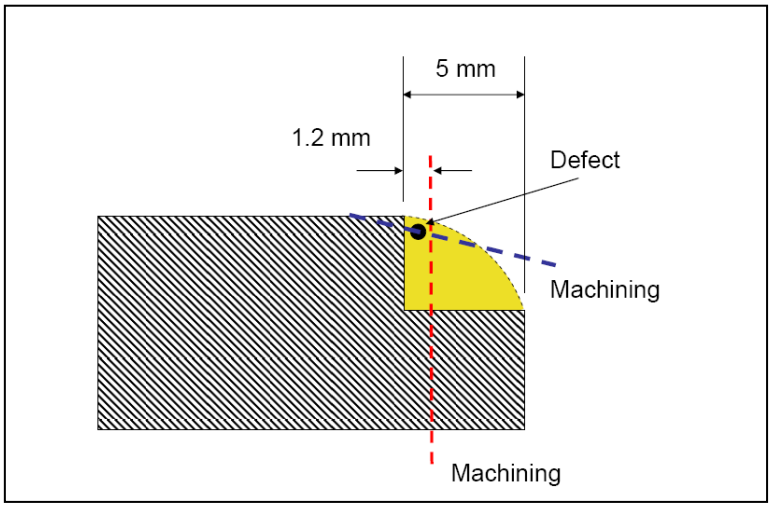

Figure 1 Typical sub-surface defect in copper cladding on a valve seat part (Courtesy of Toyota).

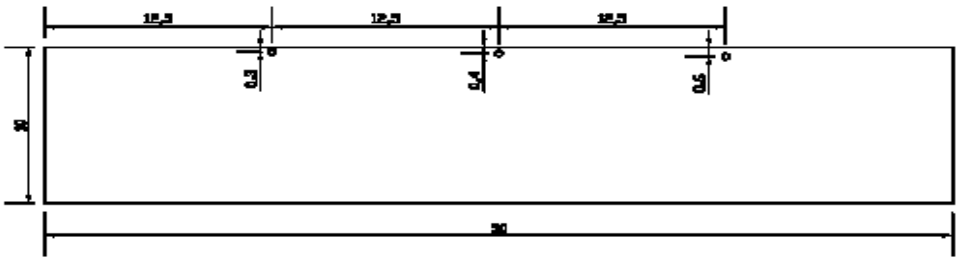

All size in mm
Hole diameters: 0.4 mm

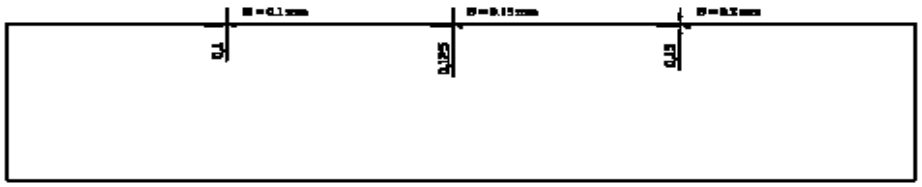

All size in mm

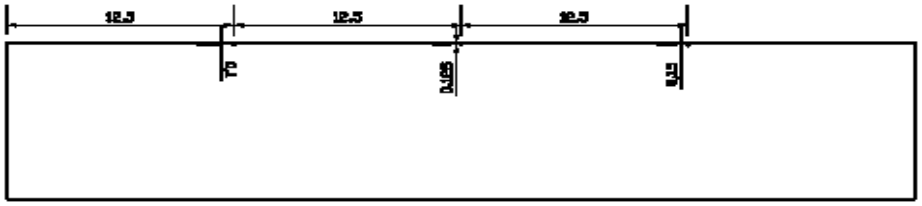

All size in mm
Hole diameters: 0.1 mm

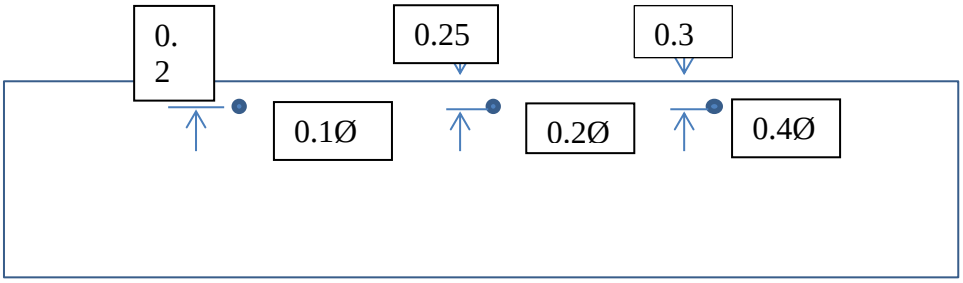

Figure 2 Type 1 designs (dimensions in mm)

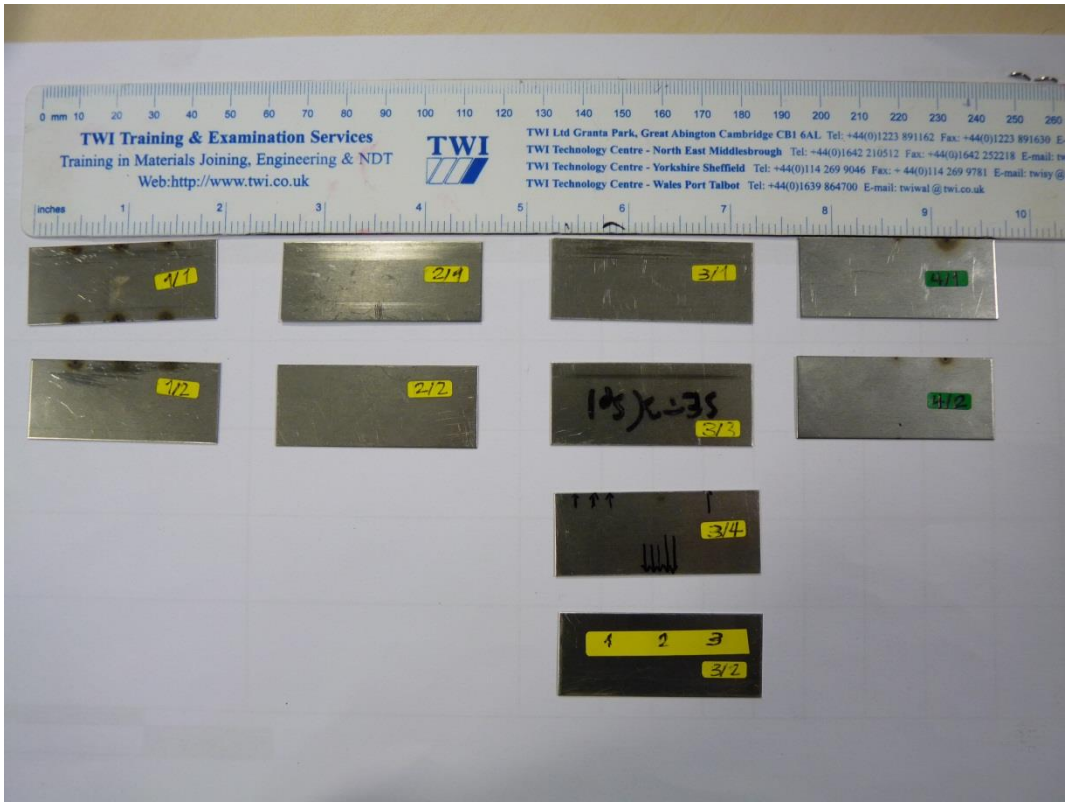

Figure 3 Type 1 Samples

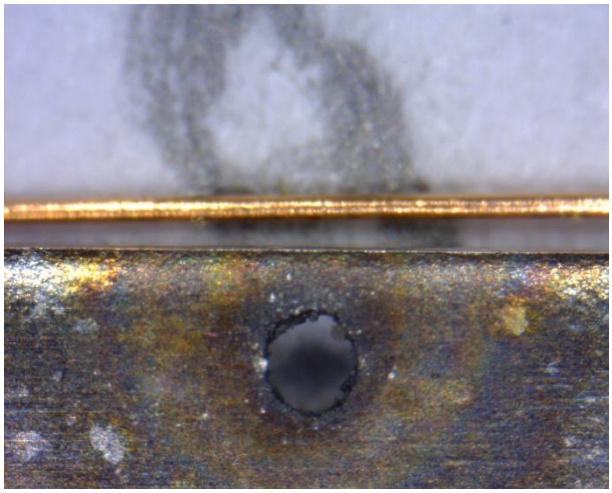

Figure 4 Typical Target produced by laser drilling in Reference Samples Type 1

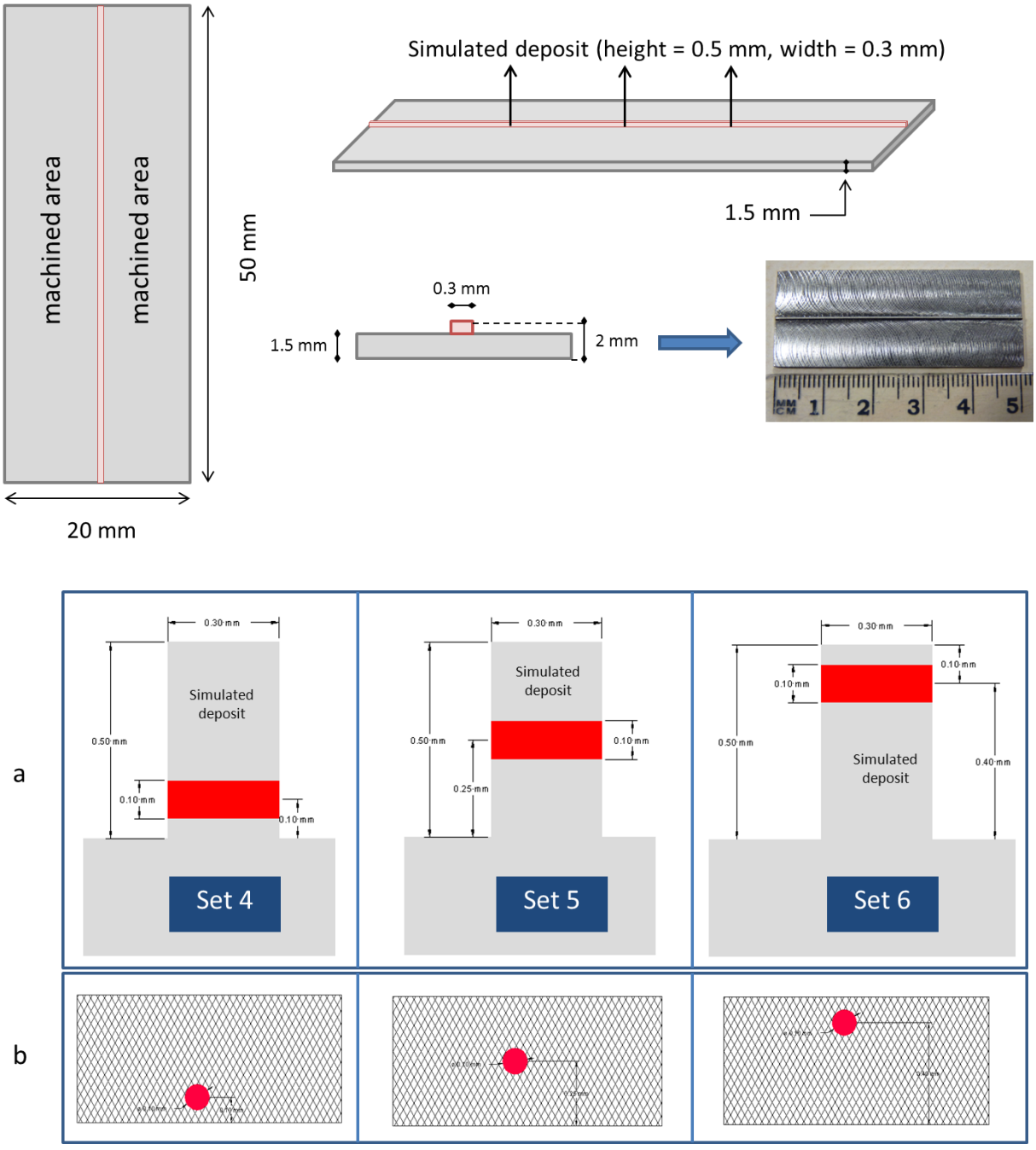

Figure 2 Overall dimensions, cross sectional view (a) and side view (b) of the simulated deposit showing the various positions of the 100 microns side drilled hole depending on the set number.

Figure 6 Type 2 Samples Manufactured by Electron Beam

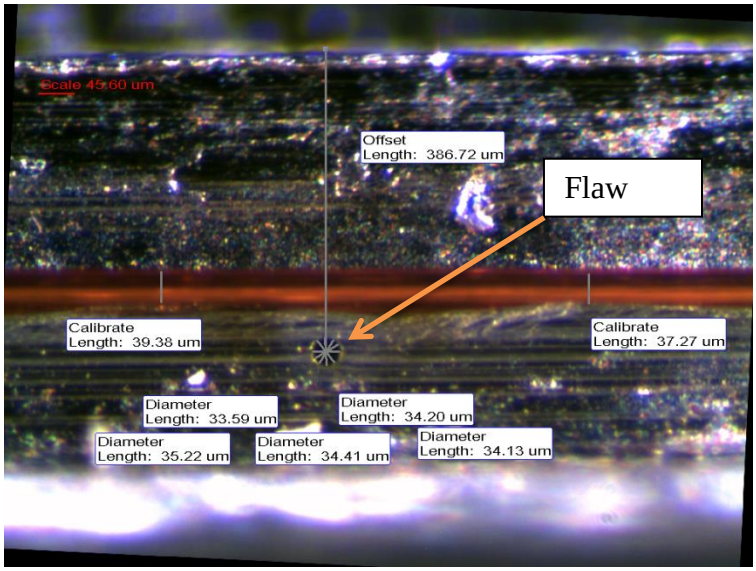

Figure 7 Example of flaw made by electron beam method (wire is 40µm)

Figure 8 Samples made by EDM Microdrilling

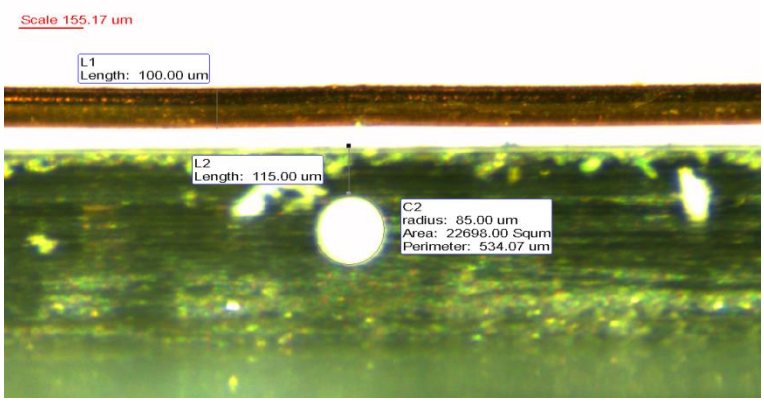

Figure 9 Sample EDM2/1

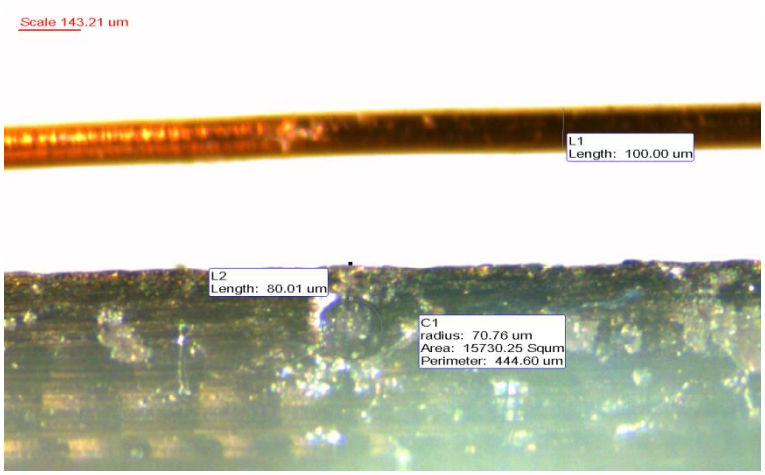

Figure 10 Sample DB1

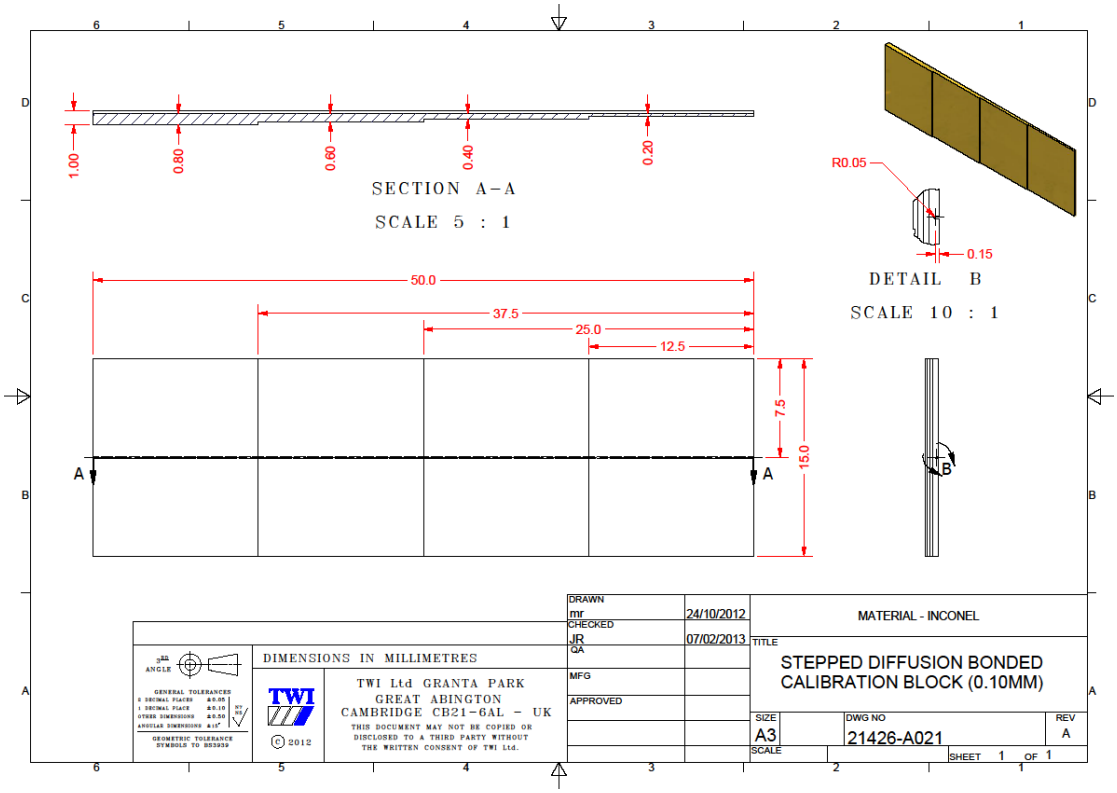

Figure 11 Type 3 Sample design (3 different sets of dimensions used)

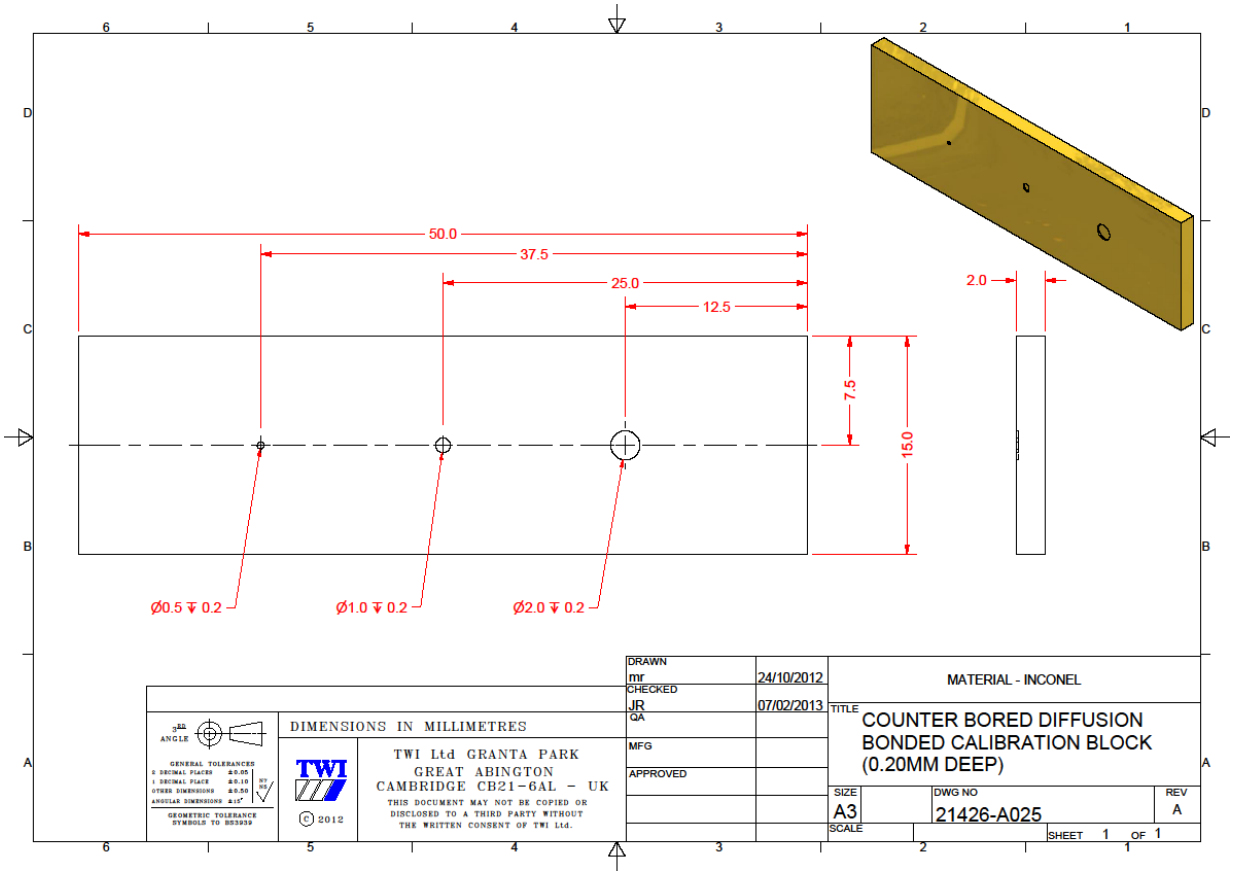

Figure 12 Type 4 Sample Design (a further block is diffusion bonded on to produce internal flaws)

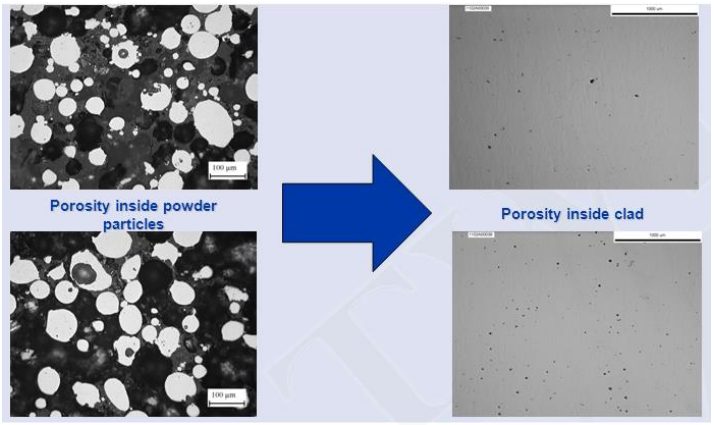

Figure 13 Porosity produced by powder containing pores

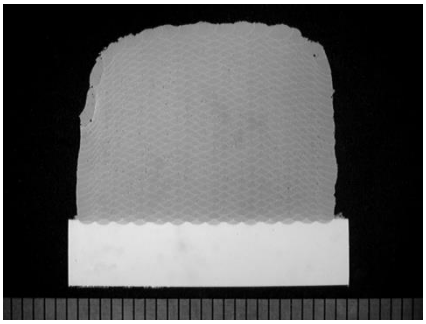

Low porosity block

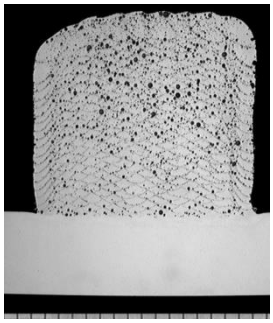

High porosity block

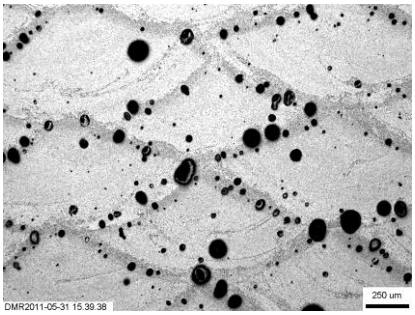

Detail of pores

Figure 14 Blocks produced demonstrating porosity

Figure 15 Single line deposits to develop defects (In 718)

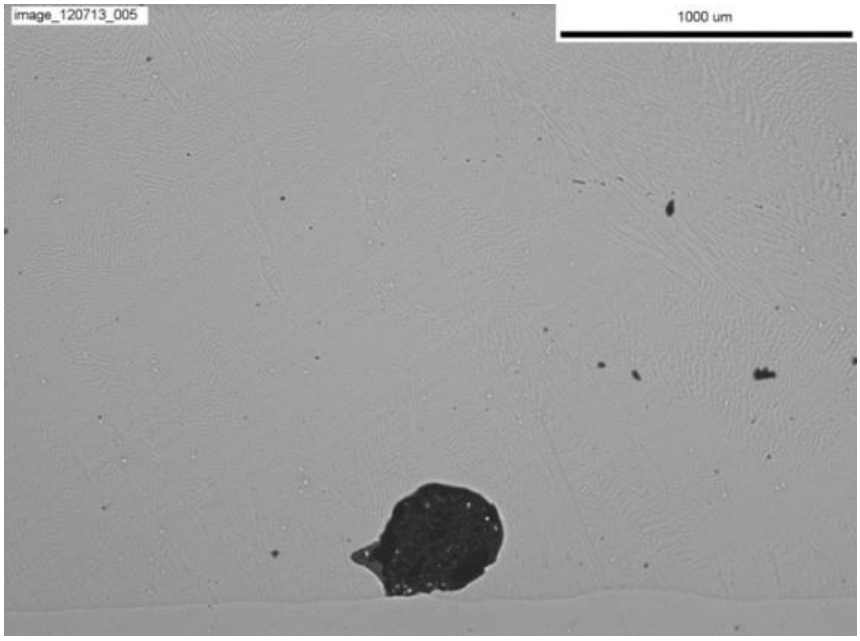

Figure 16 Detail of typical defect produced

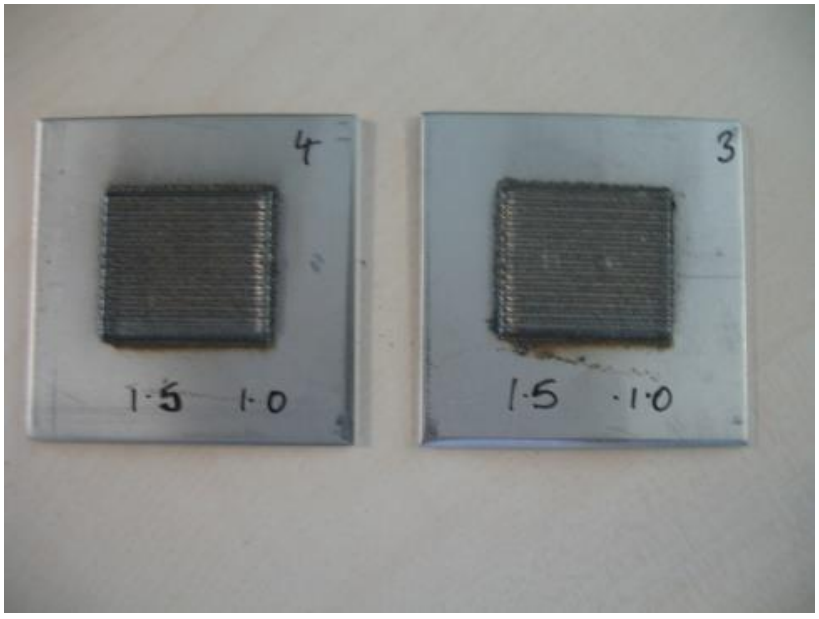

Figure 17 Coating type samples

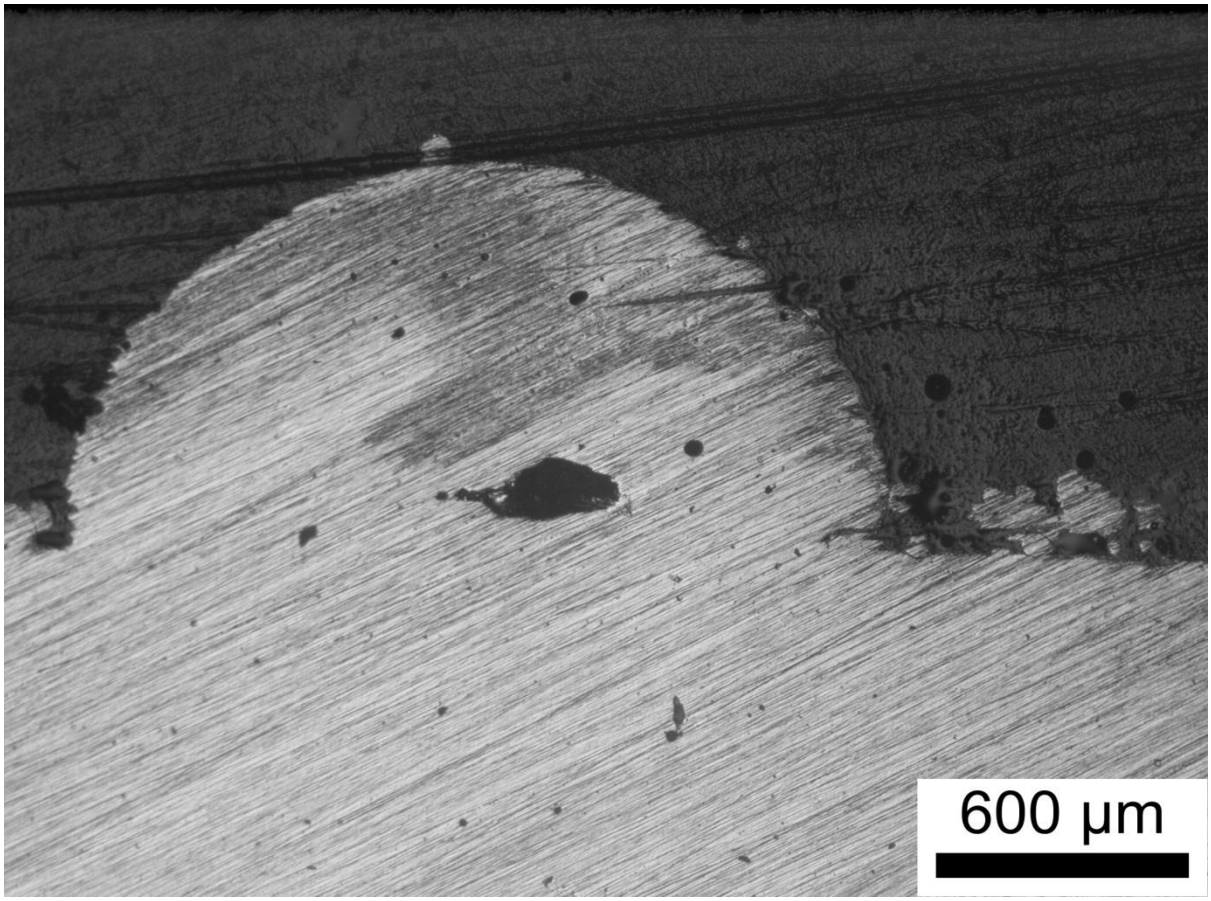

Figure 18 Flaw induced by hole drilling method

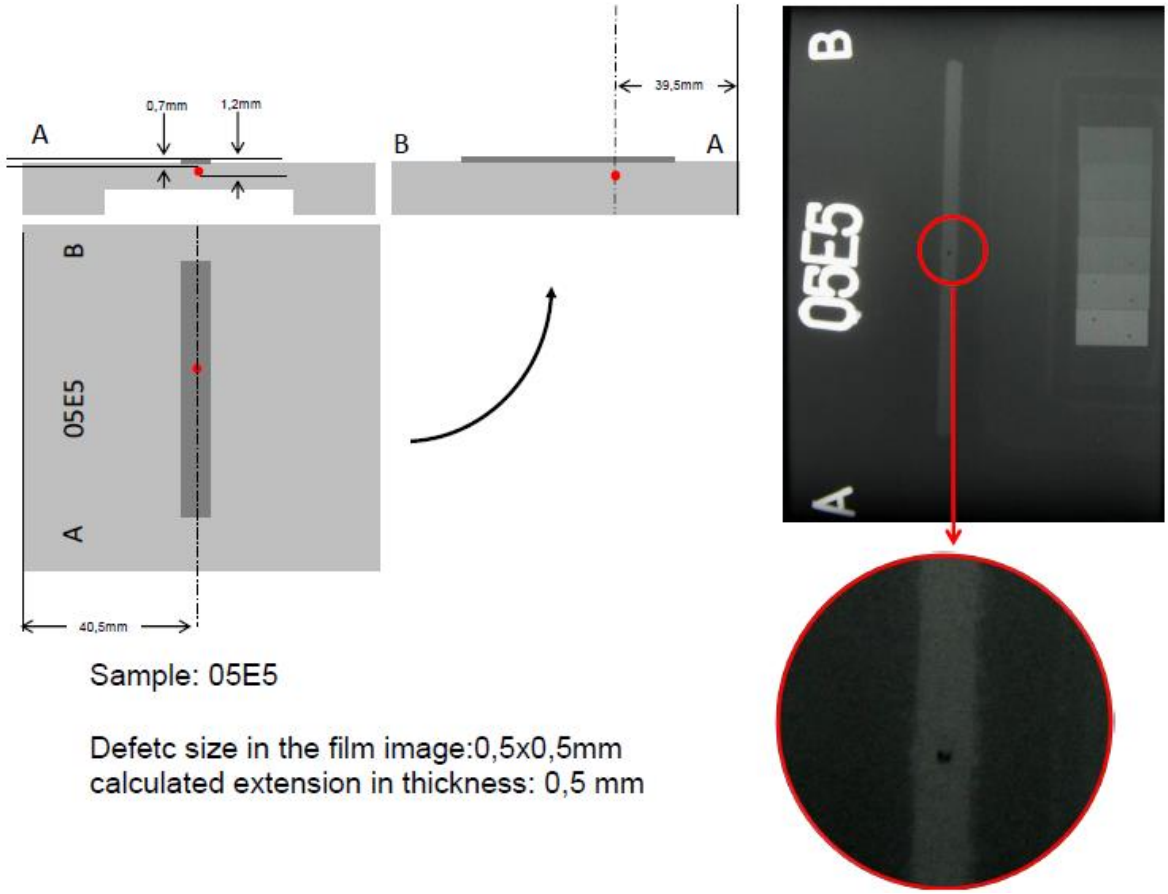

Figure 19 Radiography of flaws

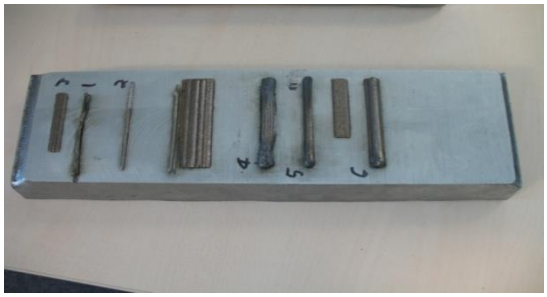

Figure 20 Samples of deposited line tracks

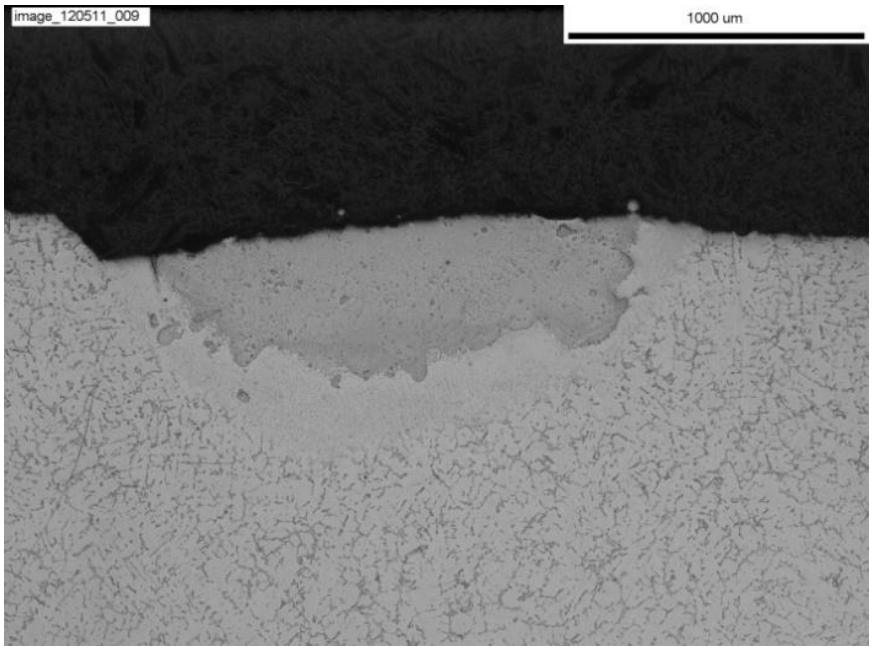

Figure 21 Section through deposit showing fine surface cracking of copper-nickel deposit onto aluminium A2C2

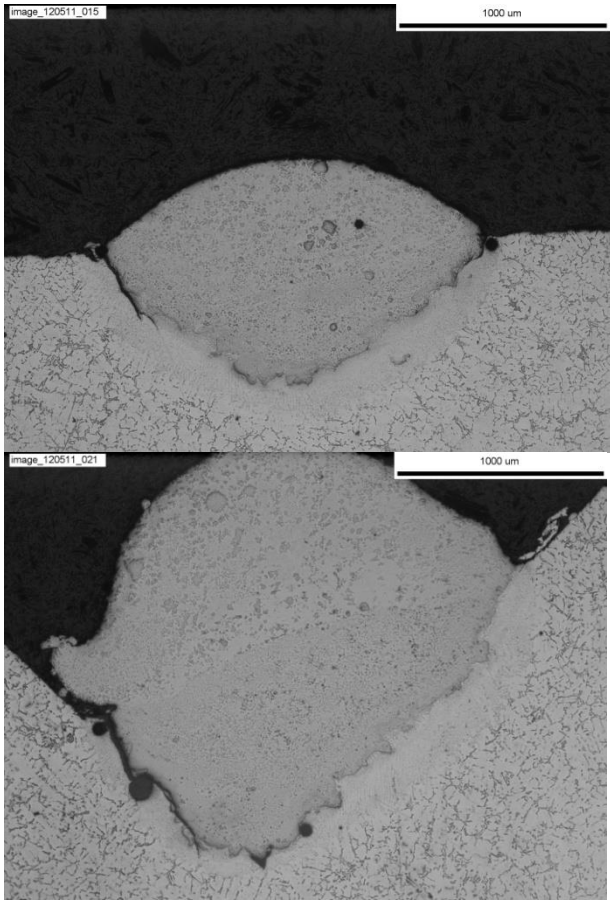

Figure 22 Figure b Deposit showing deep cracks into base of Cu-Ni deposit onto aluminium A2C2 substrate

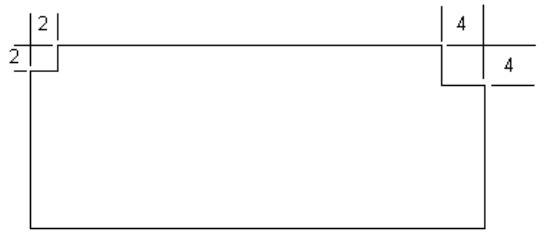

Figure 23 Cross Section of substrate

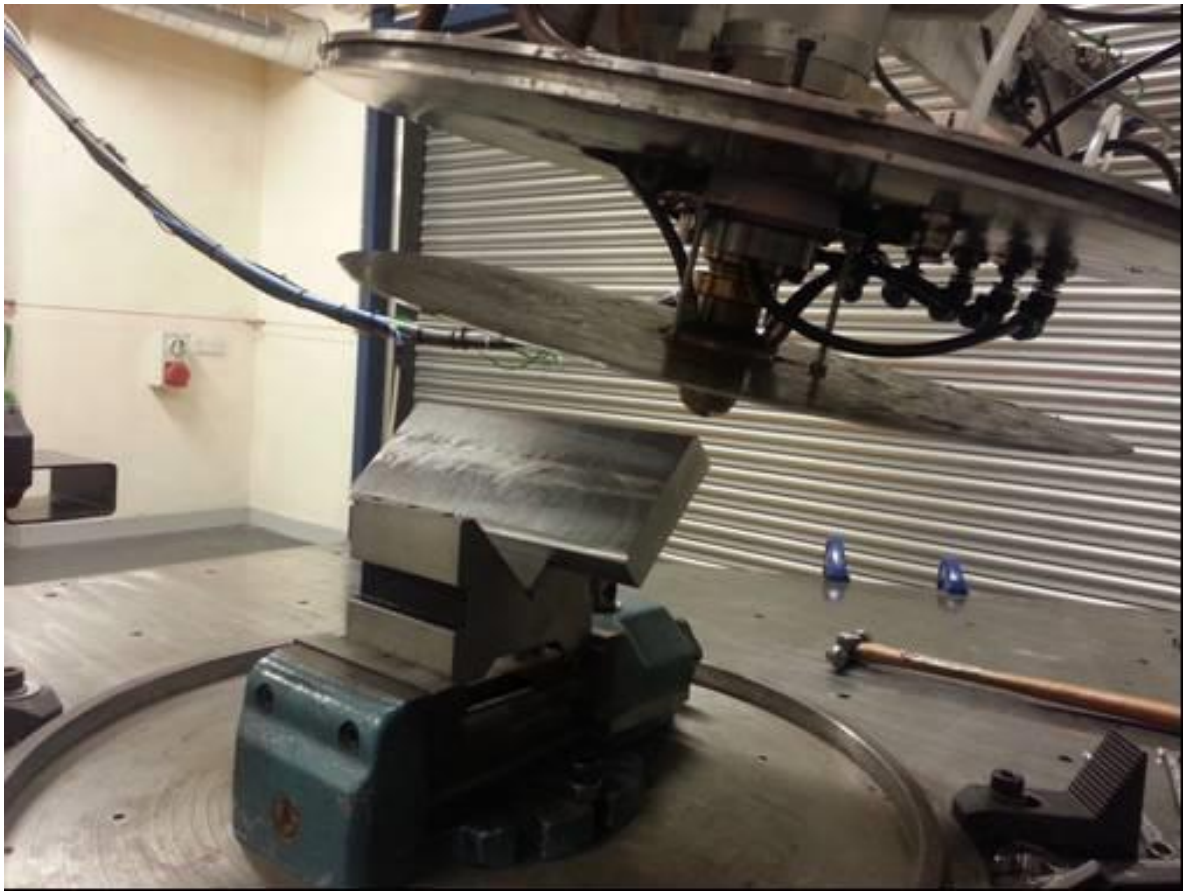

Figure 24 Equipment and set up for deposition

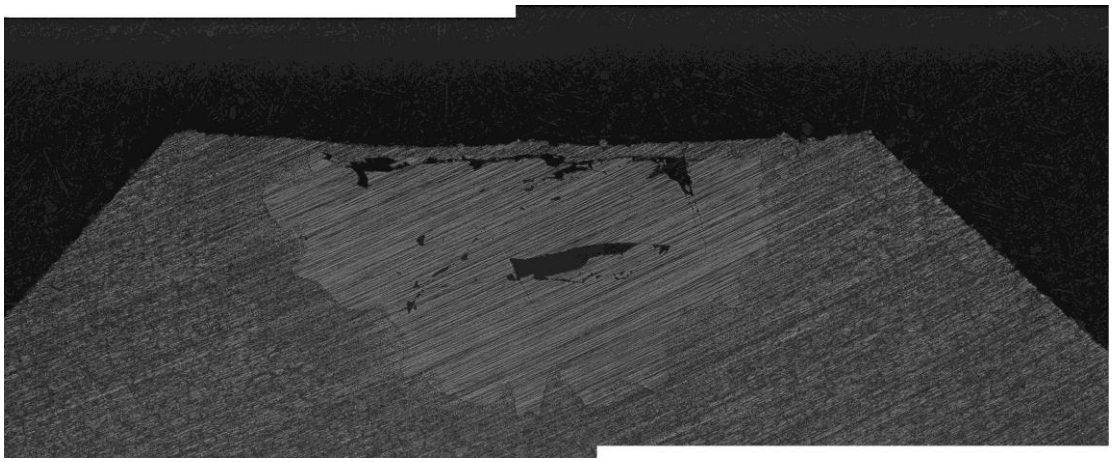

Figure 25 - Sample 1

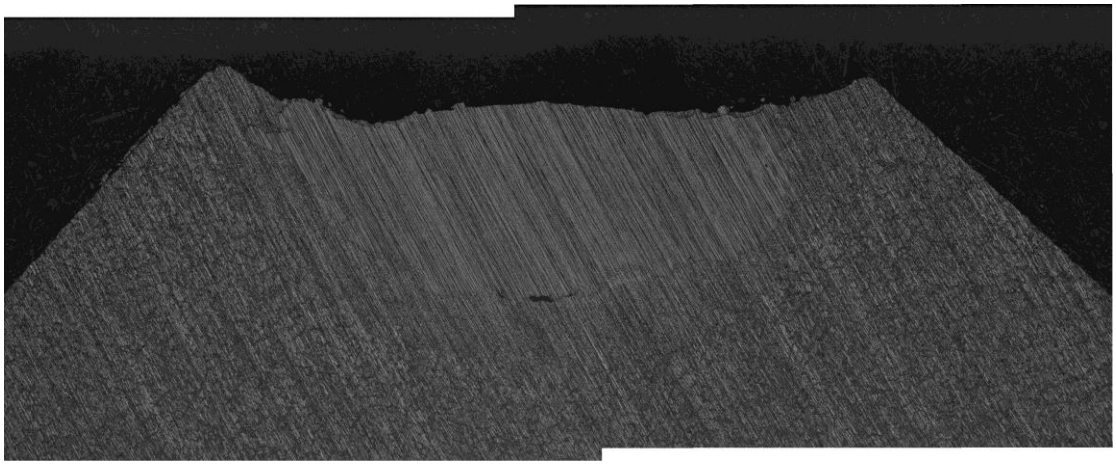

Figure 26 - Sample 2

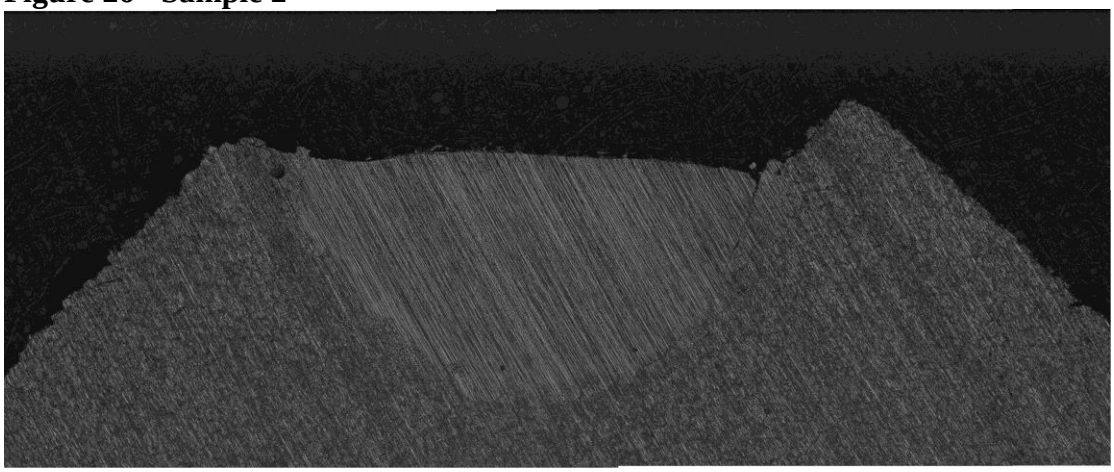

Figure 27 - Sample 3

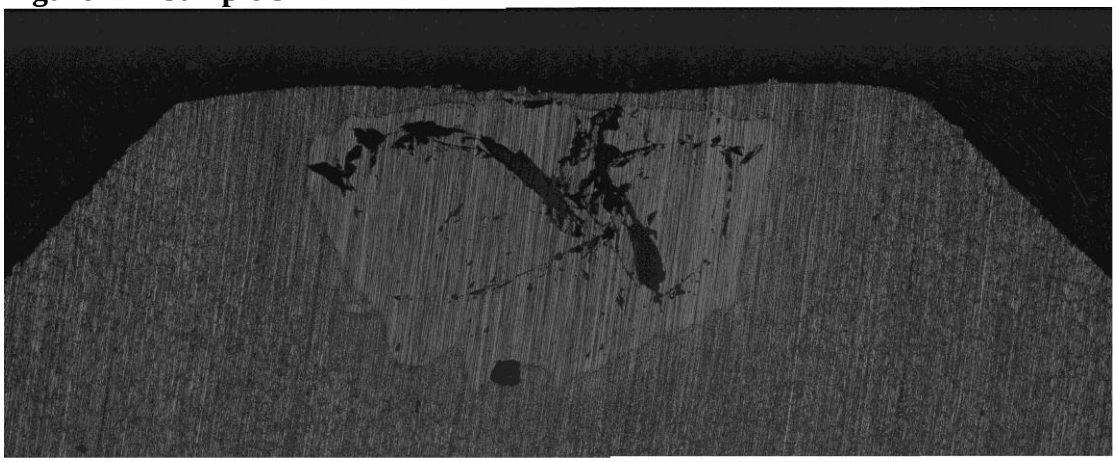

Figure 28 - Sample 4

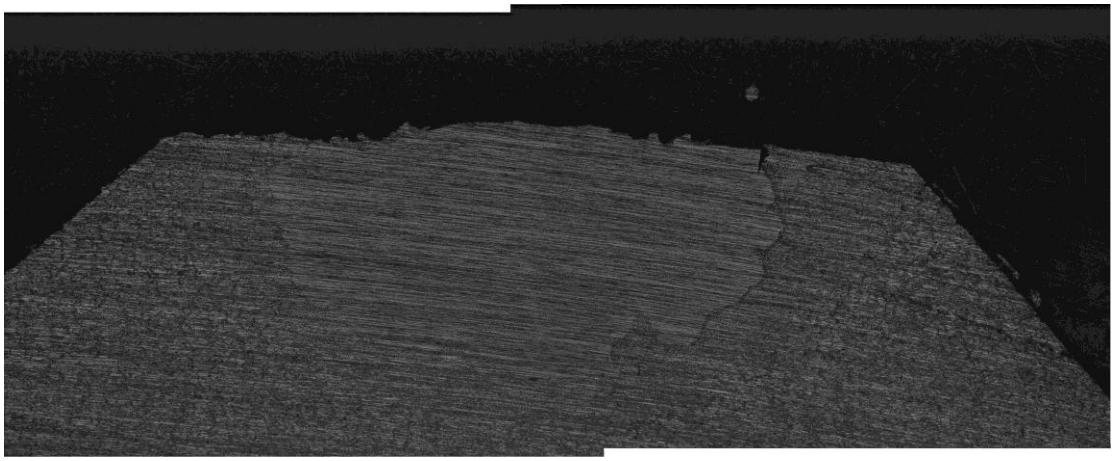

Figure 29 - Sample 5

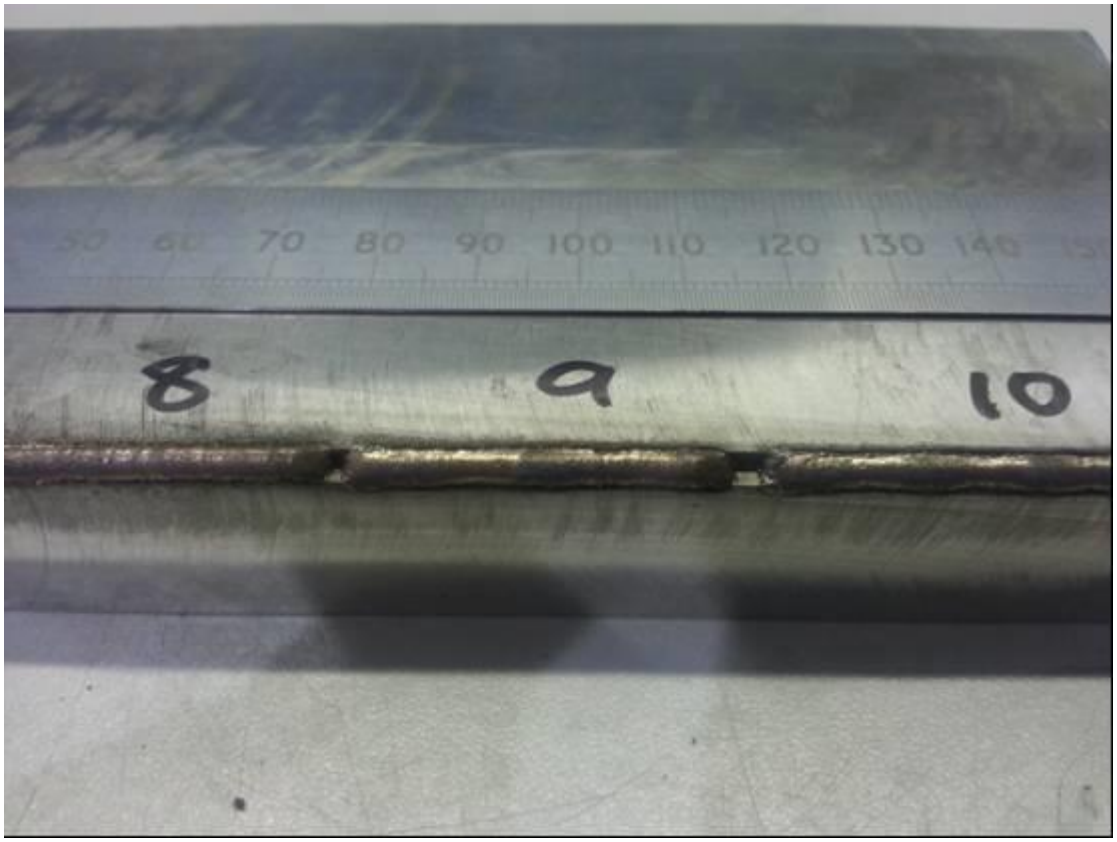

Figure 30 Test Sample with different deposit procedures

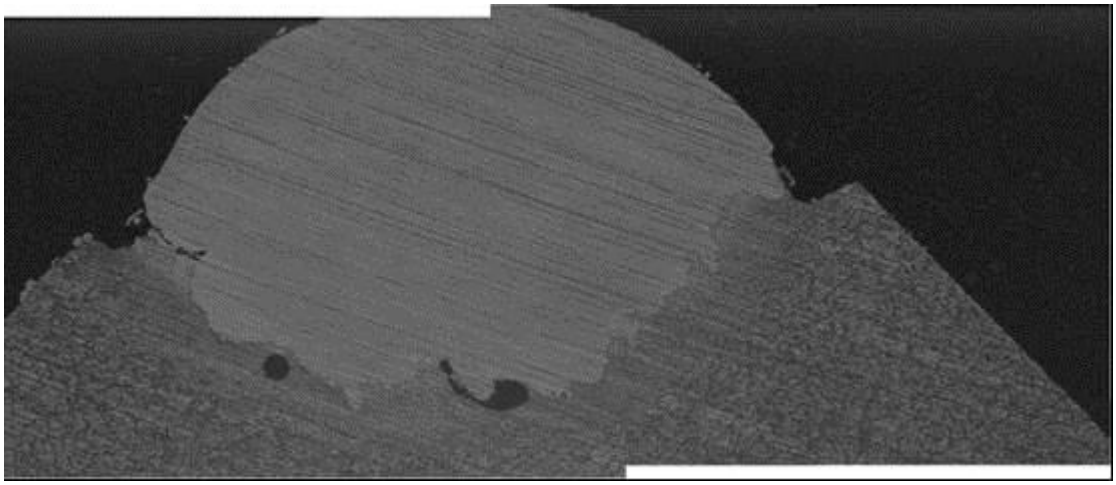

Figure 31 Sample 8

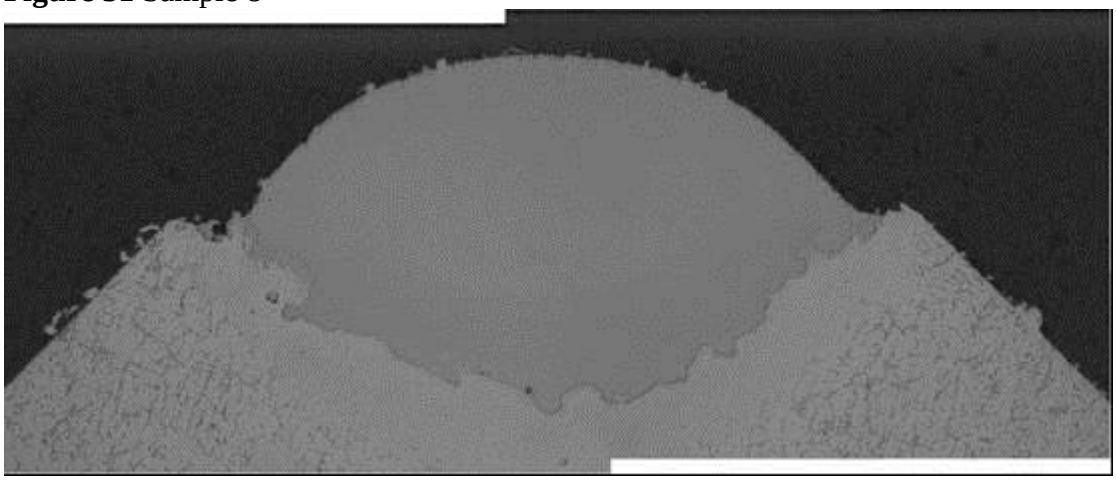

Figure 32 Sample 9

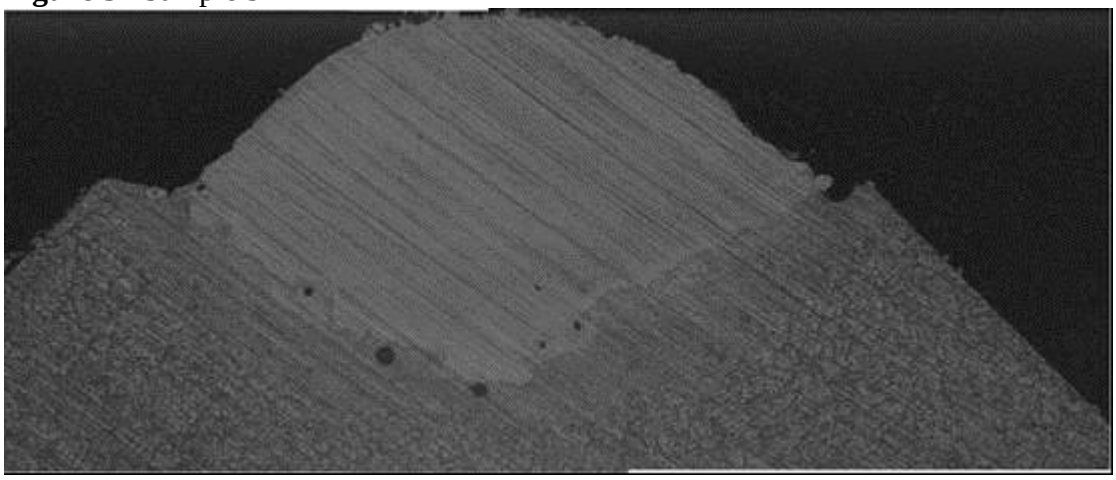

Figure 33 Sample 10

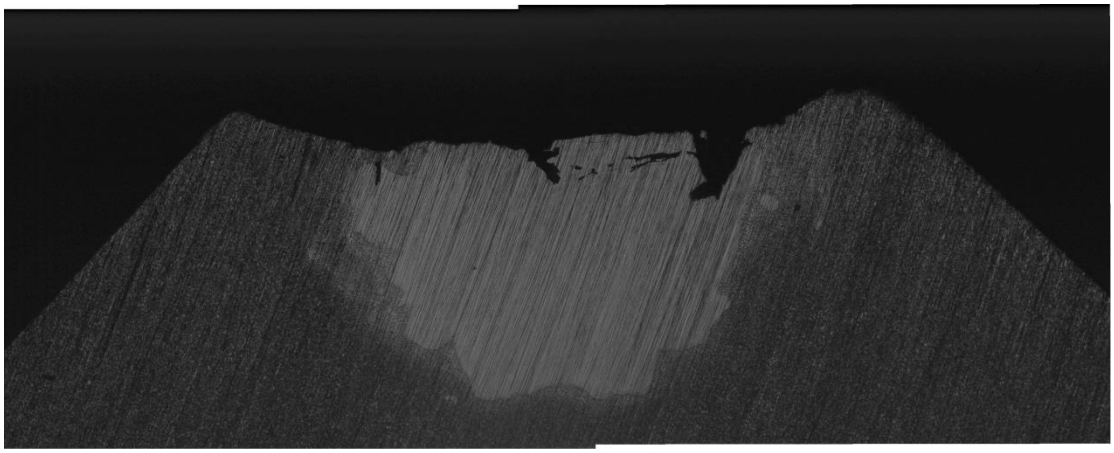

Figure 34 - Sample 11

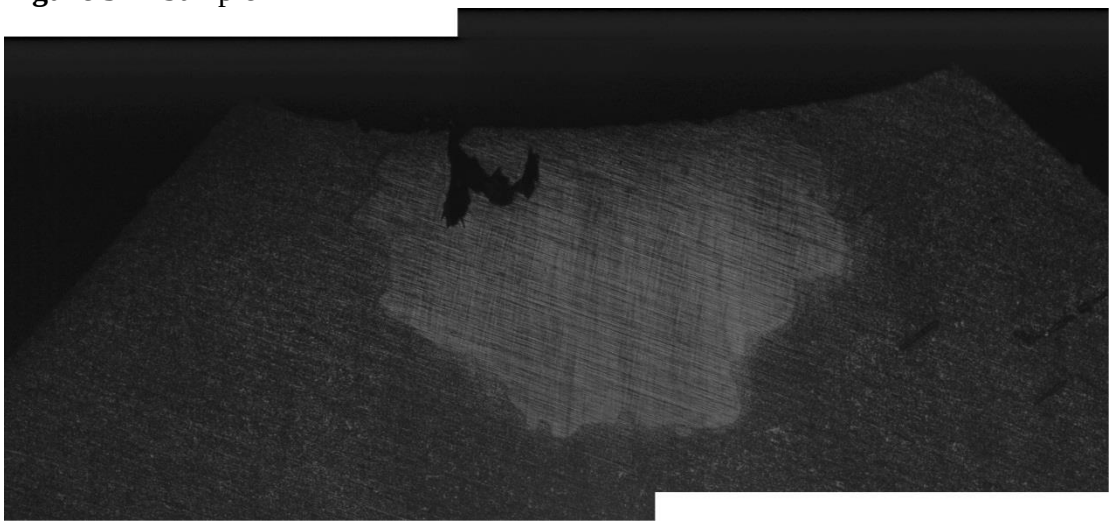

Figure 35 - Sample 12

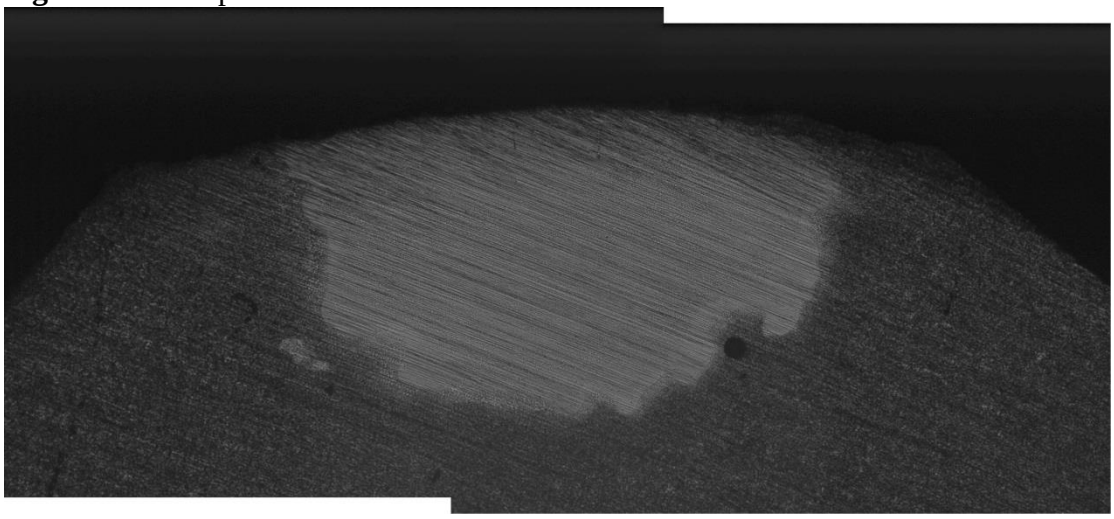

Figure 36 - Sample 13

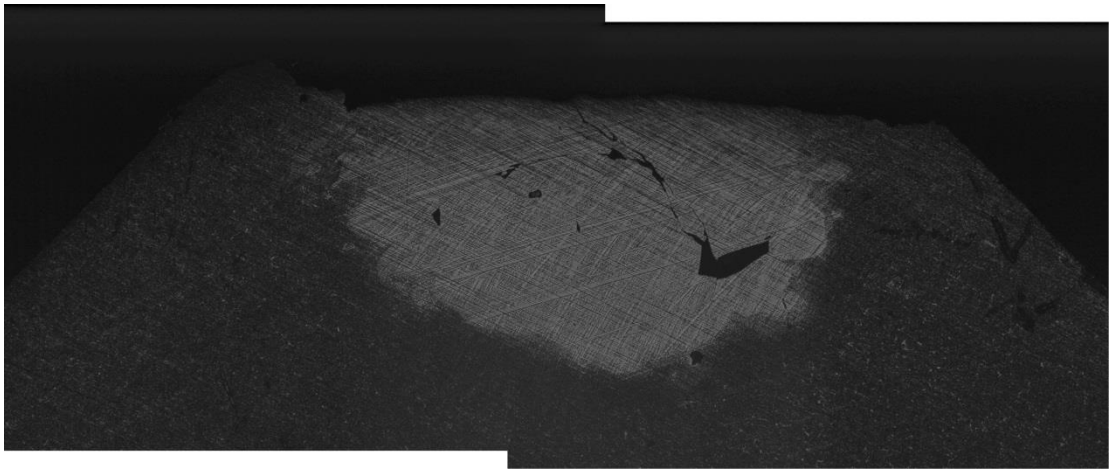

Figure 37 – Sample 14

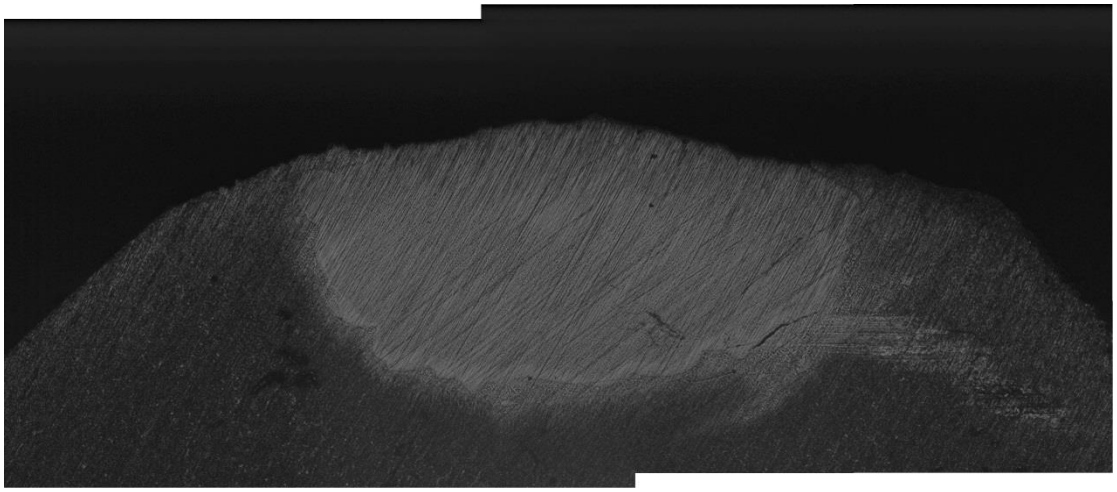

Figure 38 - Sample 15

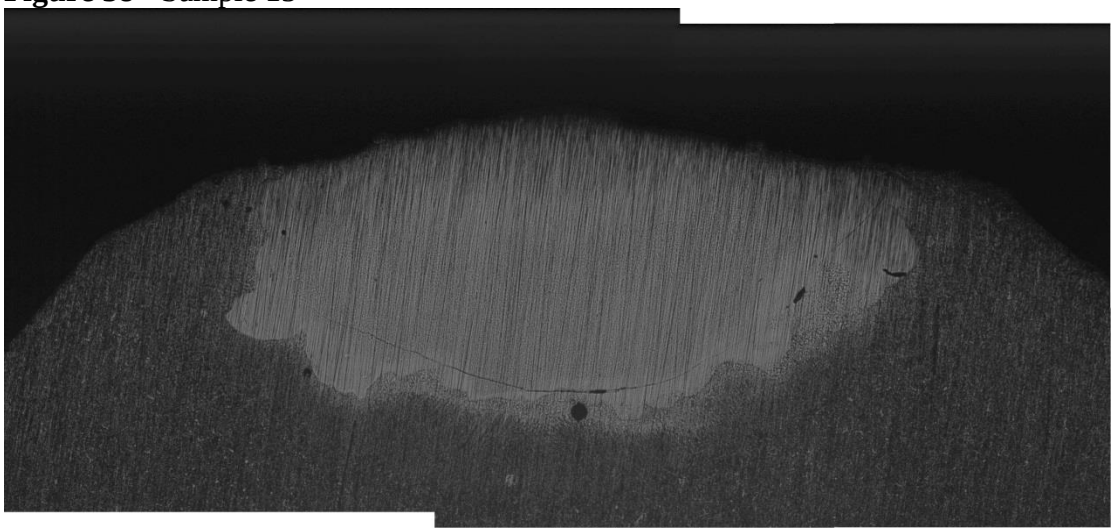

Figure 39 - Sample 16

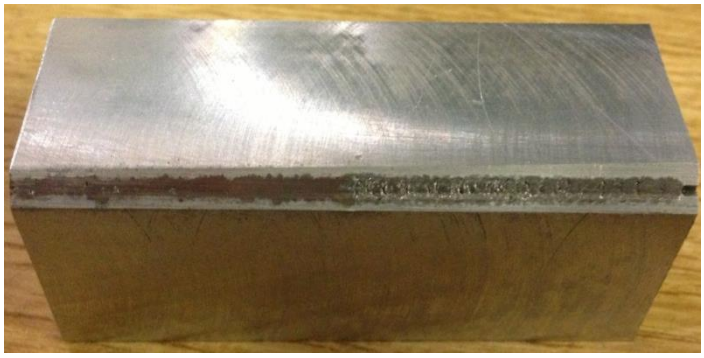

Figure 40 Sample T1 (30mm with procedure 13 and 13mm with Procedure 14)

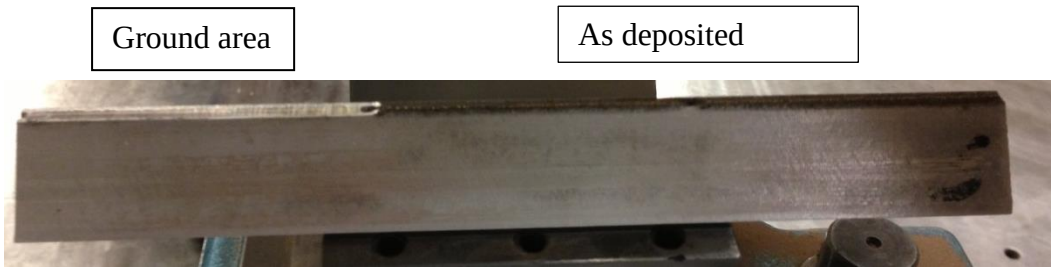

Figure 41 Experimental Sample T2 with as deposited and ground layers.

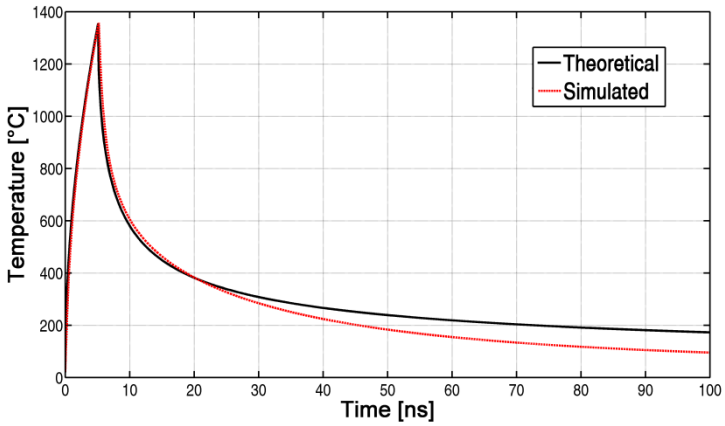

Figure 42 - Comparison between the theoretical temperature and the simulated pattern, for Inconel alloy 600.

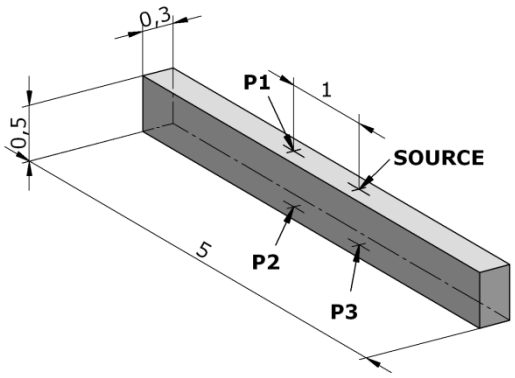

Figure 43 – Model for the comparison of the ultrasonic fields produced by different type of sources.

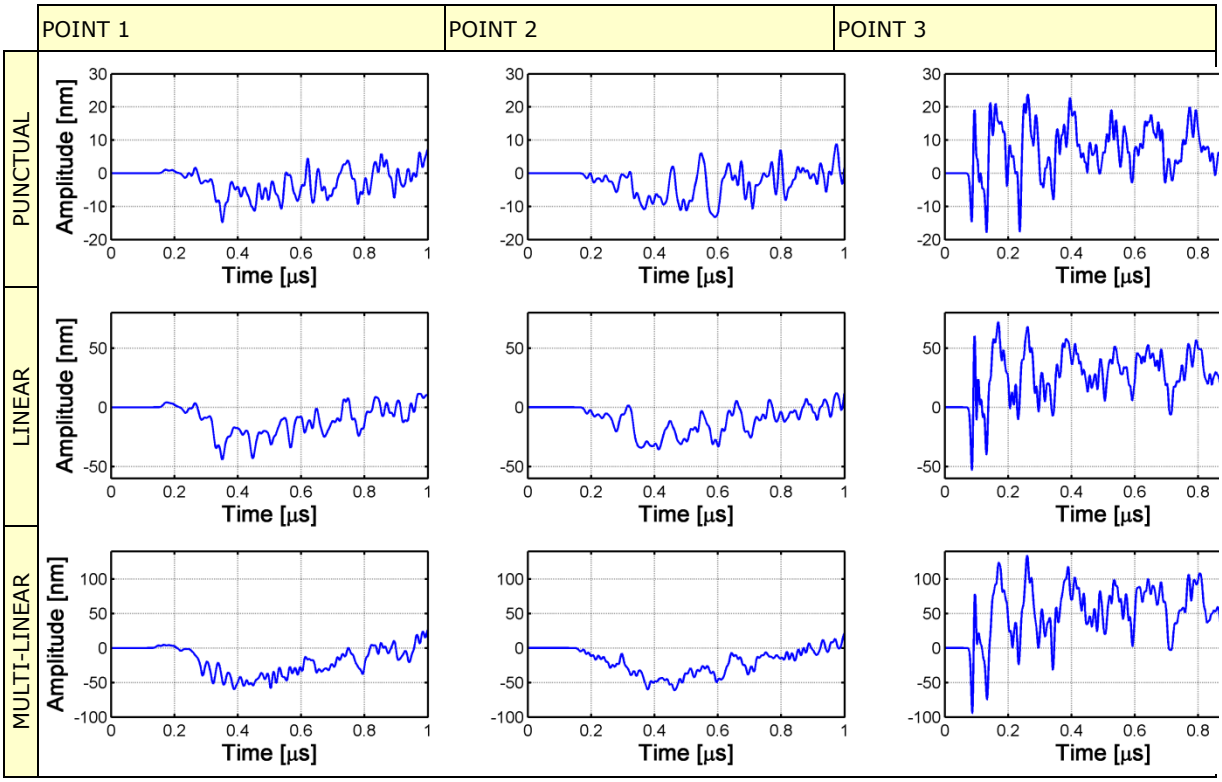

Figure 44 Displacements

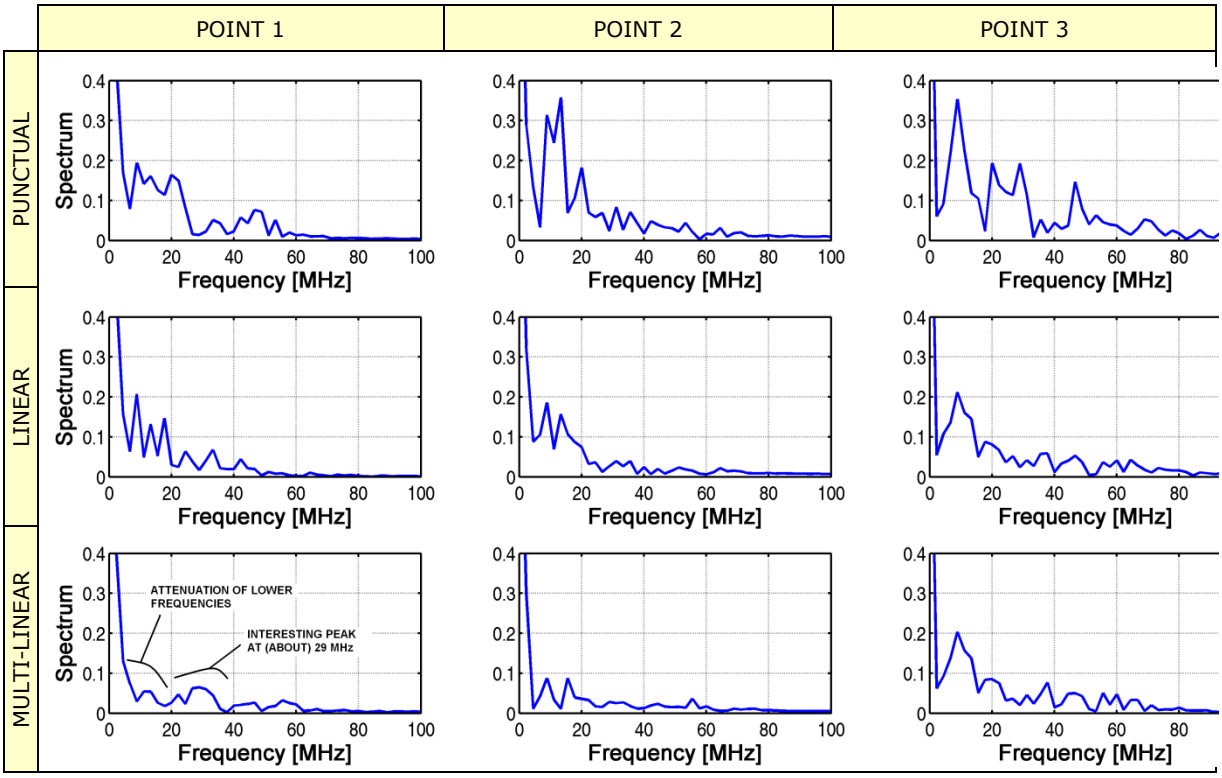

Figure 45 – Frequency spectrums

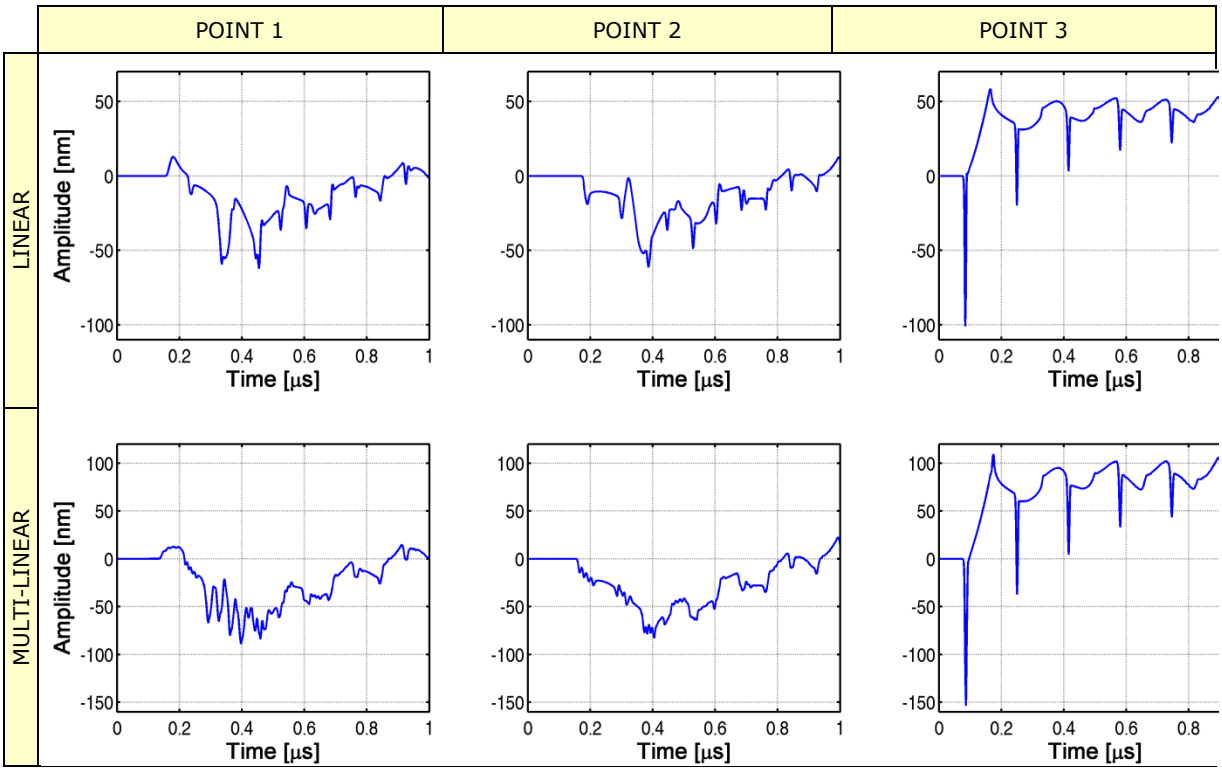

Figure 46 – Displacements obtained with the 2D model

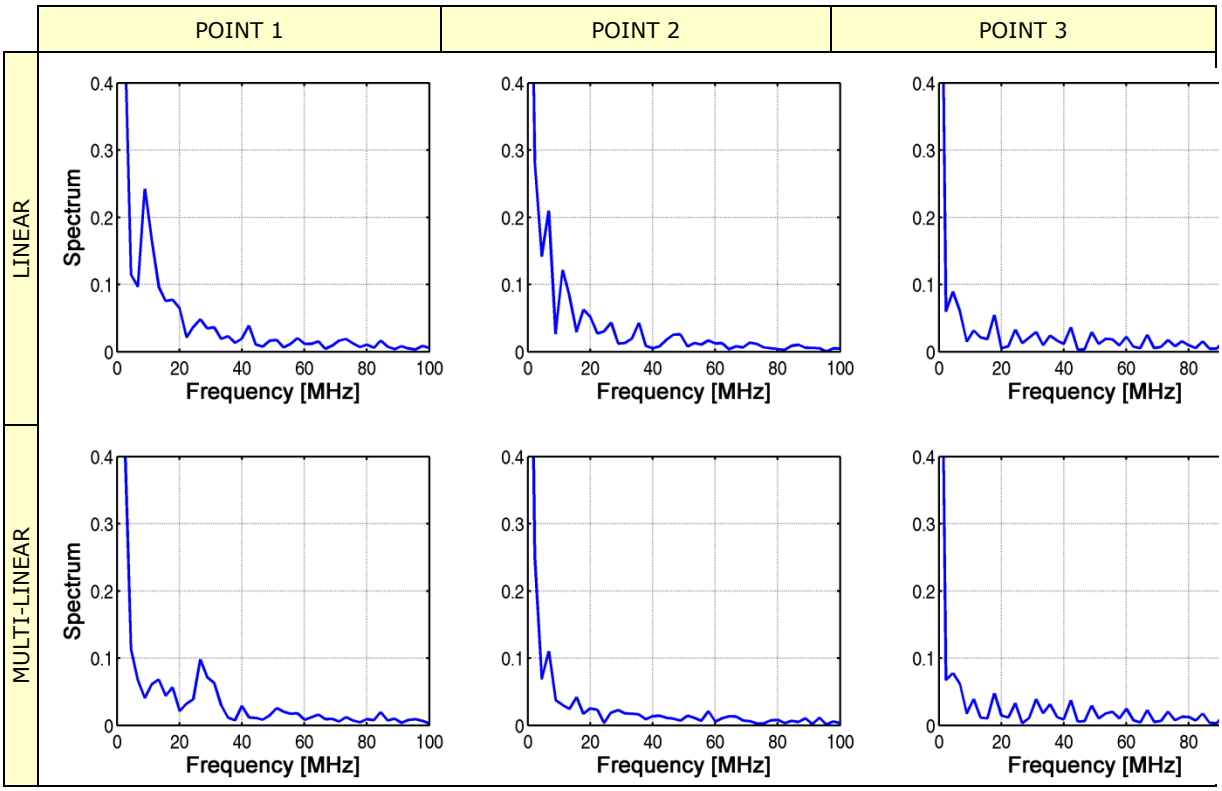

Figure 47 – Frequency spectrums obtained with the 2D model

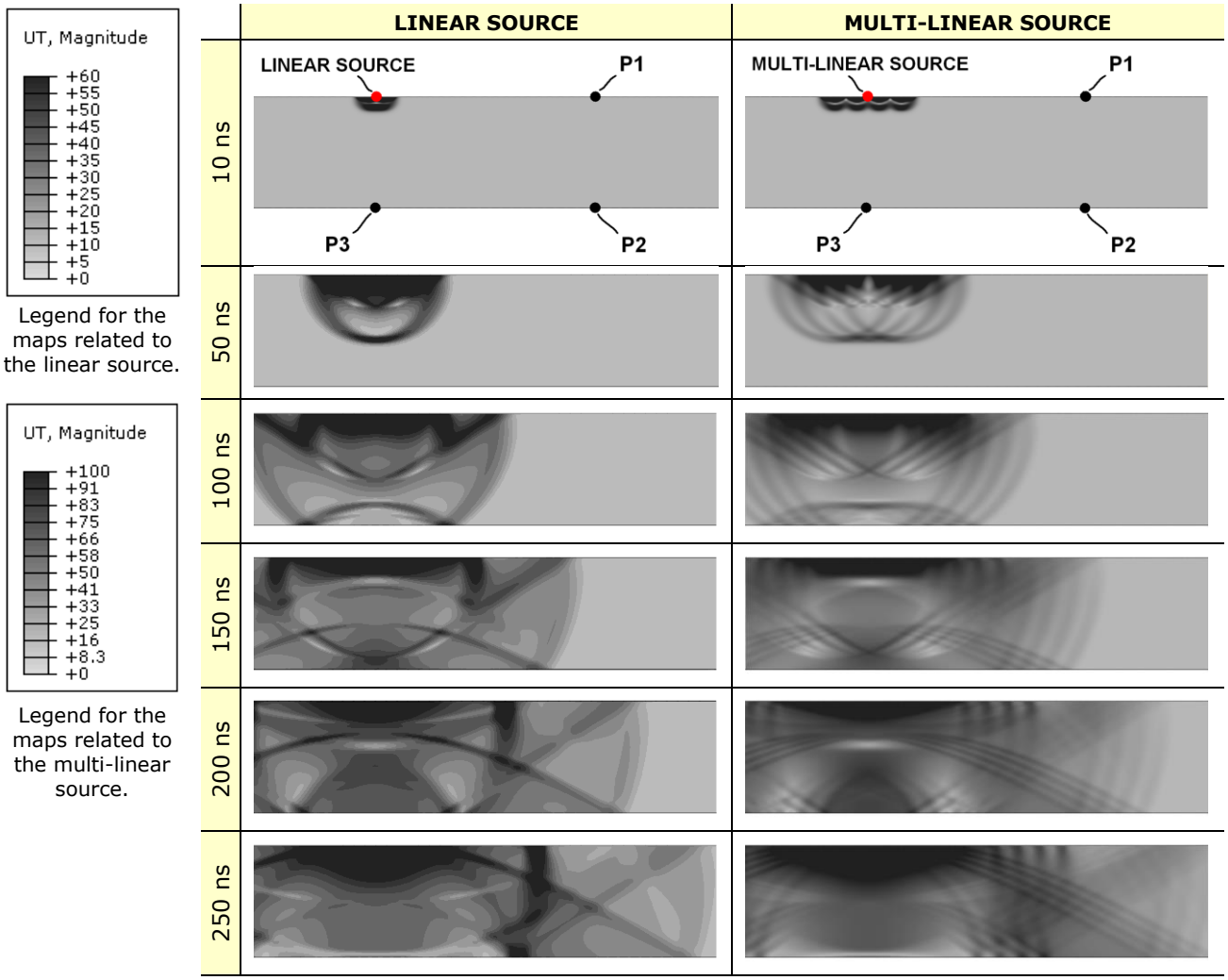

Figure 48 – Map of the displacement magnitude at different values of time.

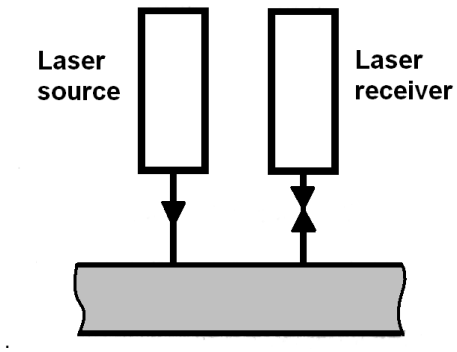

Figure 49 – Single-sided conceptual configuration, especially suitable for surface-wave measurements and the time-of-flight technique [1].

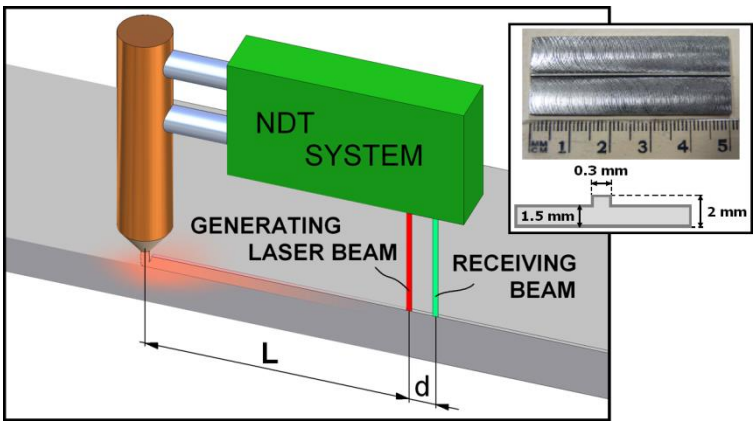

Figure 50 – The NDT system moving together with the LMD nozzle and checking the presence of flaws.

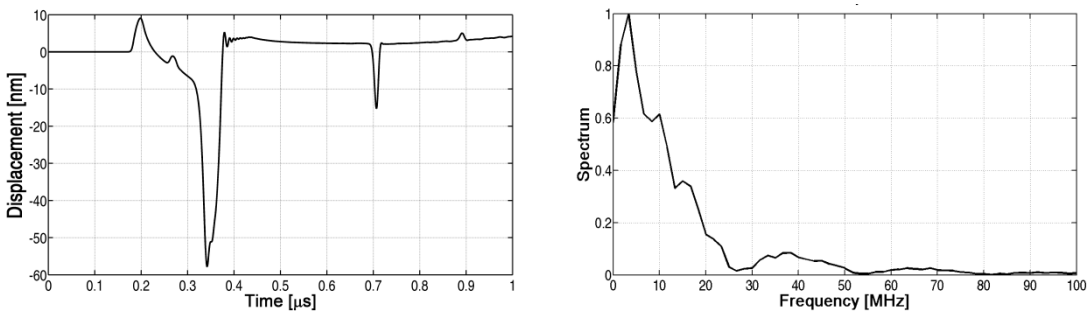

Figure 51 – Standard displacement collected at the receiving point (a) and its frequency spectrum (b).

(a)

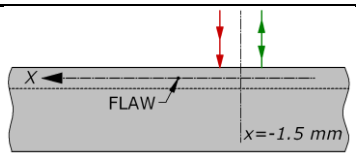

Inspection at $x = -1.5$ mm from flaw

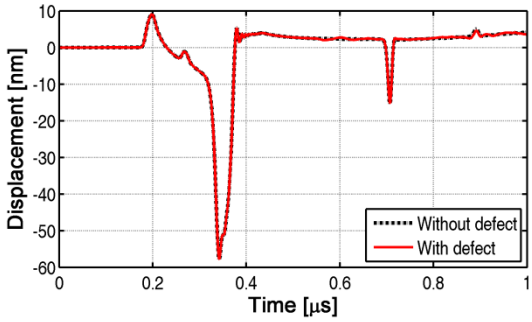

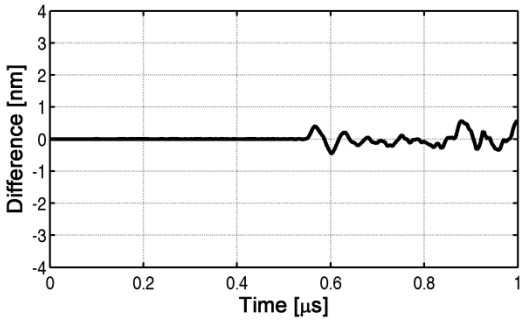

(b)

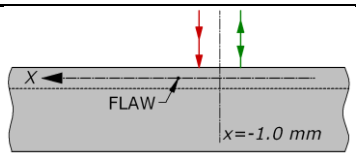

Inspection at $x = -1.0$ mm from flaw

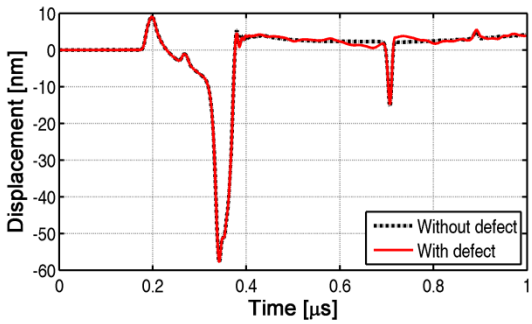

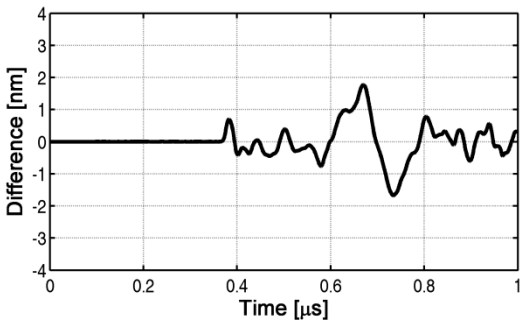

(c)

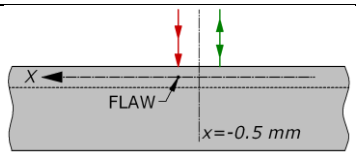

Inspection at $x = -0.5$ mm from flaw

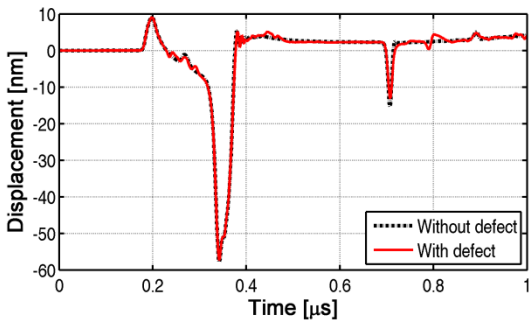

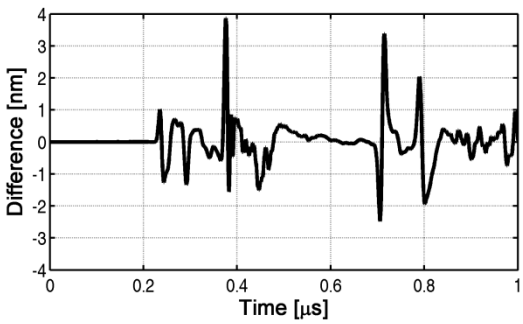

(d)

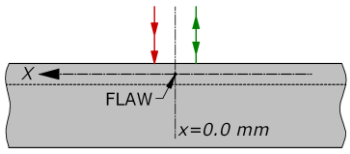

Inspection at $x = 0.0$ mm from flaw

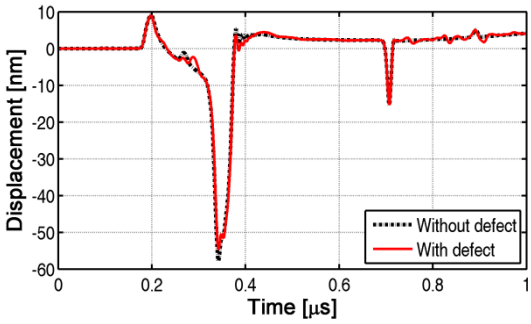

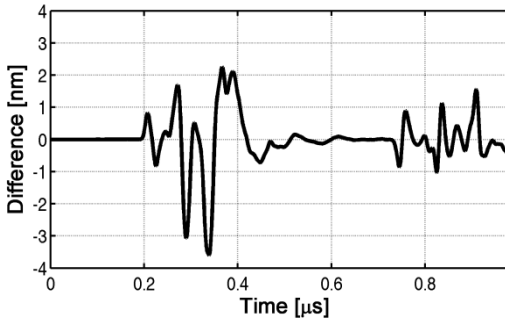

(e)

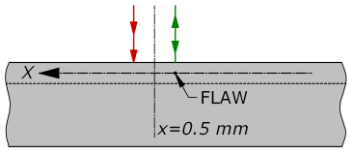

Inspection at $x = 0.5$ mm from flaw

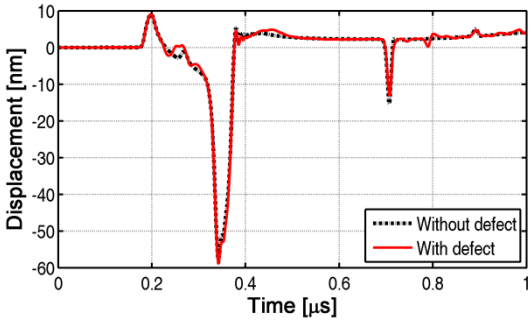

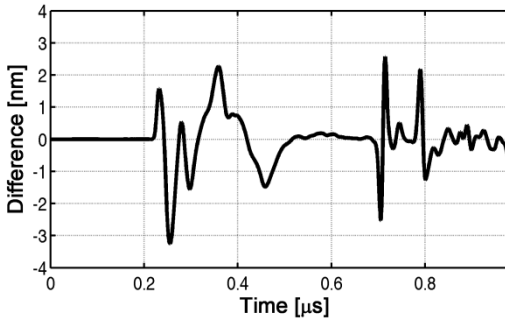

(f)

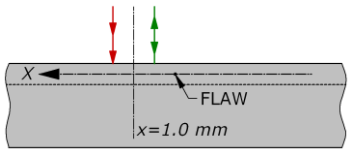

Inspection at $x = 1.0$ mm from flaw

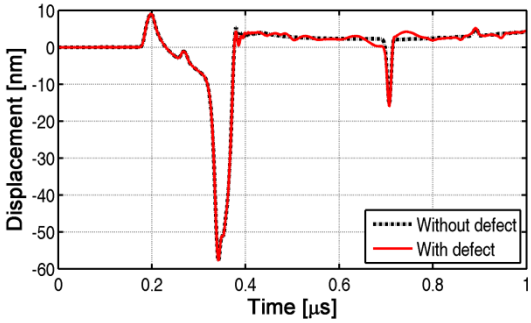

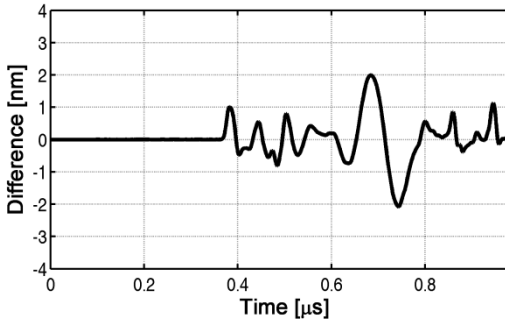

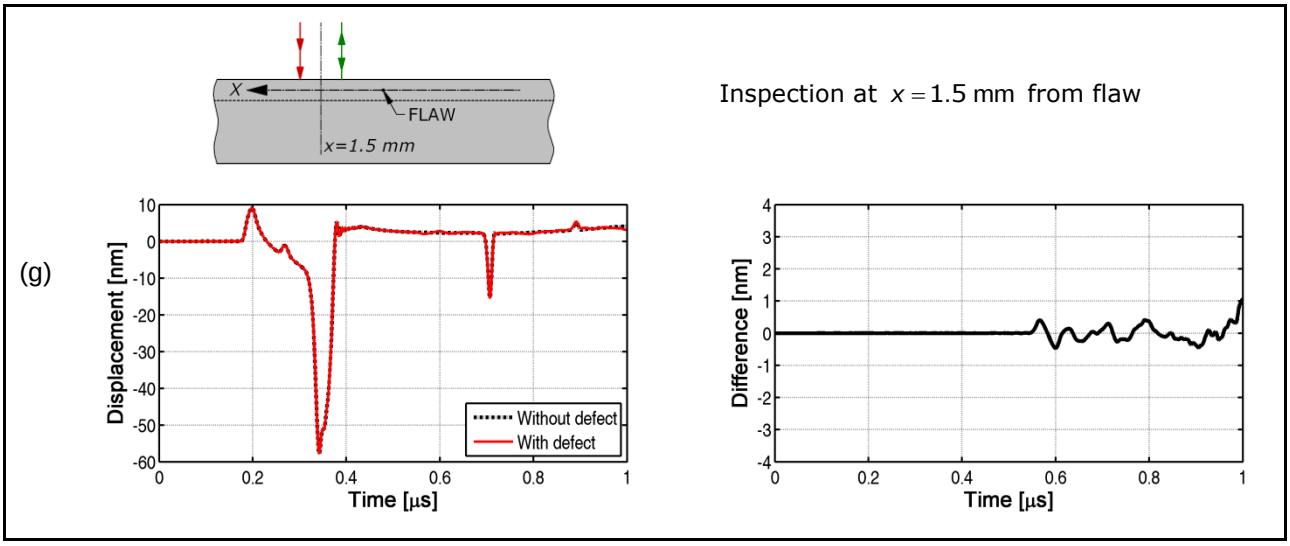

Figure 52 – Comparison between the displacement simulated in the model without defect and each displacement collected by the seven simulations in the model with the defect, developed across the flaw with increment of 0.5 mm. Linear source.

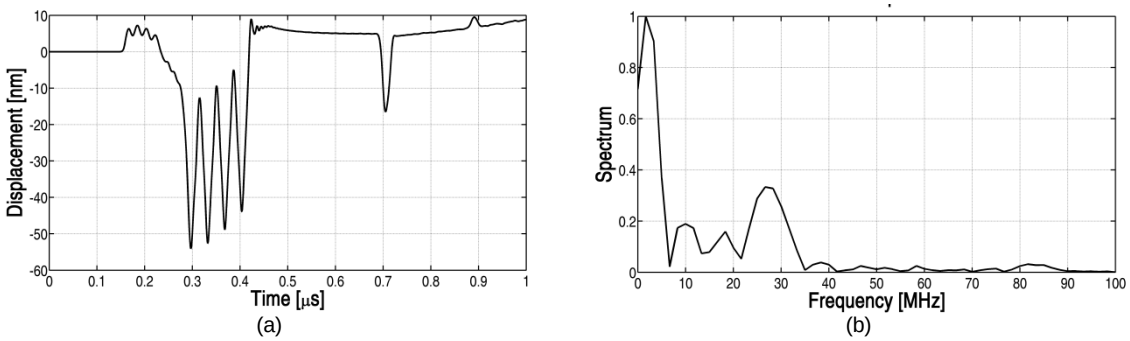

Figure 53 – Standard displacement collected at the receiving point (a) and its frequency spectrum (b).

(a)

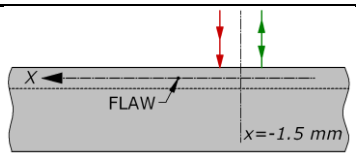

Inspection at $x = -1.5$ mm from flaw

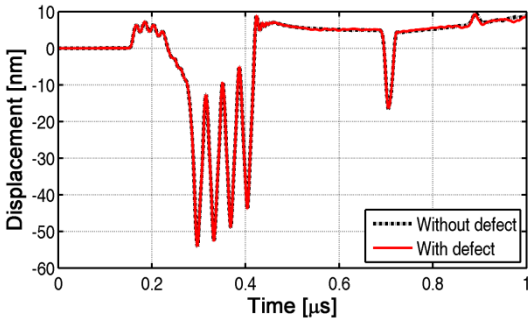

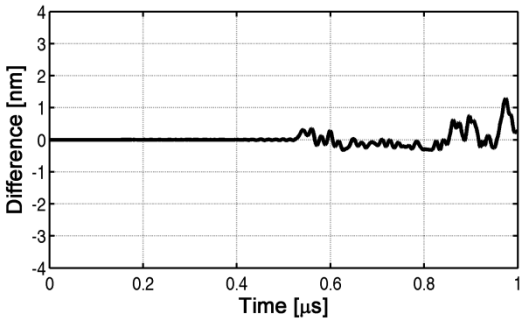

(b)

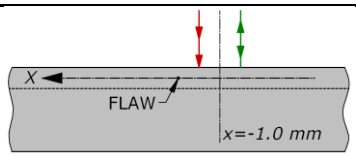

Inspection at $x = -1.0$ mm from flaw

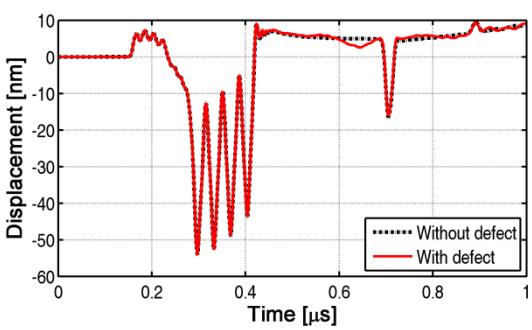

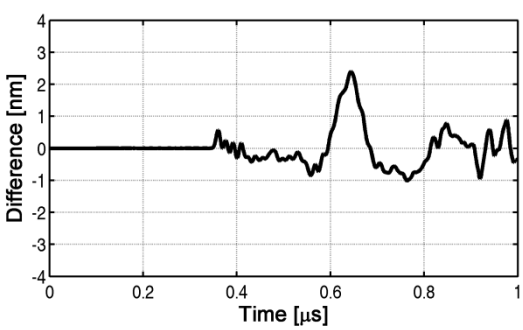

(c)

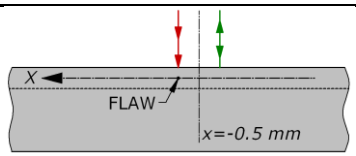

Inspection at $x = -0.5$ mm from flaw

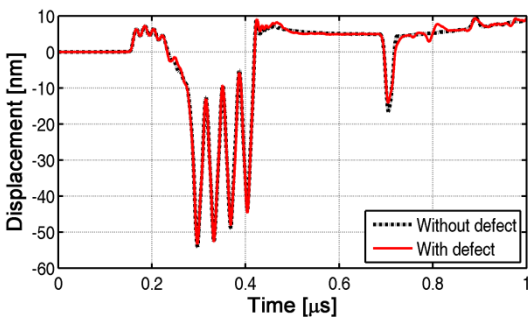

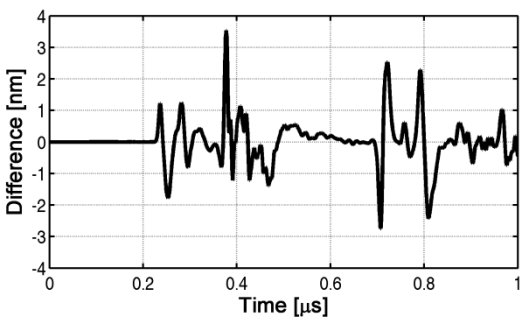

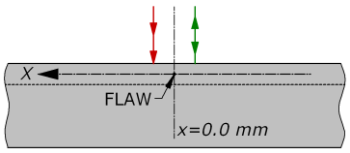

Inspection at $x = 0.0$ mm from flaw

(d)

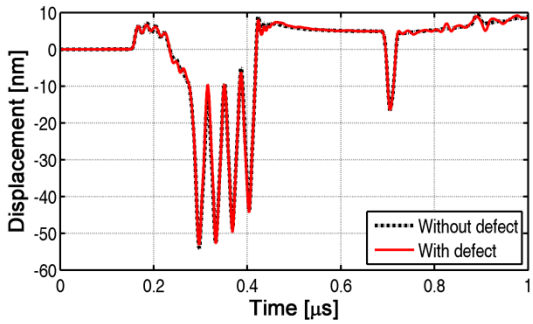

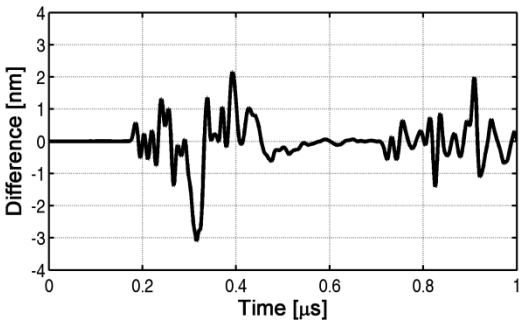

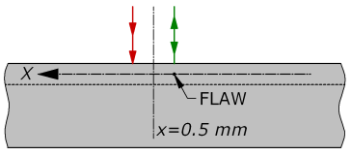

Inspection at $x = 0.5$ mm from flaw

(e)

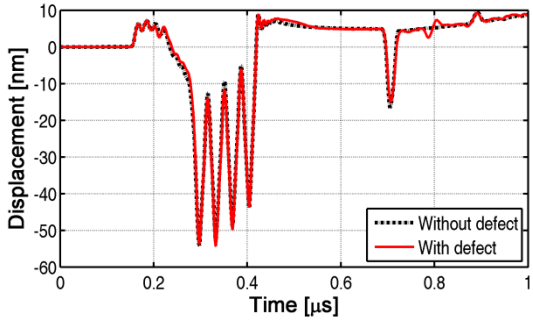

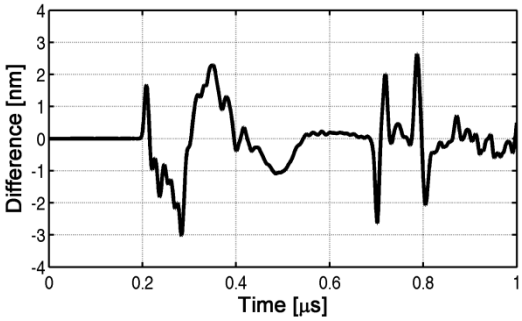

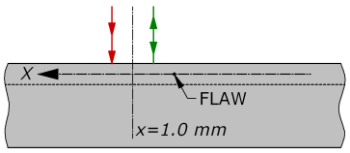

Inspection at $x = 1.0$ mm from flaw

(f)

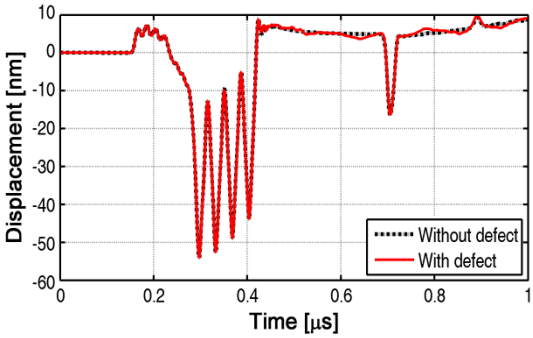

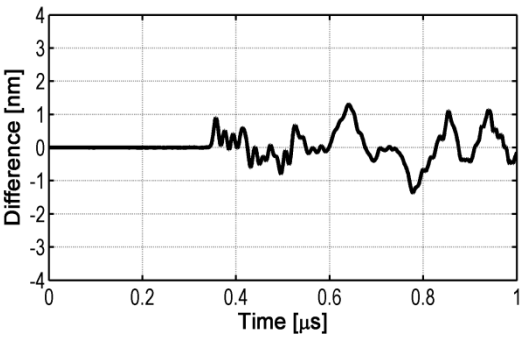

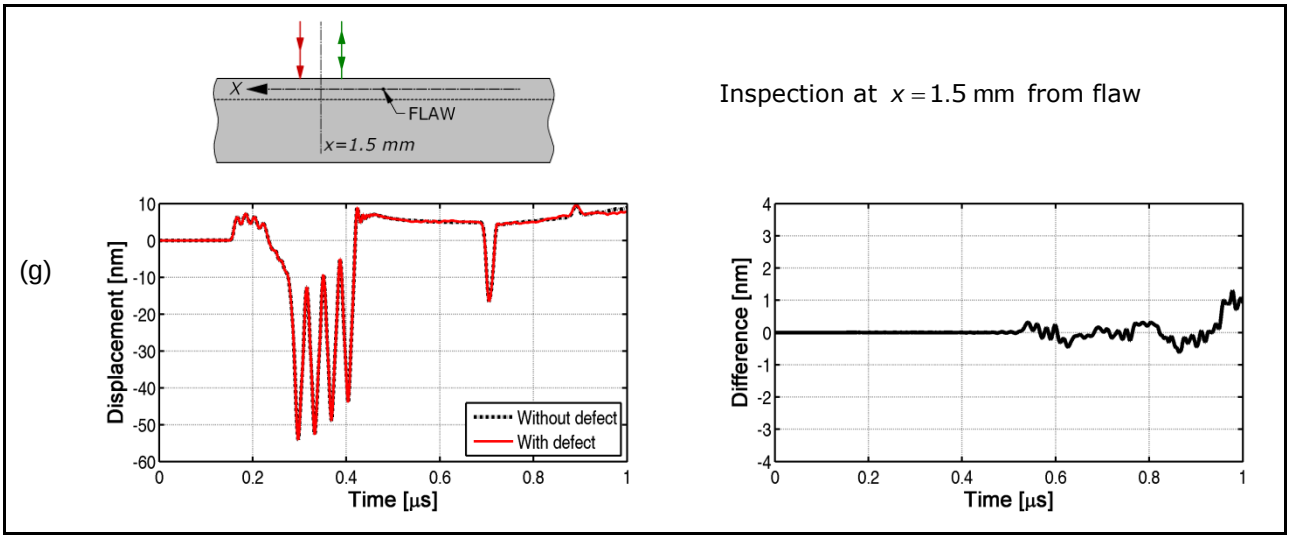

Figure 54 – Comparison between the displacement simulated in the model without defect and each displacement collected by the seven simulations in the model with the defect, developed across the flaw with increment of 0.5 mm. Multi-linear source.

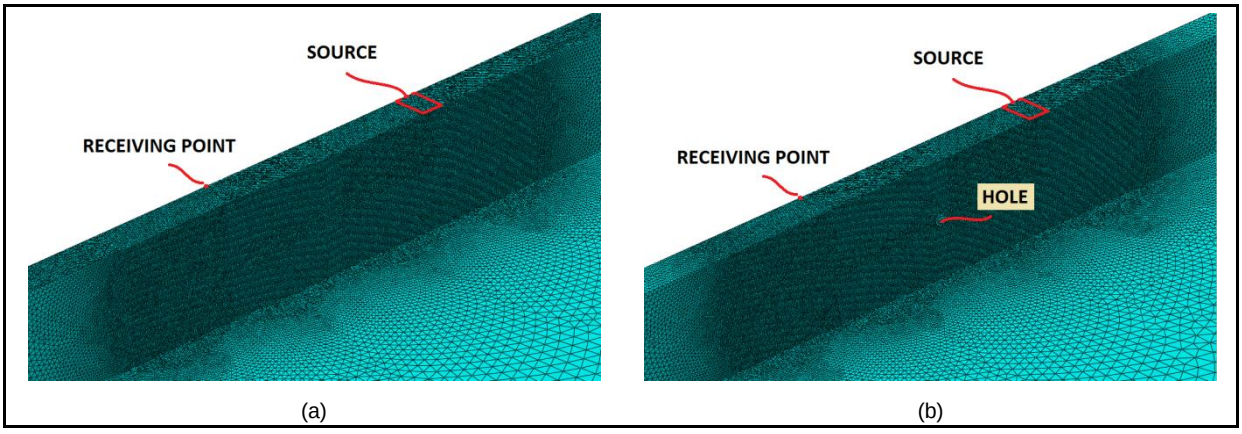

Figure 553 – Particular of the meshed model without defect (a) and of the model with the hole (b).

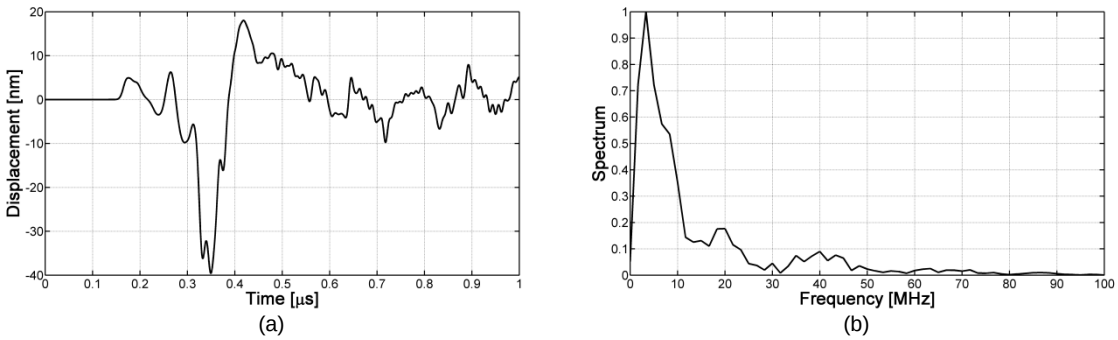

Figure 56 – Displacement collected at the receiving point in the 3D standard model (a) and its frequency spectrum (b).

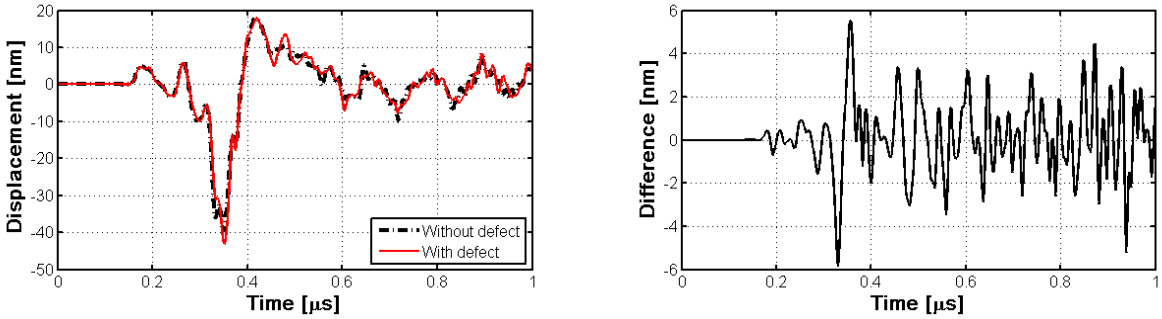

Figure 57 – Comparison between the displacement simulated in the 3D model without defect and the displacement collected in the model with the hole, considering the NDT system at $x = 0$ mm (see the used reference system).

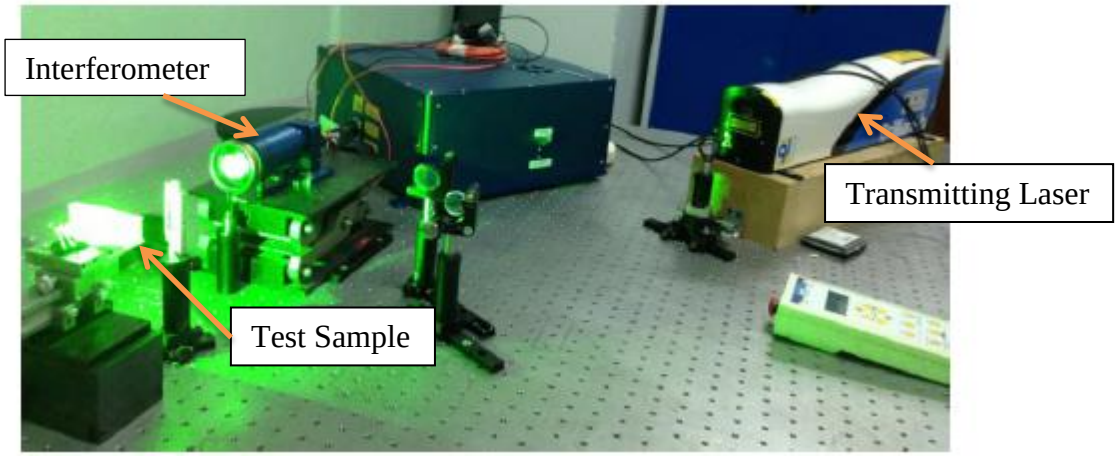

Figure 58 Laboratory set up for the laser UT

Figure 59 Interferometer Control Box

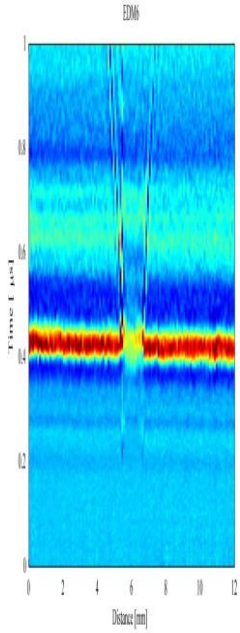

Figure 60 Indication from a reference sample flaw with the laboratory system

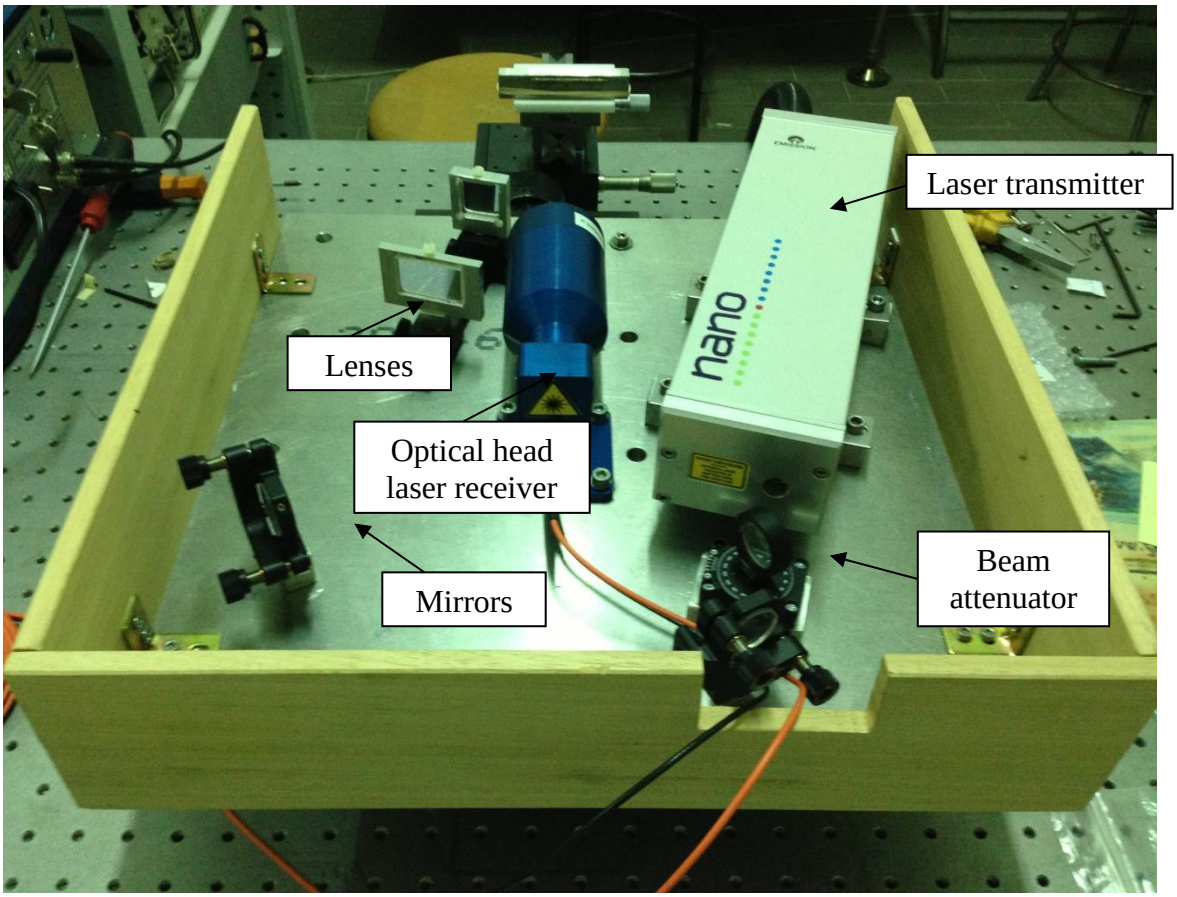

Figure 61. Components of the laser ultrasonic prototype mounted on the plate.

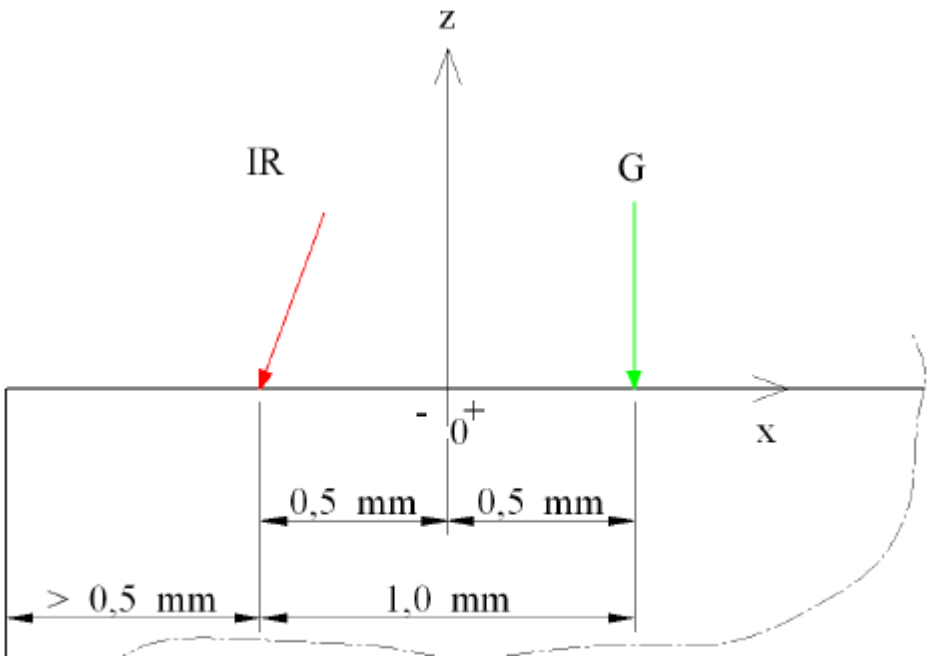

Figure 62 Positions to be set up in the inspection procedure

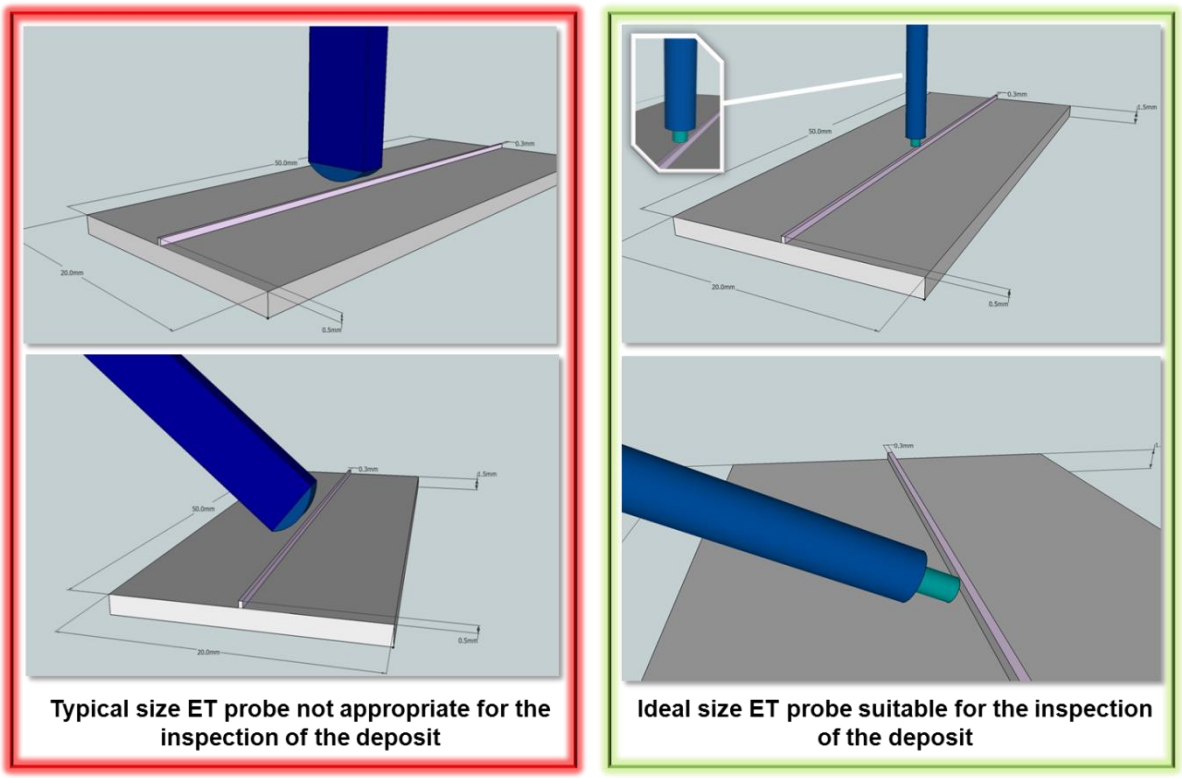

Figure 63 Sizes of eddy current probe and deposit sizes

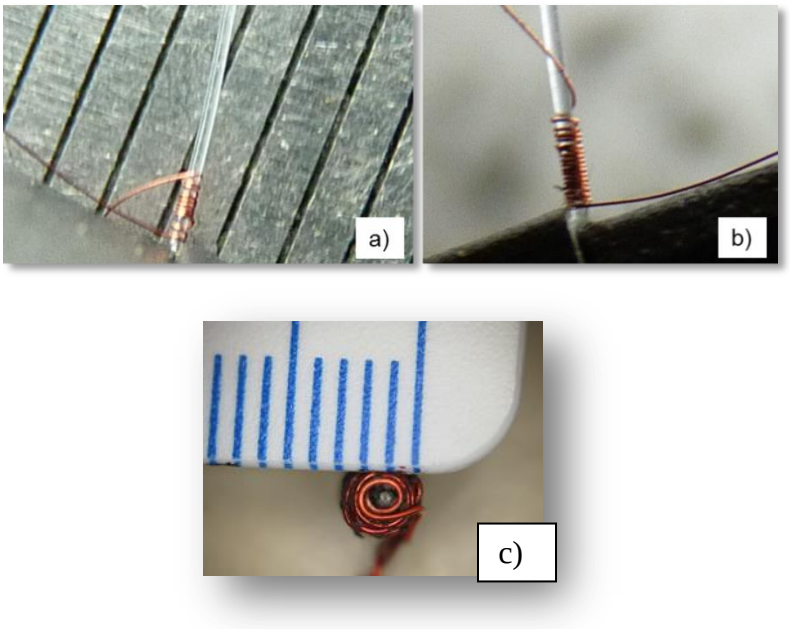

Figure 64 (a,b) Small coil mounted on Nylon Brush Bristle (scale is mm) **(c)** Tapered winding

	2MHz	1MHz	500KHz
Tapered Probe	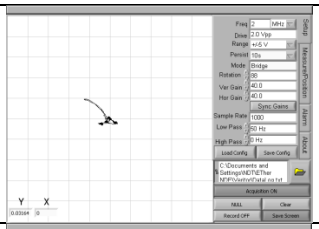	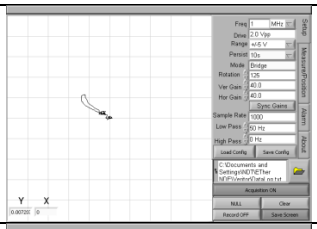	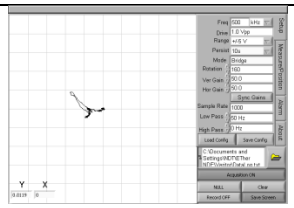
Commercial Probe	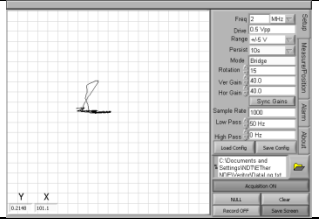	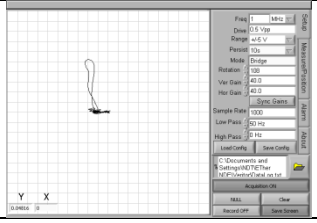	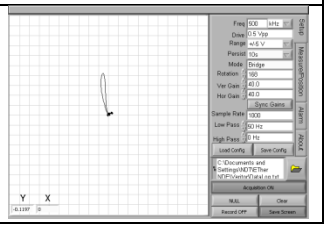

Figure 65 Results from different probes and different frequencies

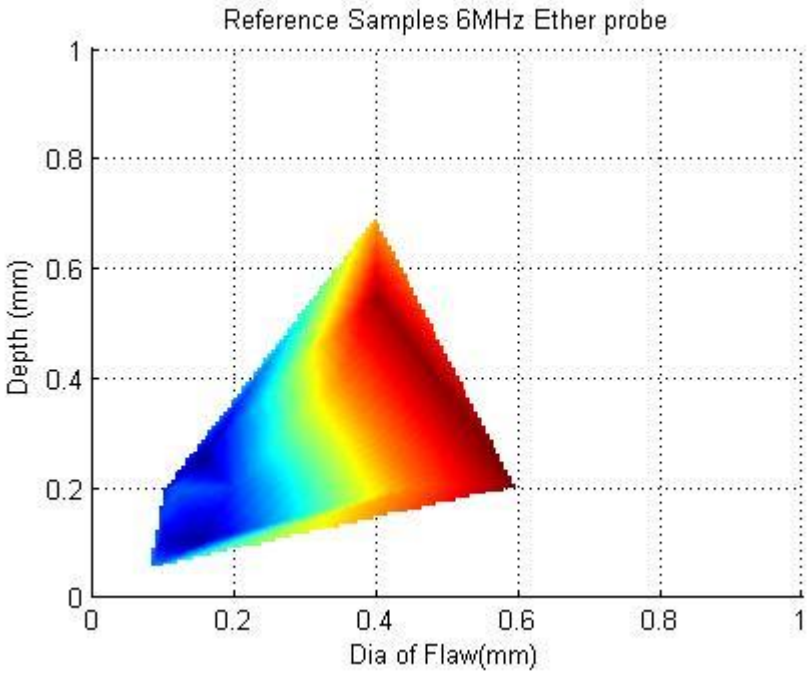

Figure 66 Results at 6MHz using the Ether 6Mhz probe

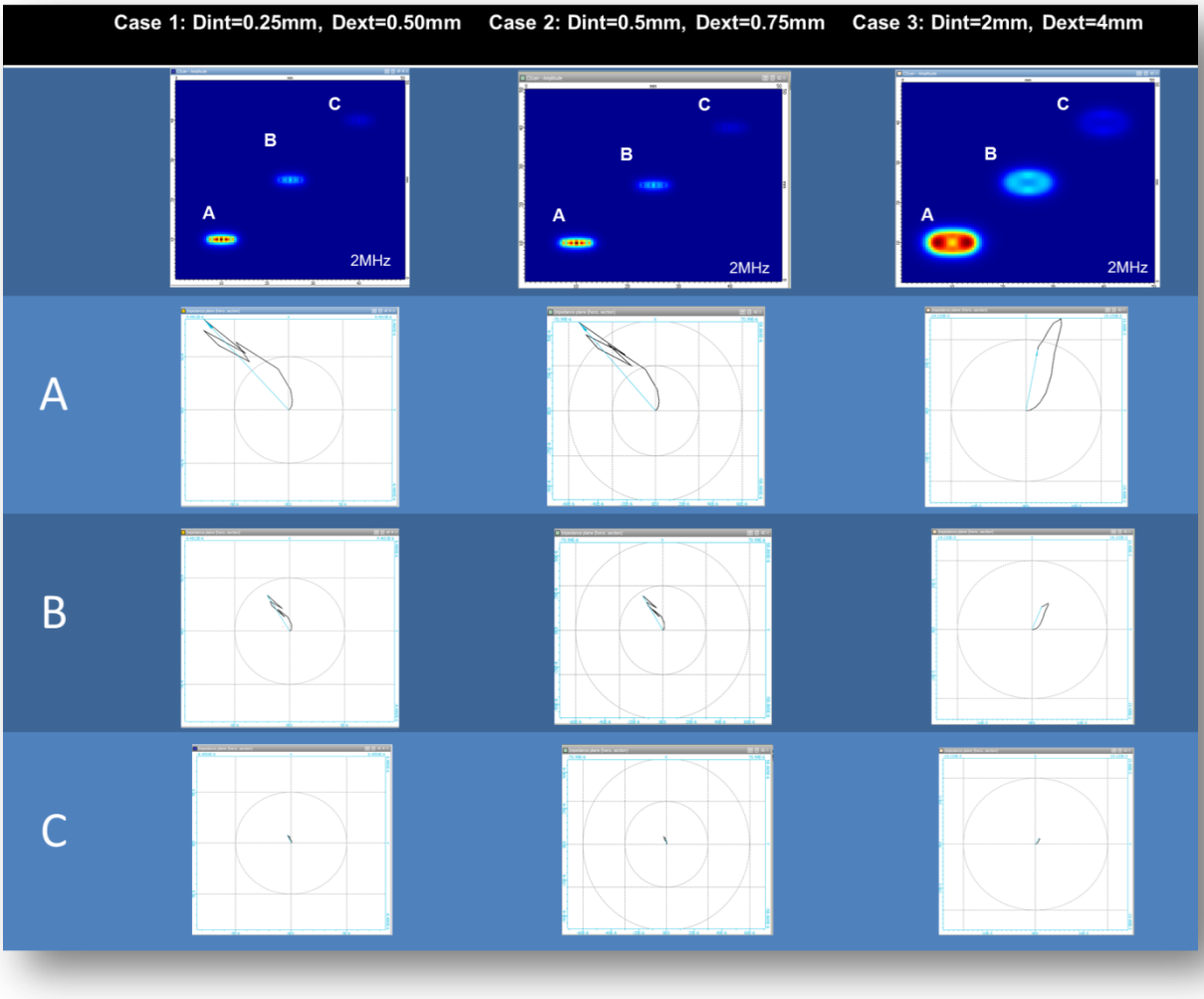

Figure 67 Results from the modelling experiments performed at 2MHz for the three cases investigated.

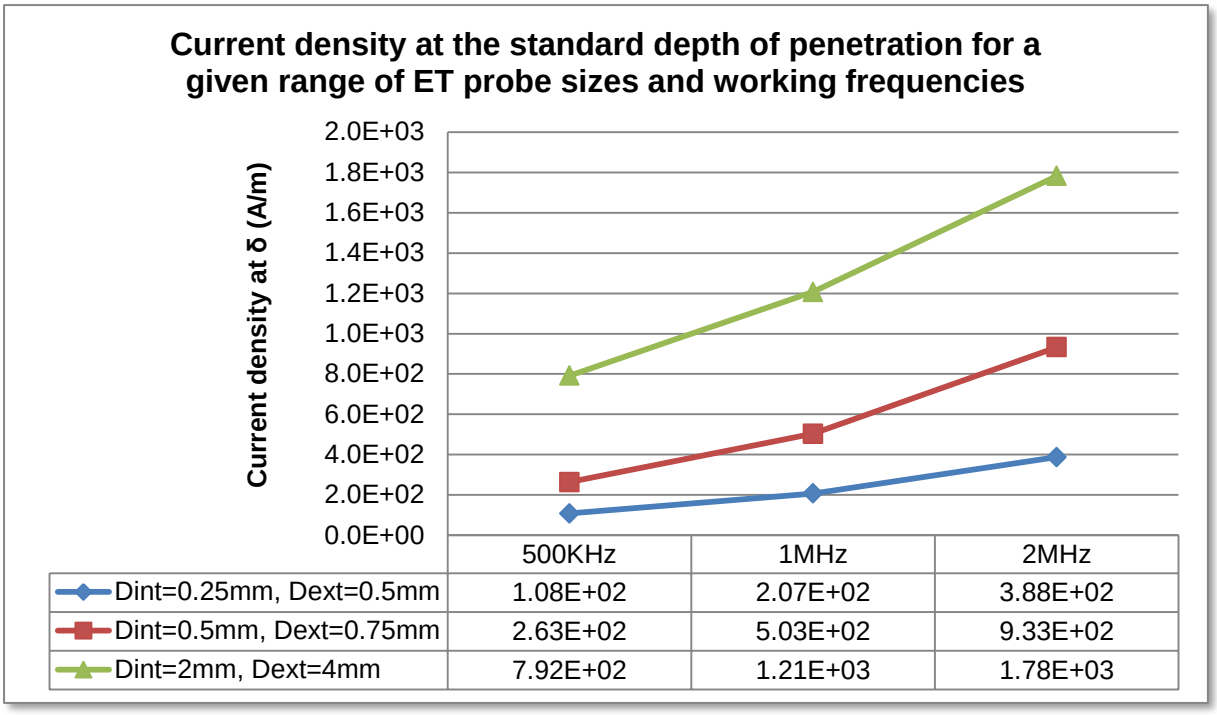

	500KHz	1MHz	2MHz
Dint=0.25mm, Dext=0.5mm	1.08E+02	2.07E+02	3.88E+02
Dint=0.5mm, Dext=0.75mm	2.63E+02	5.03E+02	9.33E+02
Dint=2mm, Dext=4mm	7.92E+02	1.21E+03	1.78E+03

Figure 68 Variation of the current density at the standard depth of penetration for the 3 simulated cases.

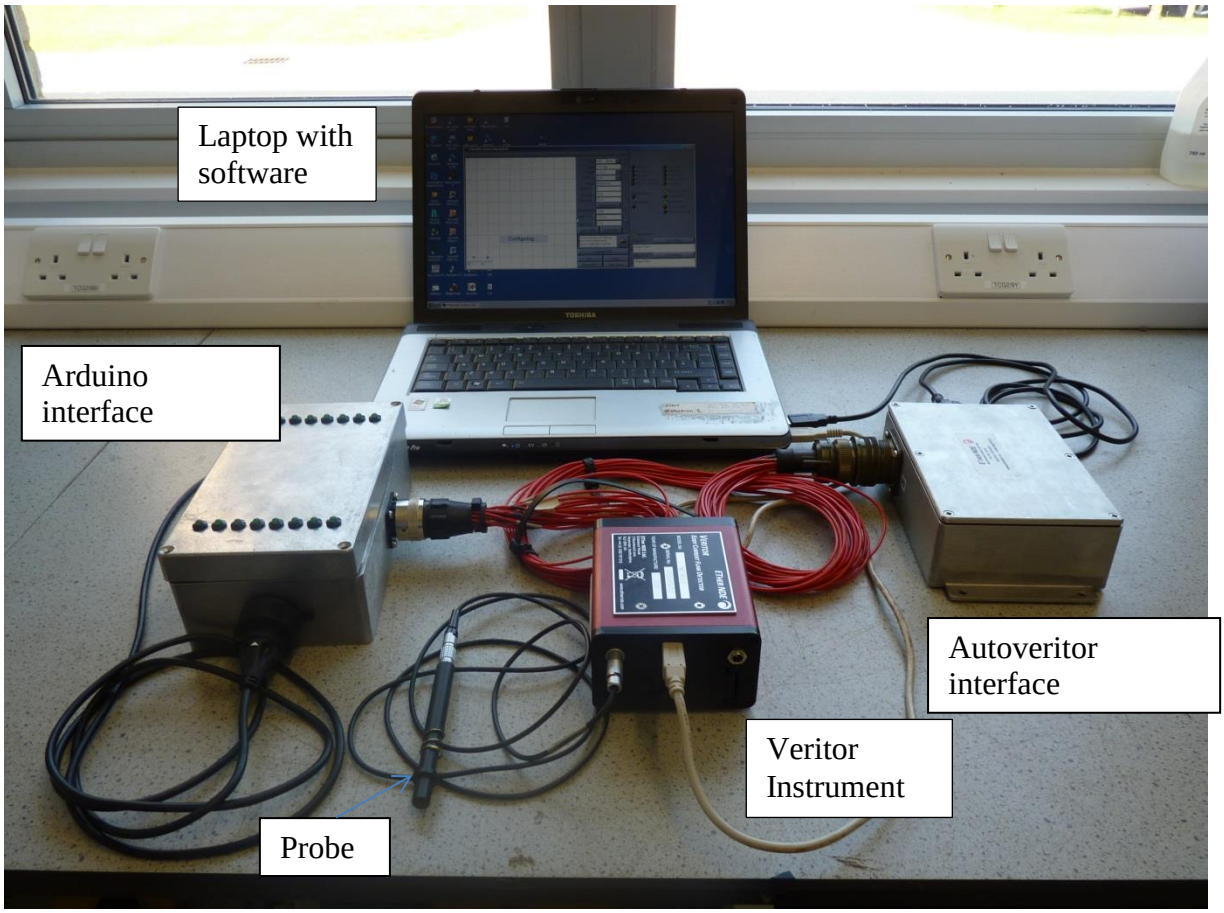

Figure 69 Components of complete eddy current system

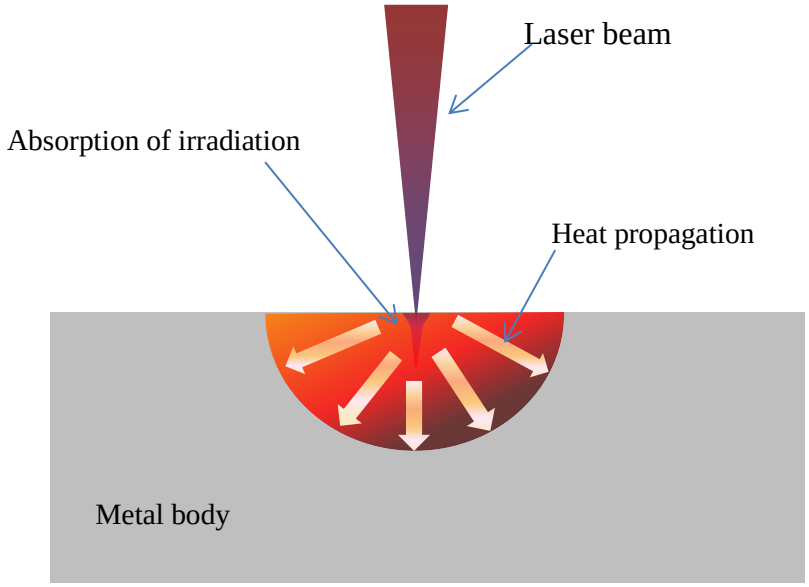

Figure 70. Heat propagation in a laser irradiation heated metal body**.**

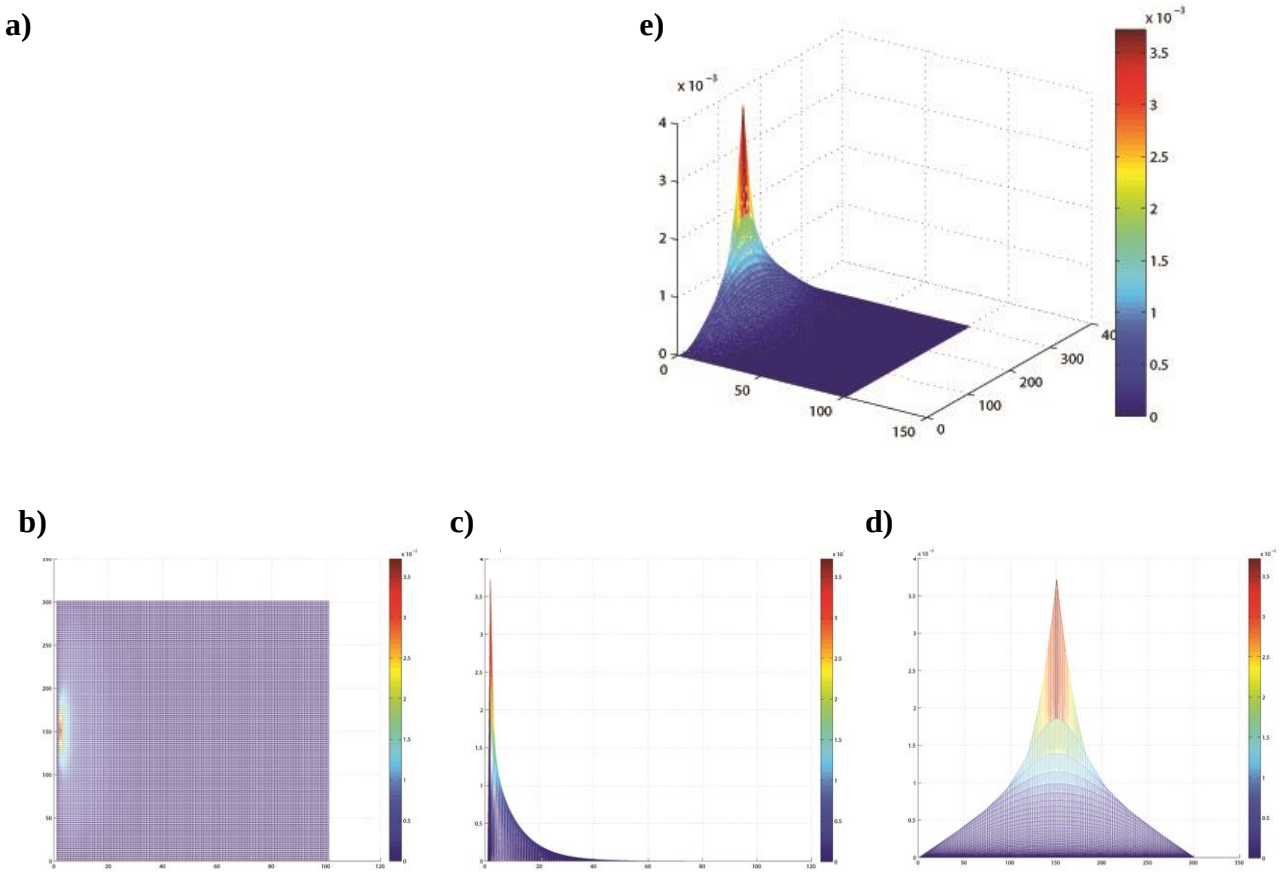

Figure 71 a) Heat content across 300µm LPD profile, 5ms after the laser pulse impact. b) The 3D temperature curves, plotted for time, temperature and position and (c), (d) and (e) present heat content over the line profile, heat change over time and heat change over location.

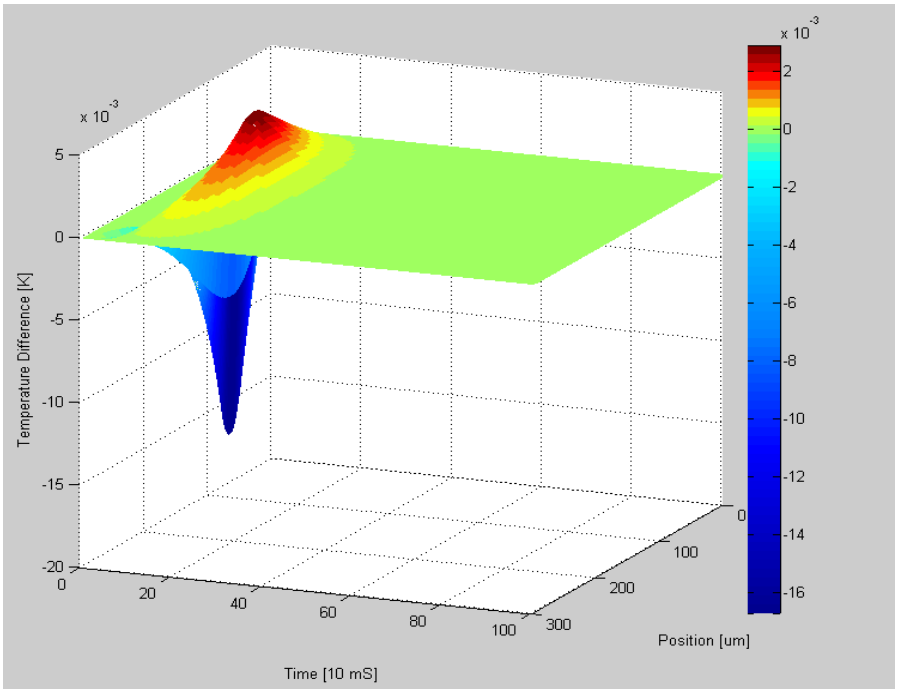

Figure 72. Temperature difference showing non-defective heat content profile subtracted from defective plotted against time, temperature and position

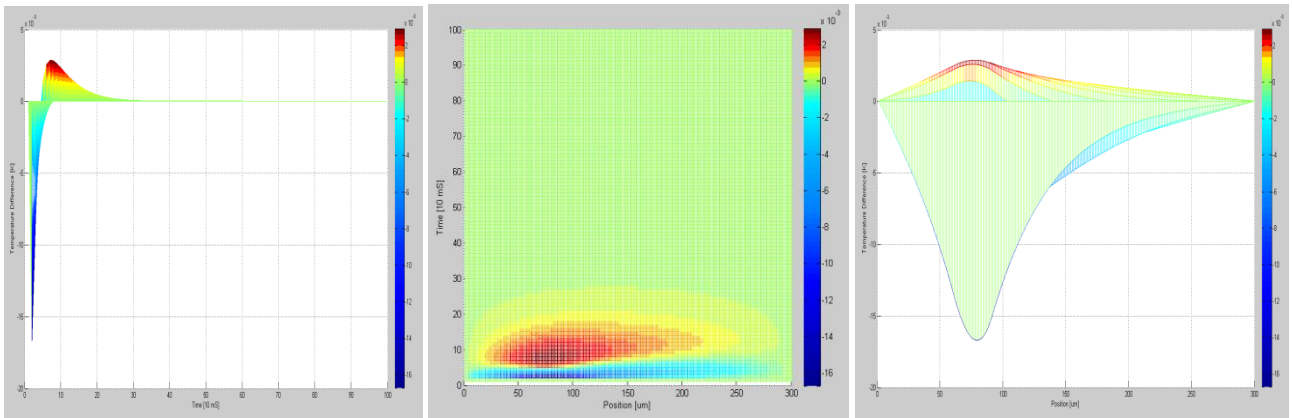

(a) (b) (c)

Figure 73: Predicted variance of heat content across LPD track (defective – non-defected side) showing a) aggregate temperature difference over time b) temperature difference across the entire LPD (0 - 300 µm, the incident laser impacts at 150 µm) over time
c) temperature range over the LPD profile

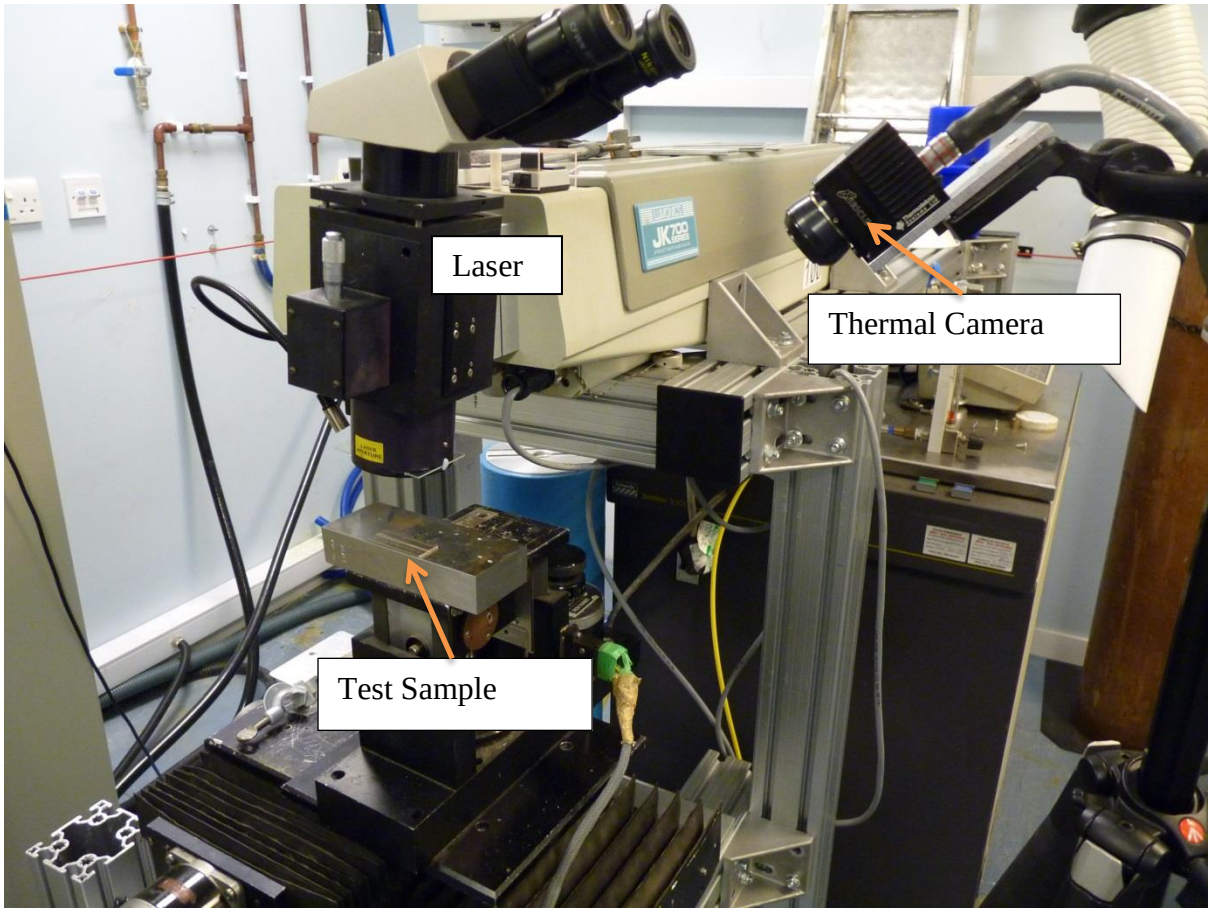

Figure 74 Initial Set Up for Thermography Inspection

Figure 75 Recording of laser pulse striking surface at 20mSec intervals during and after laser pulse

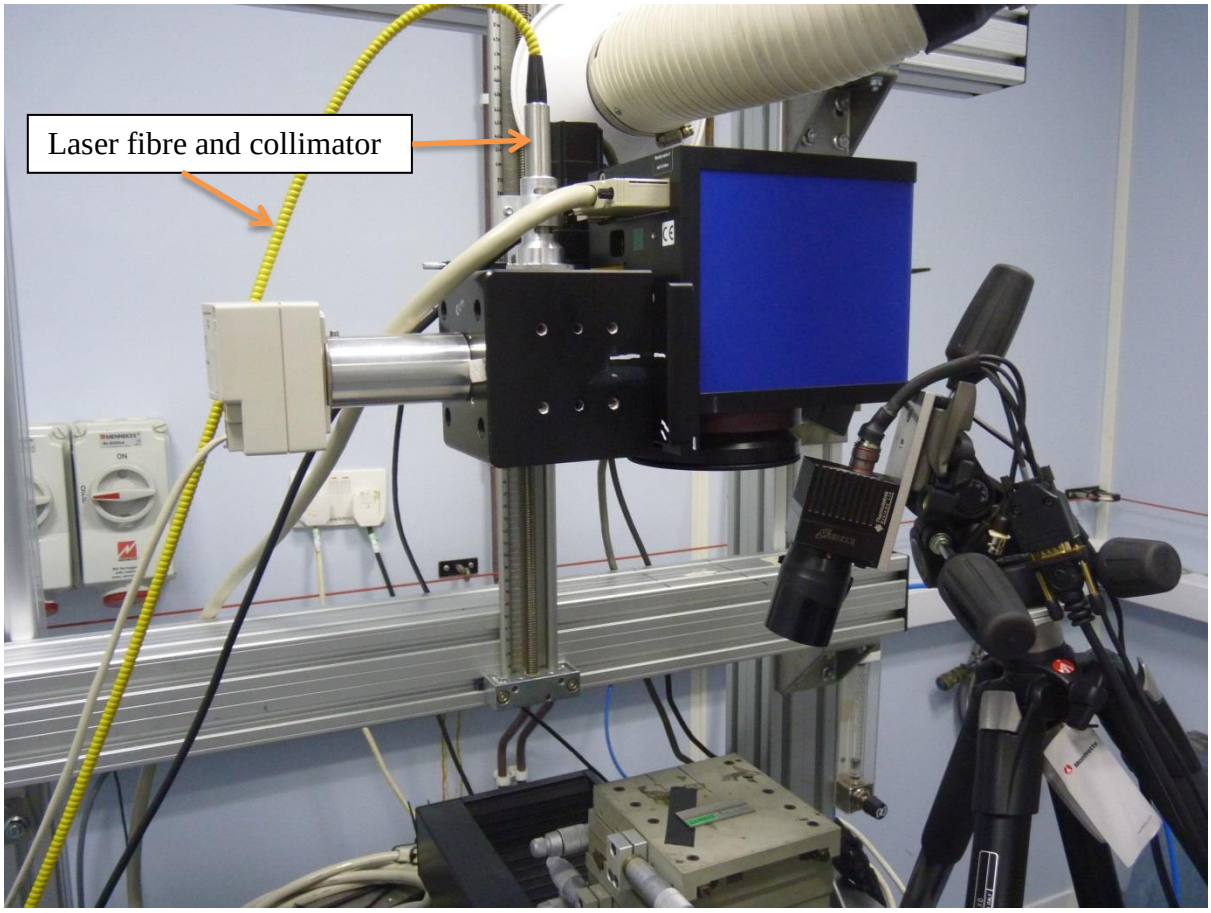

Figure 76 Second arrangement of laser thermography system

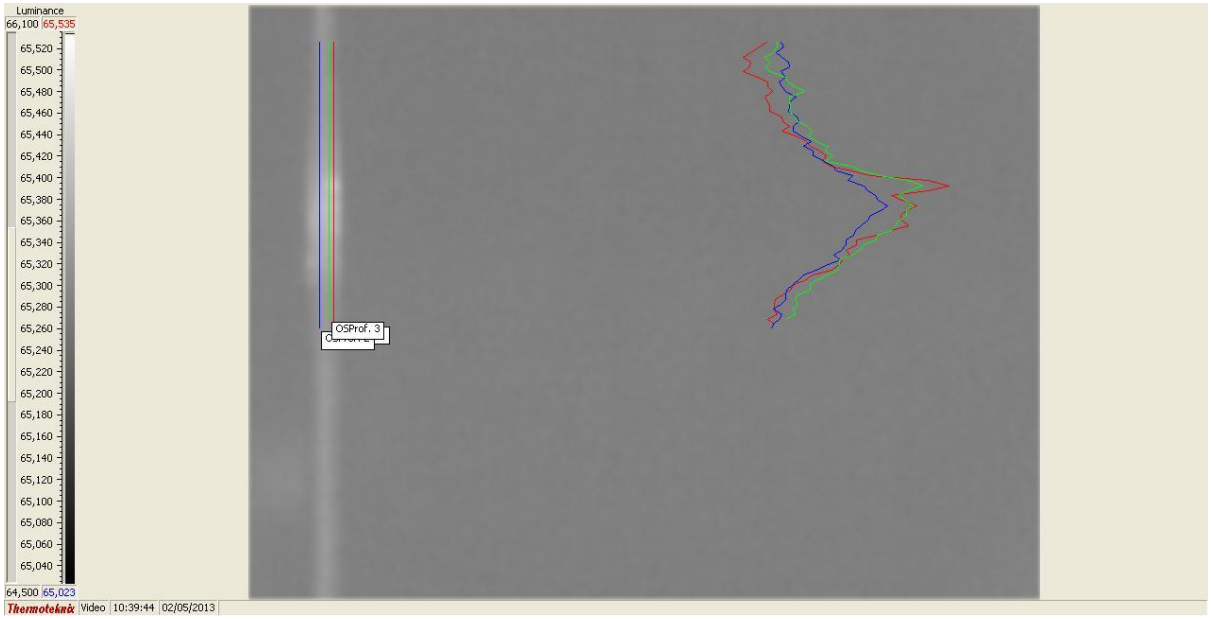

Figure 77 Zoomed image of flaw with profile using the Thermagram software

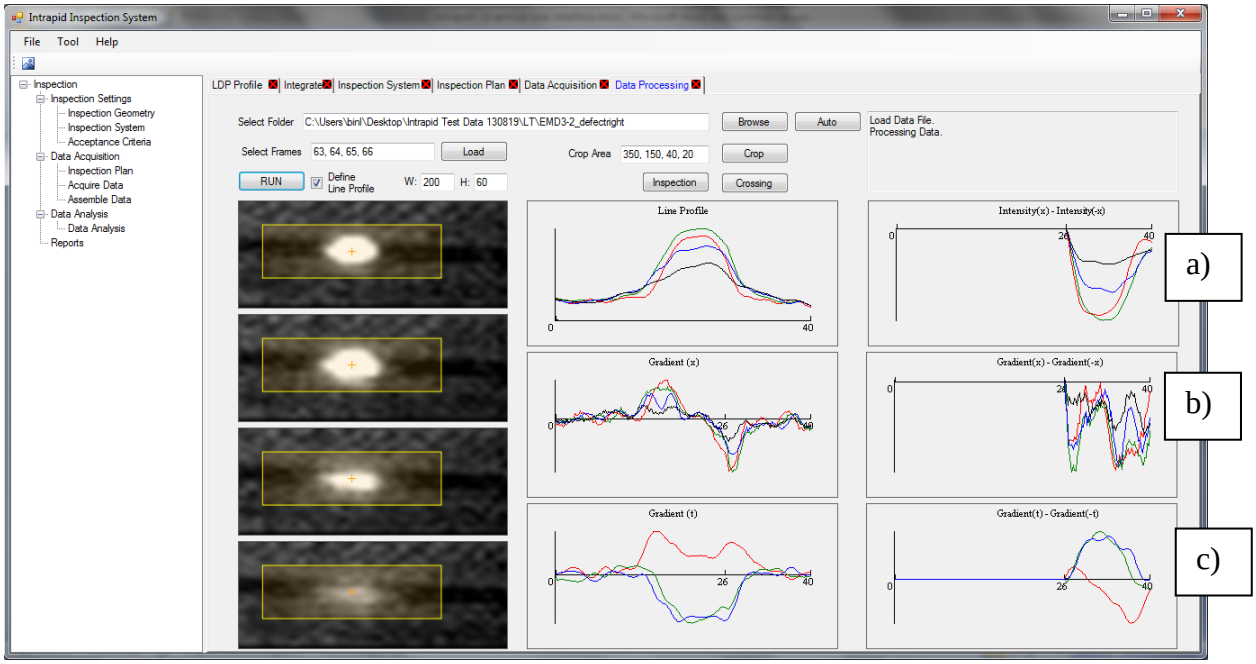

Figure 78: The INTRAPID laser Thermography GUI displaying the four frames to be analysed and a) Line Profile Analysis, b) Spatial Derivative Analysis and c) the Time Derivative Analysis

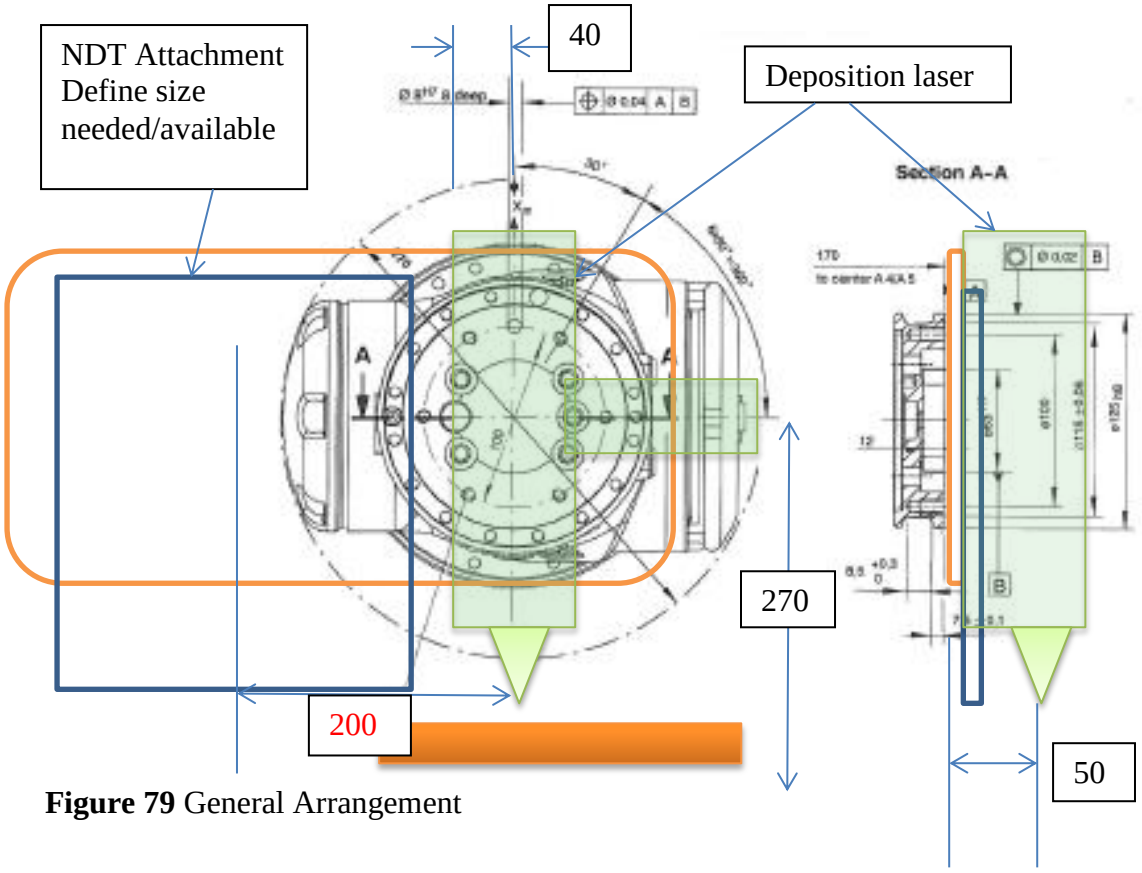

Figure 79 General Arrangement

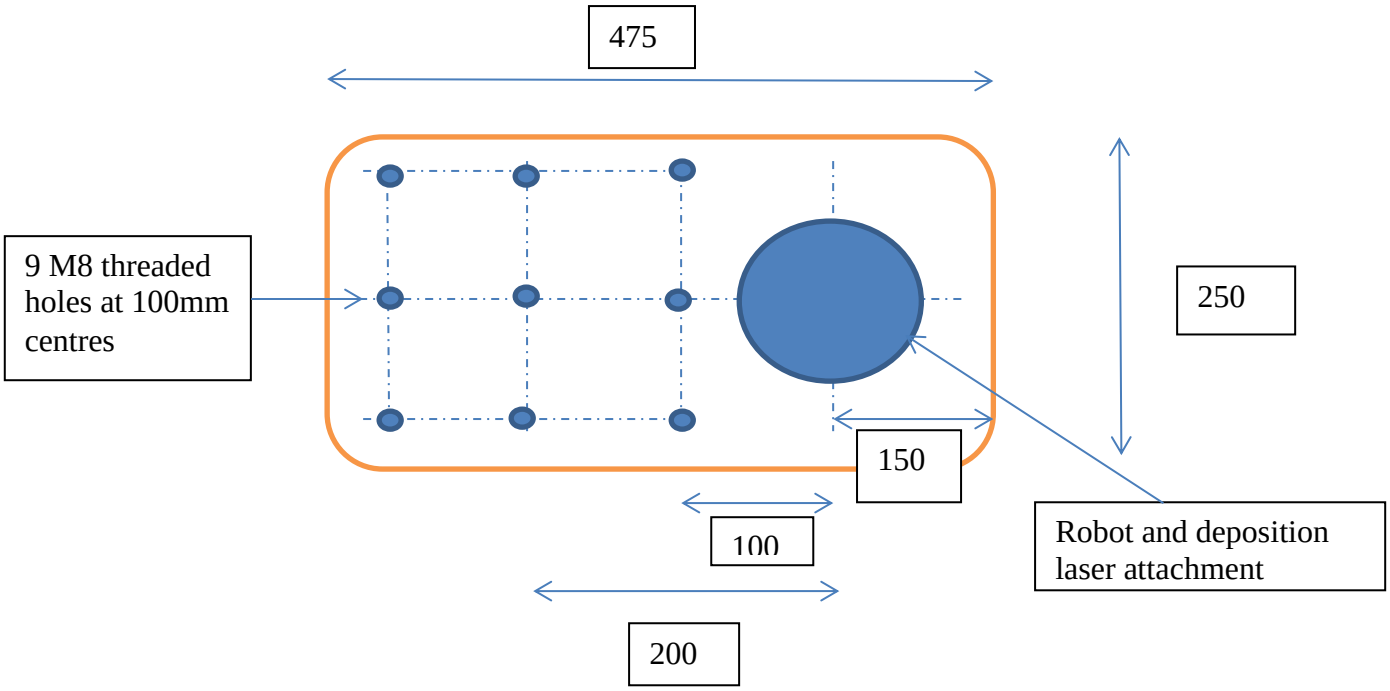

Figure 80 Robot Plate (10mm Aluminium)

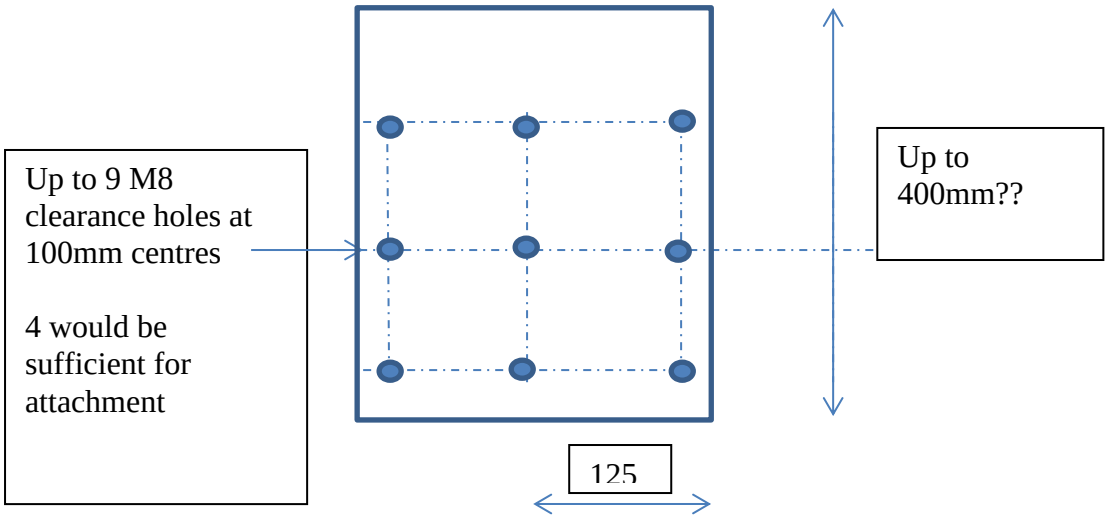

Figure 81 NDT Plates (excluding details for equipment holders etc)

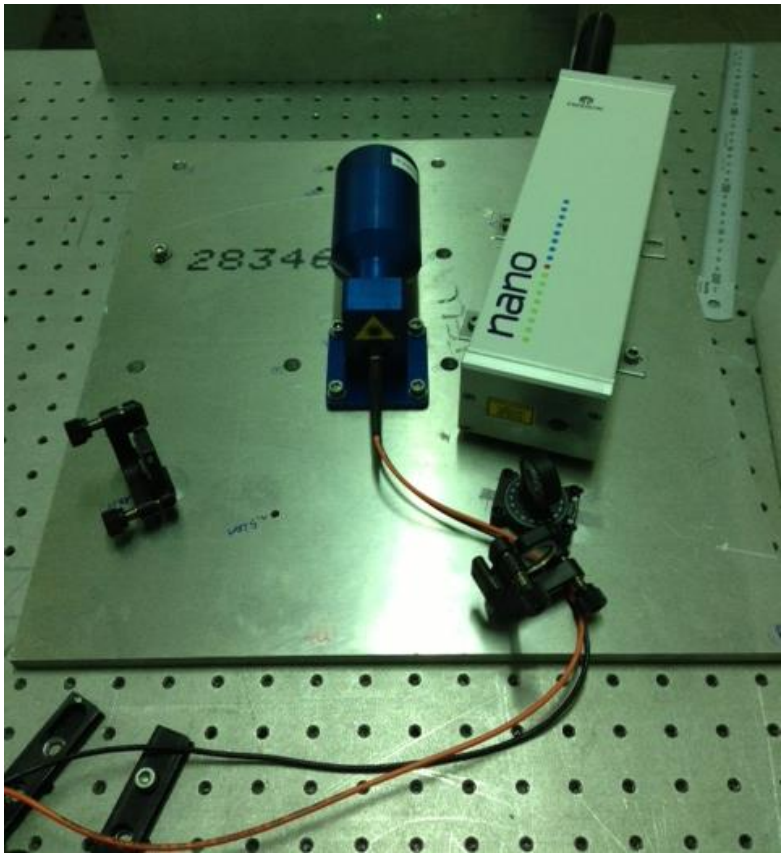

Figure 82 Laser UT System under construction on adaptor plateInterferometer on left, transmitting t laser on right

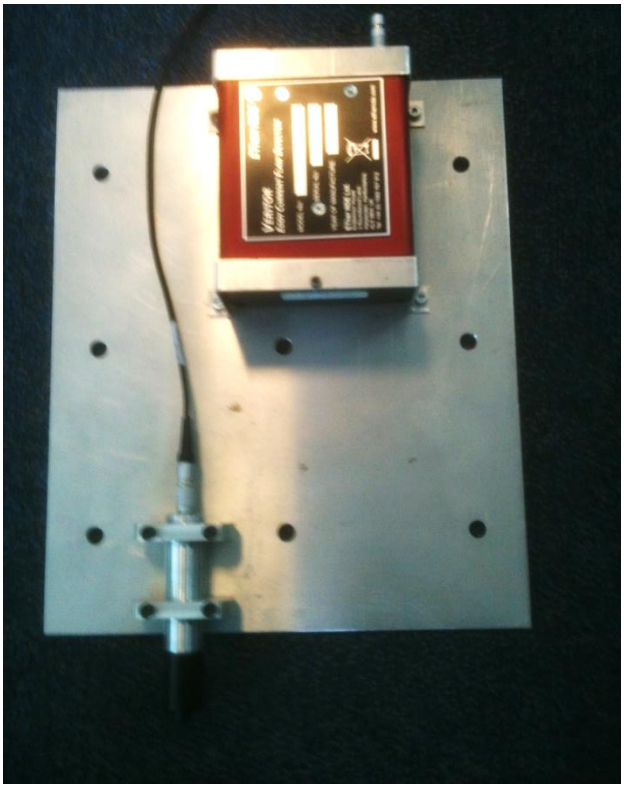

Figure 83 Eddy Current System on adaptor plate

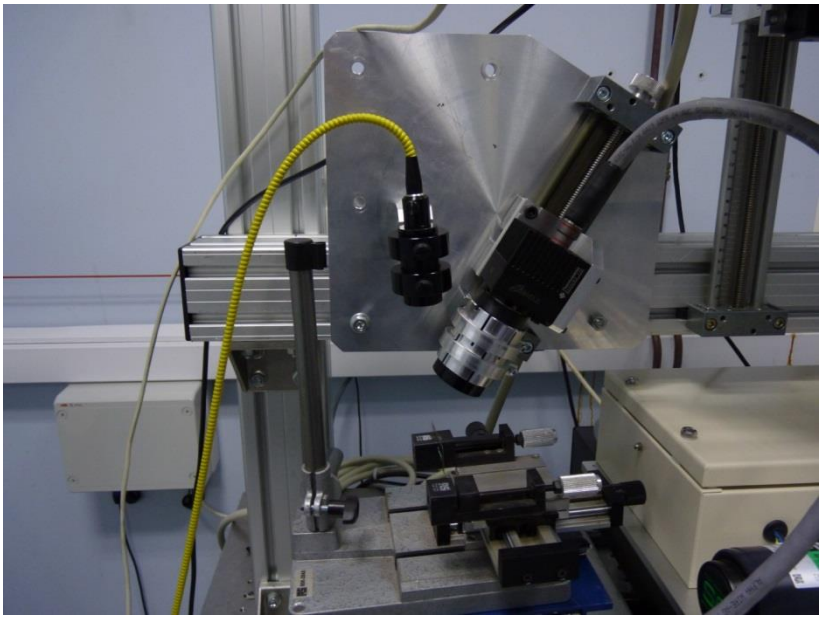

Figure 84 Laser Thermography System mounted on plate (laser on left, camera on right)

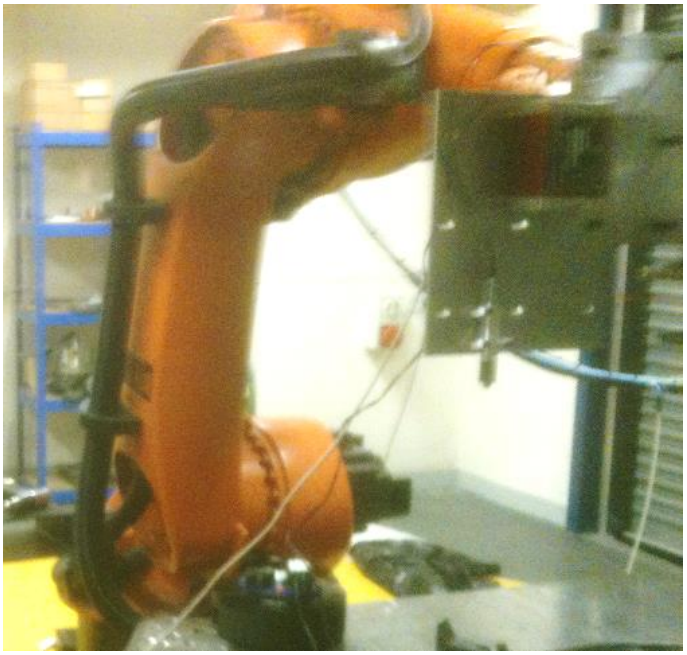

Figure 85 Eddy Current System Mounted on Robot

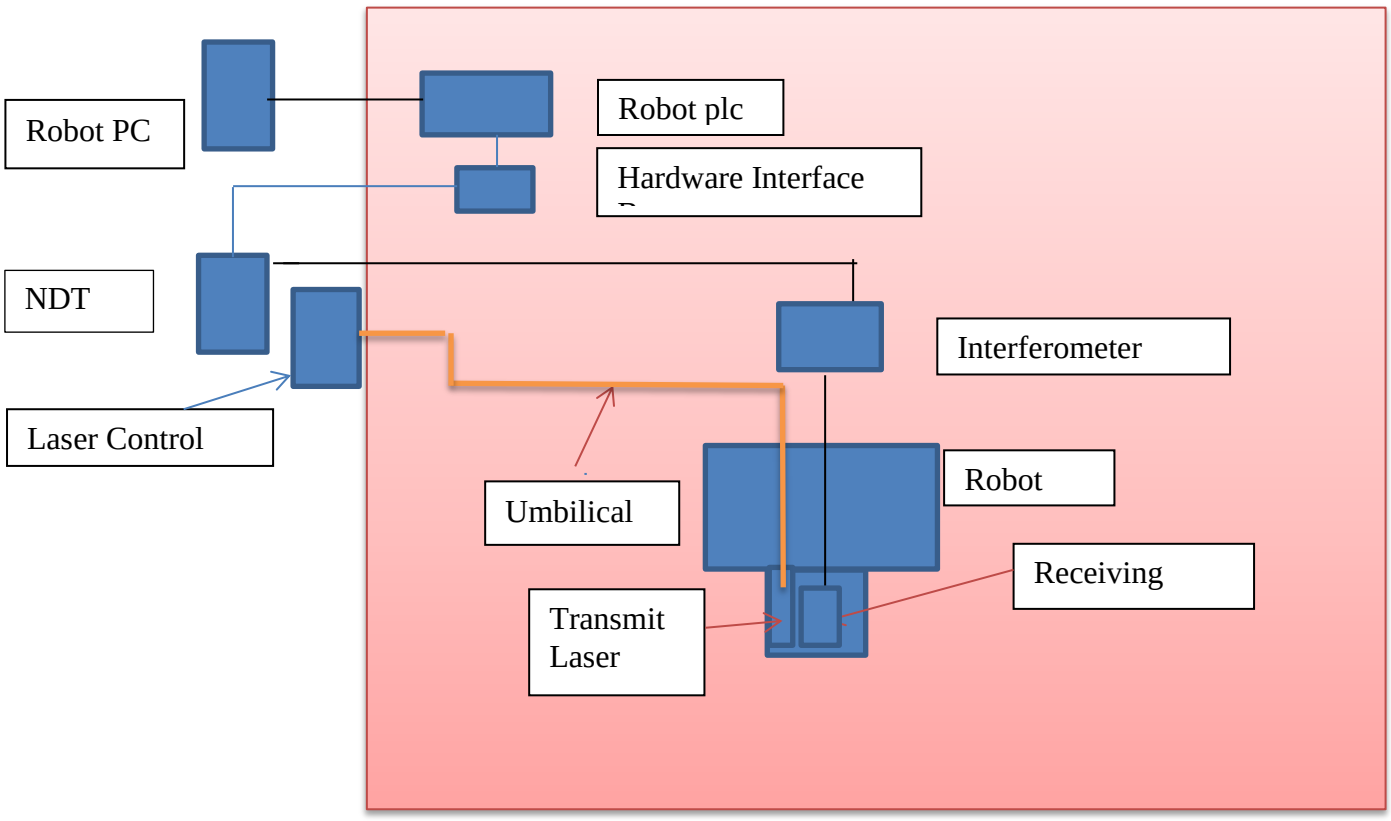

Figure 86 Schematic of Laser Ultrasonic System

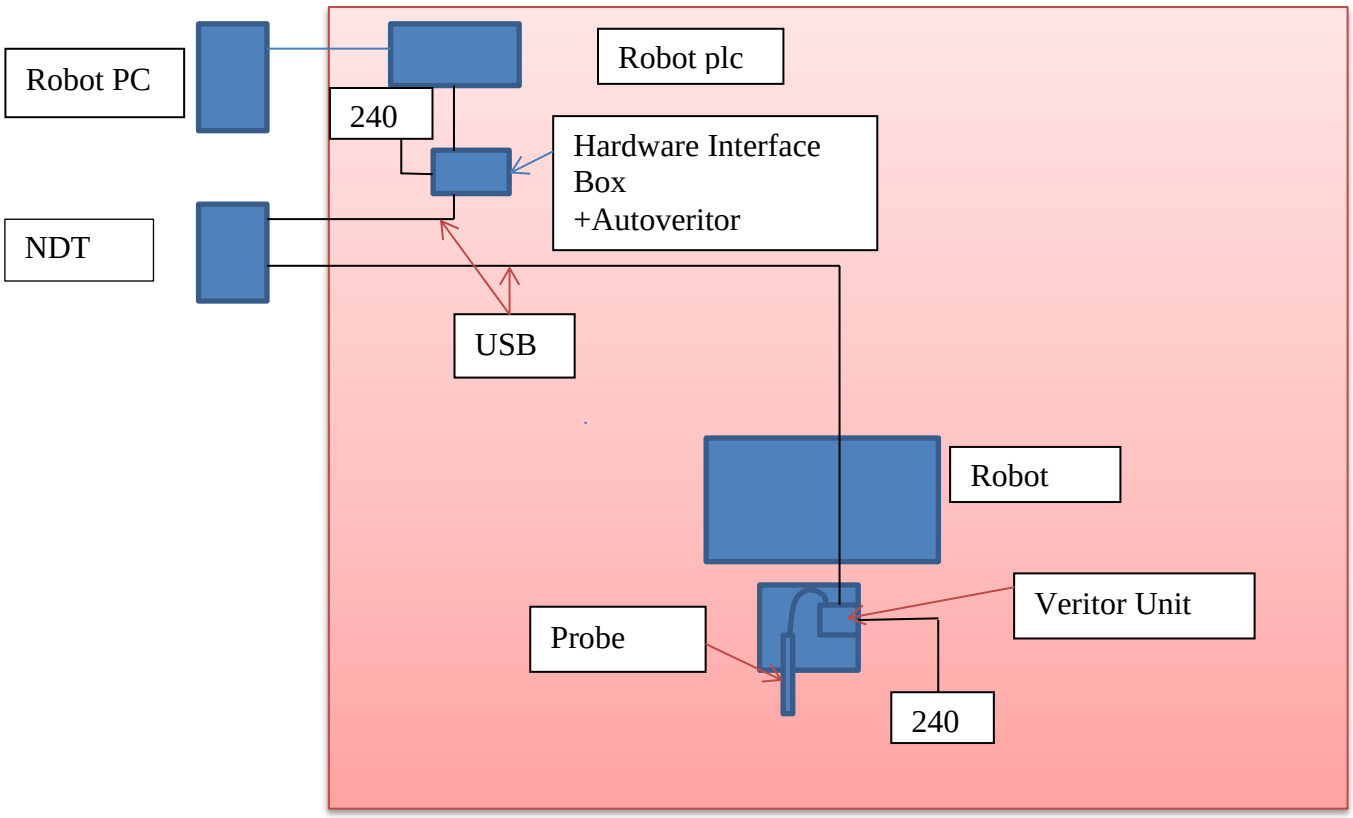

Figure 87 Eddy Current interconnections schematic (USB leads 15m and 5m)

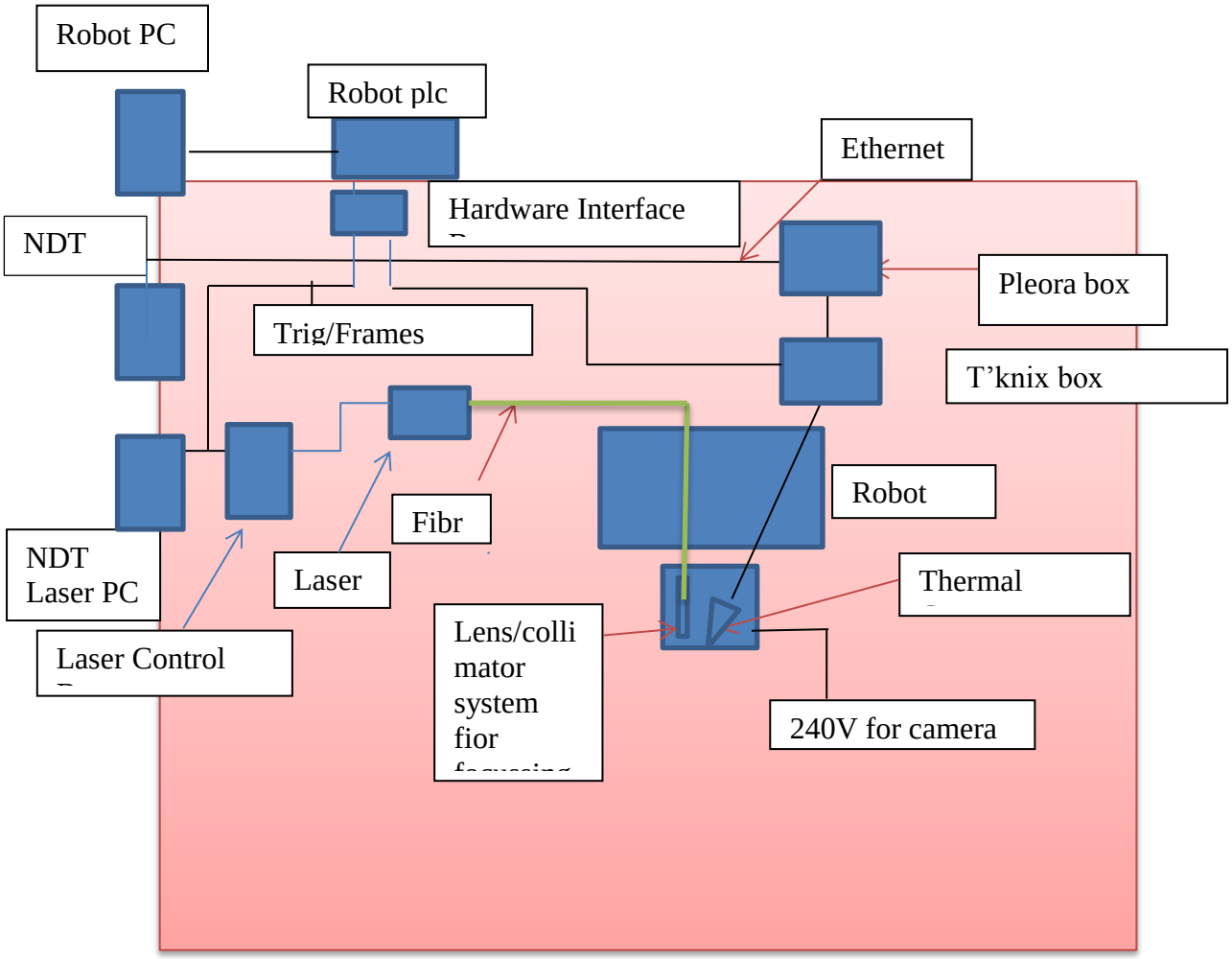

Figure 88 Schematic for Laser Thermography

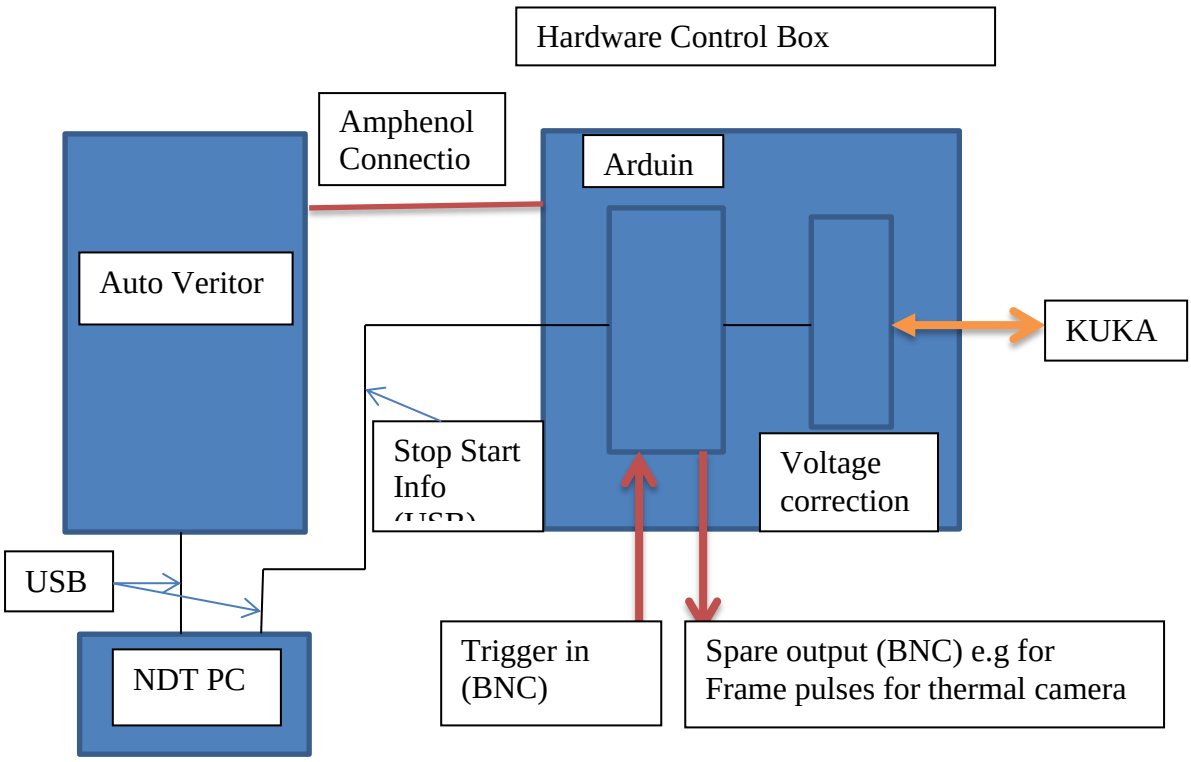

Figure 89 Detail of Hardware Interface Box. The autoveritor is only connected for the eddy current system

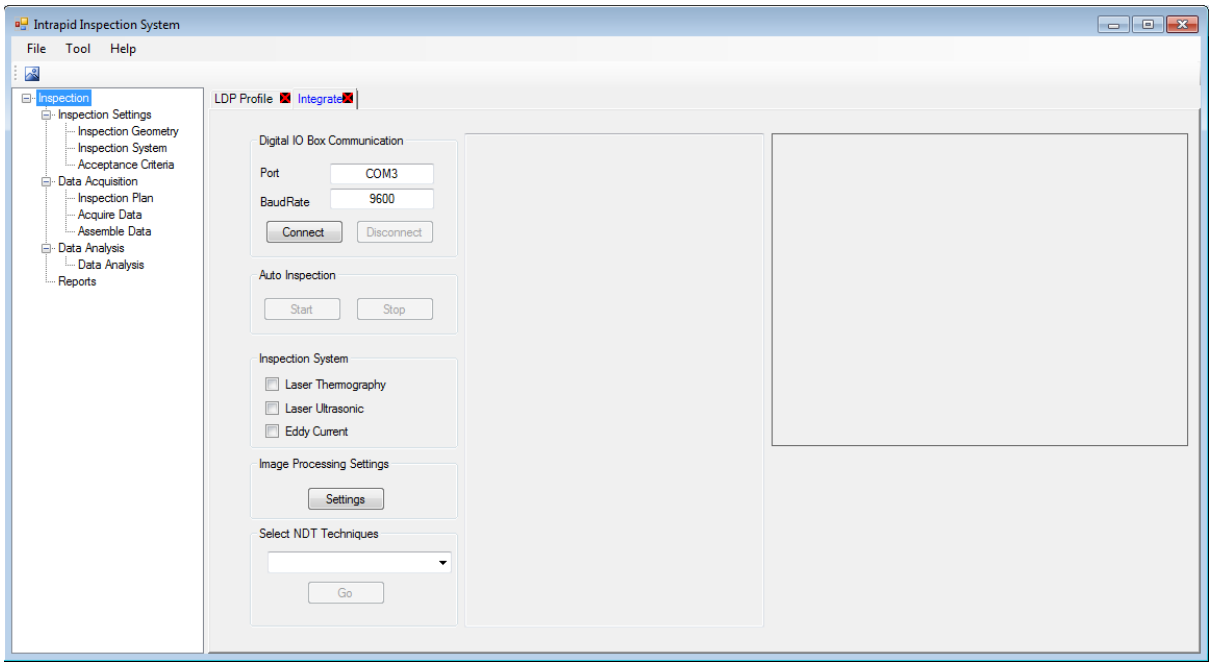

Figure 90 Initial Screen

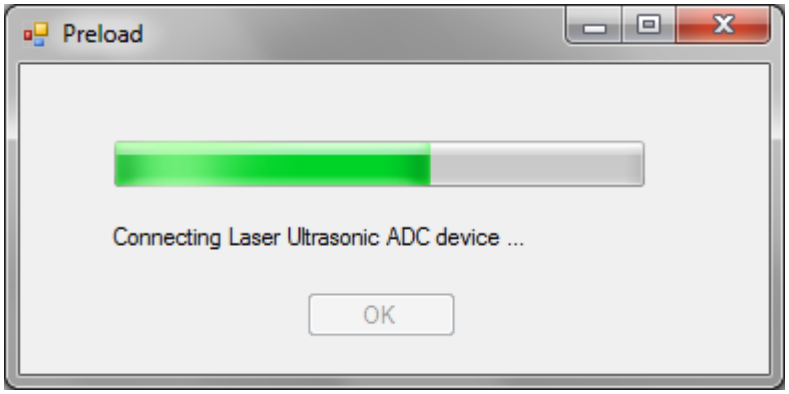

Figure 91 Connecting hardware

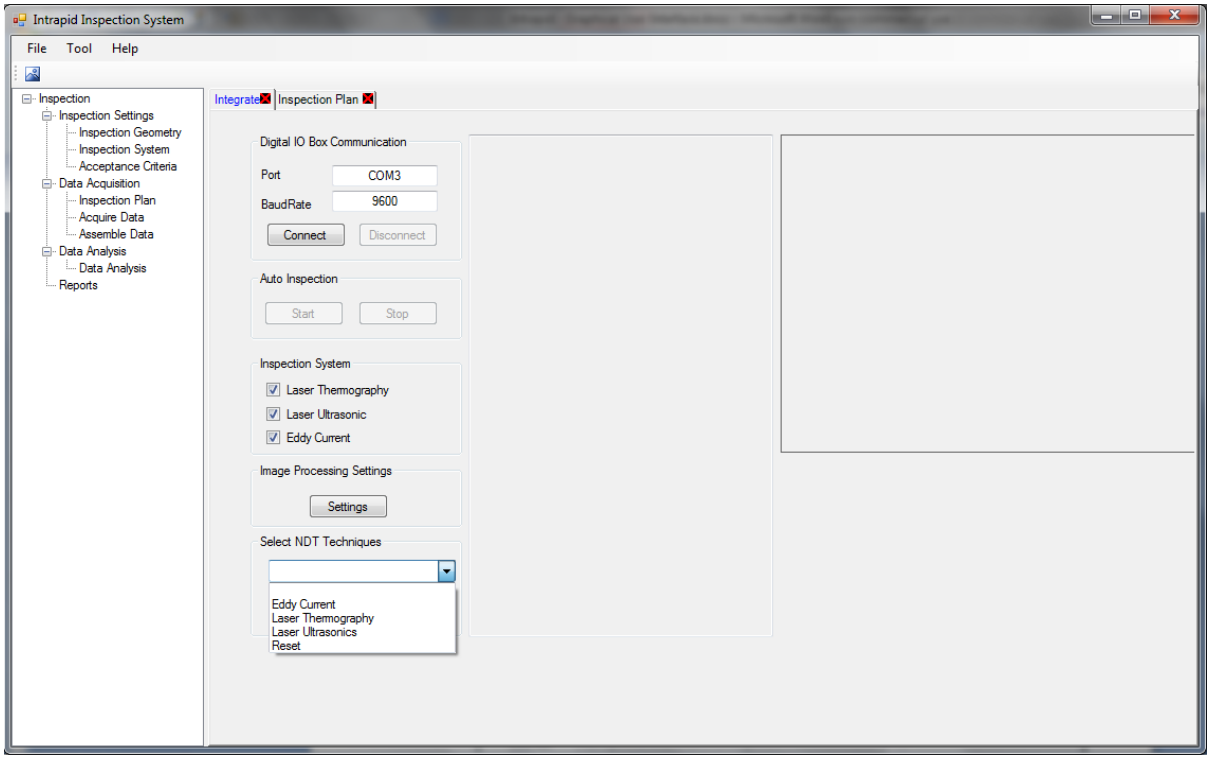

Figure 92 Selection of Inspection Options

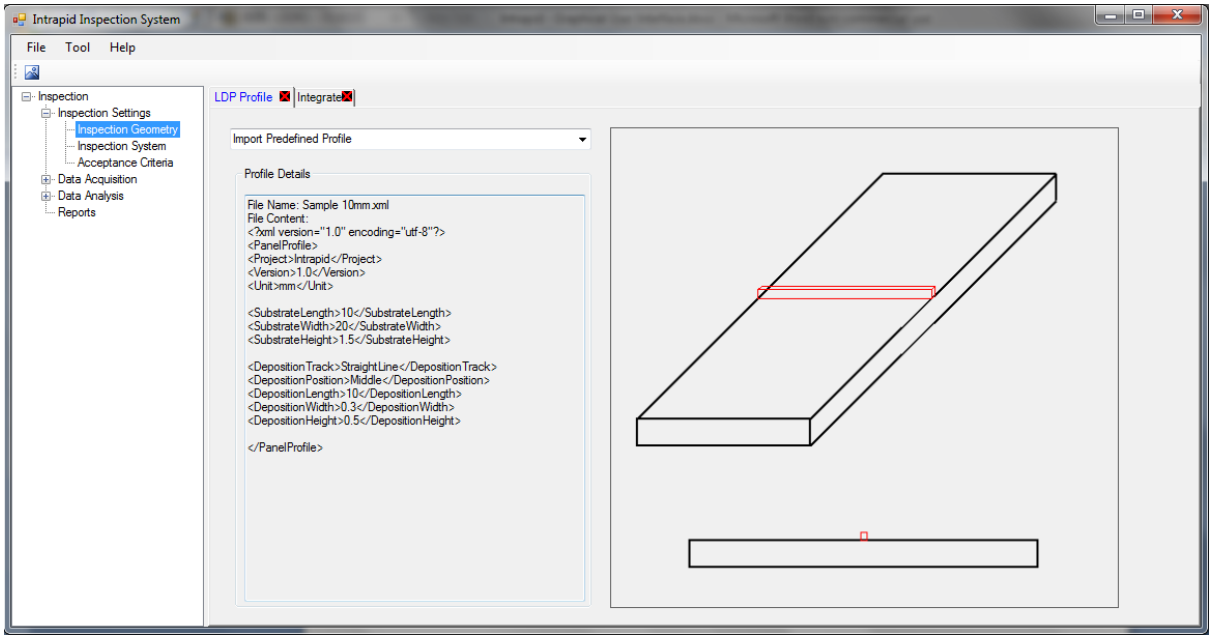

Figure 93 Importing the component geometry

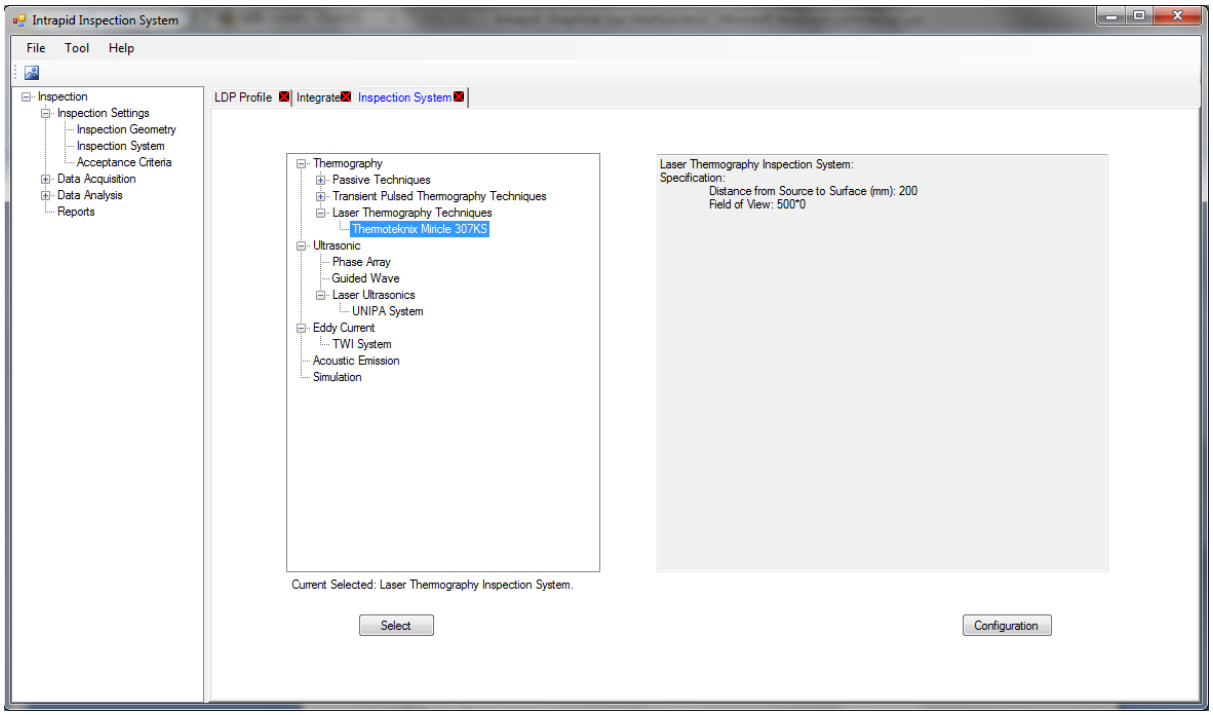

Figure 94 Selecting the Inspection Instrument parameters

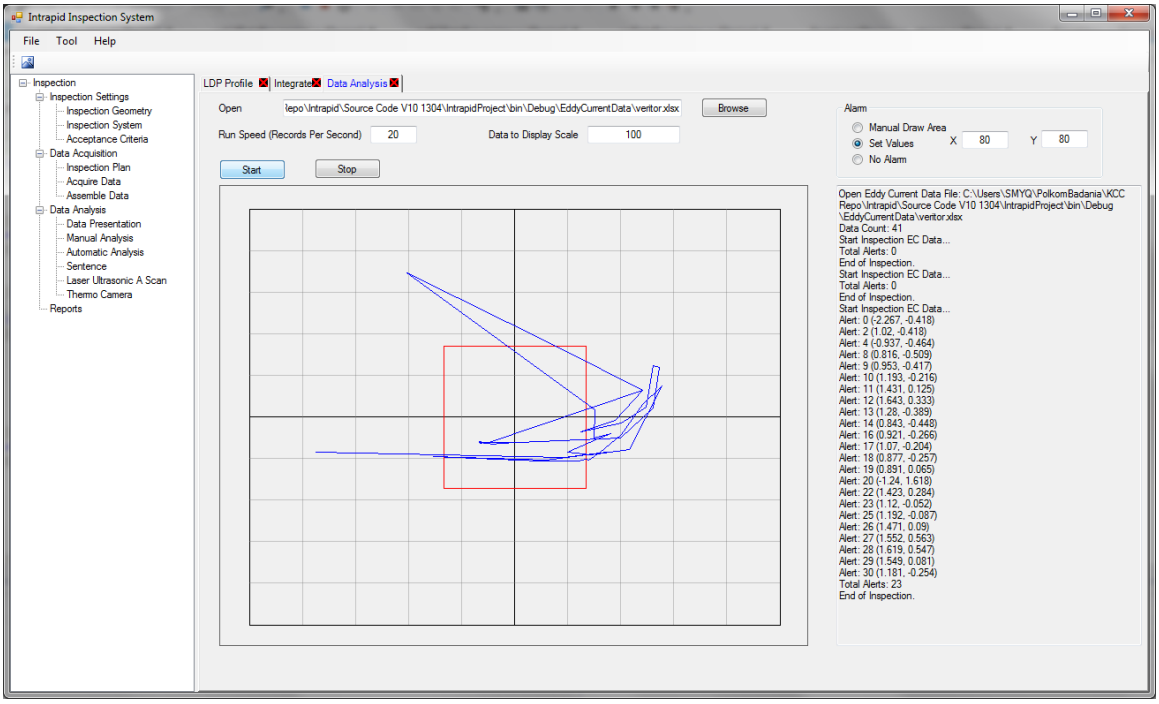

Figure 95 Recorded eddy current data showing automated defect detection region

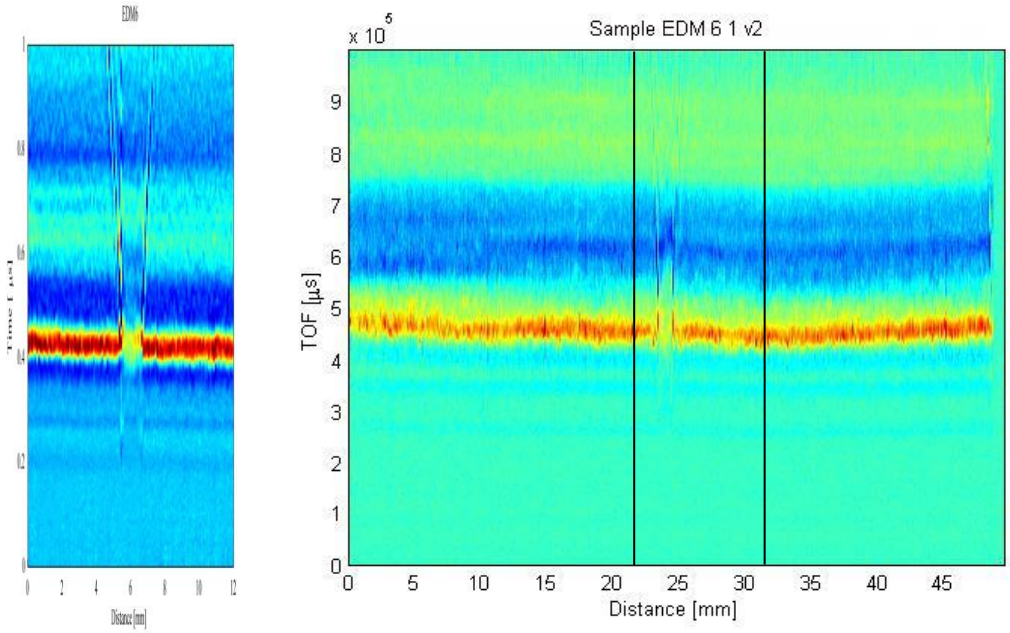

(a) (b)

Figure 96 Comparison of the 3D maps on sample EDM 6-1 between the prototype in the lab (a) and the prototype mounted on the robot (b).

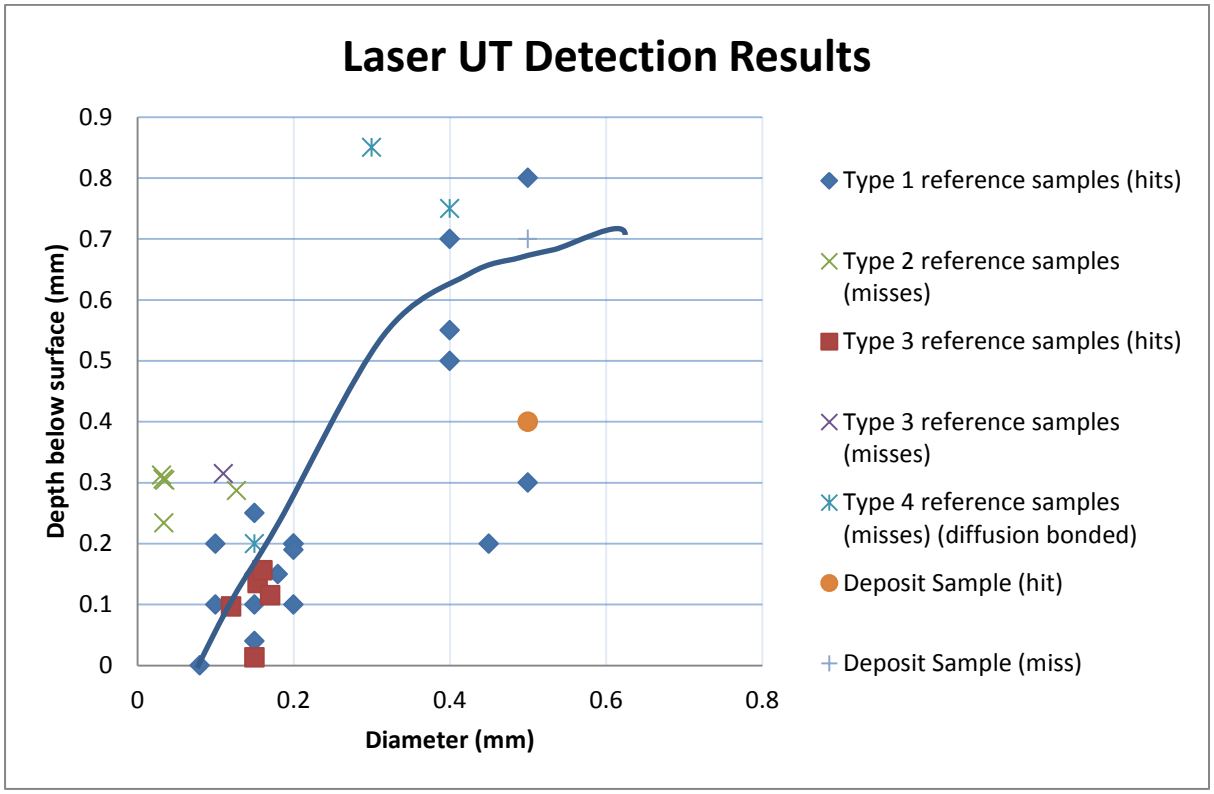

Figure 97 Summary Detection Results for Laser Ultrasonics (all Inconel samples)

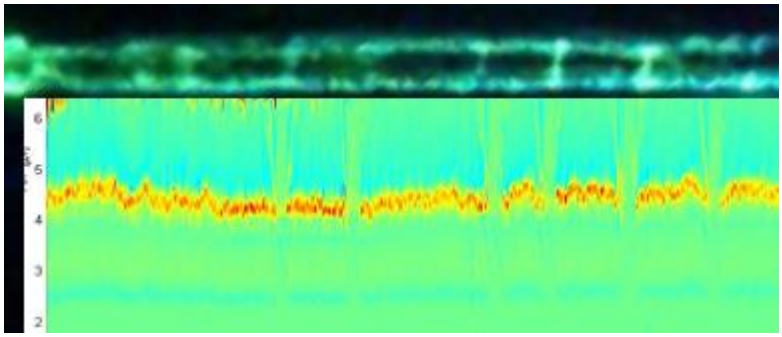

Figure 98 Comparison of Dye Penetrant and Laser UT data (automated scan)

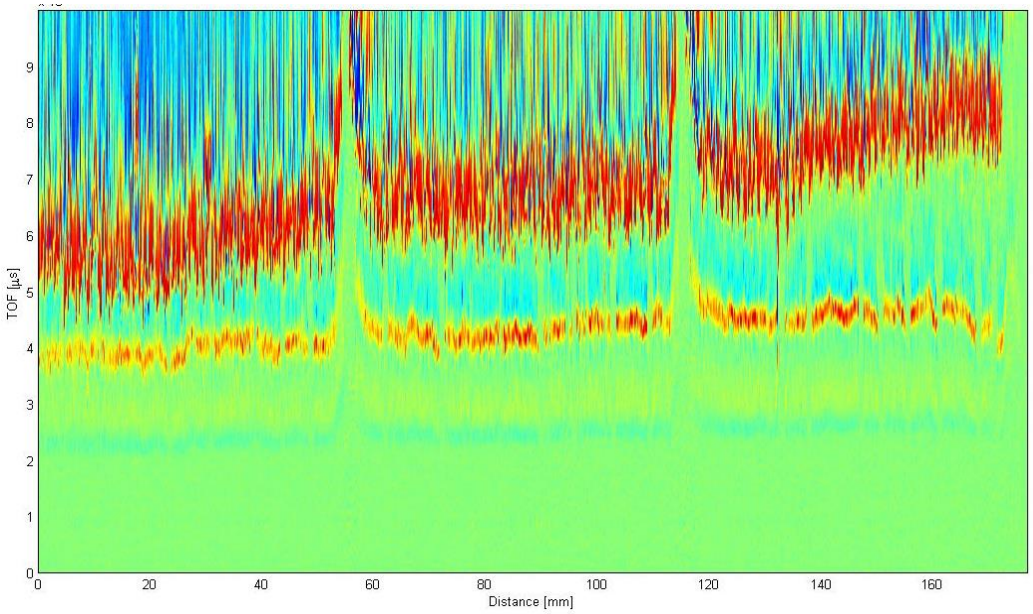

Figure 99 Displacement map acquired on CuNi alloy sample #2 (surface as deposited).

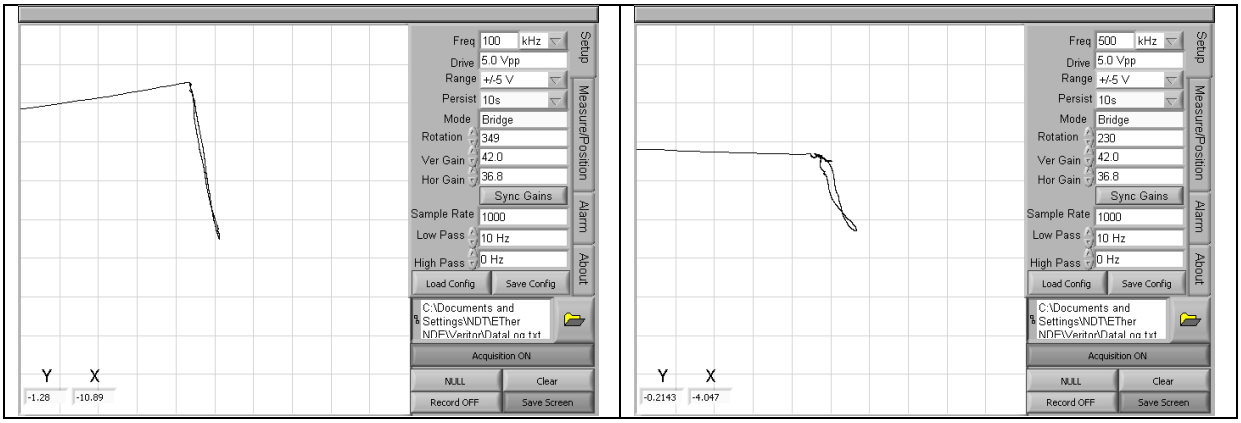

Figure 100 Effect of scanning the probe across a deposited layer (machined flat) at 100KHz (left) and 500KHz.

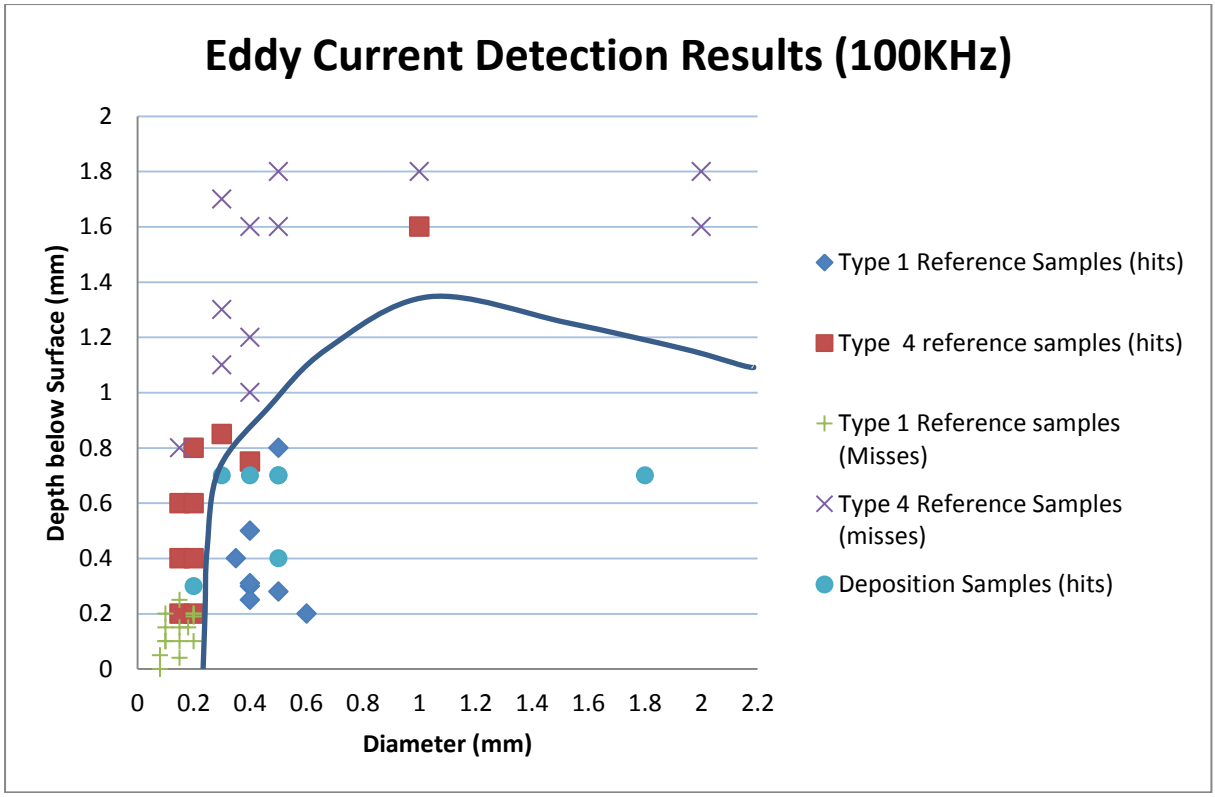

Figure 101(a) Results for Eddy Current Testing at 100KHz (all results)

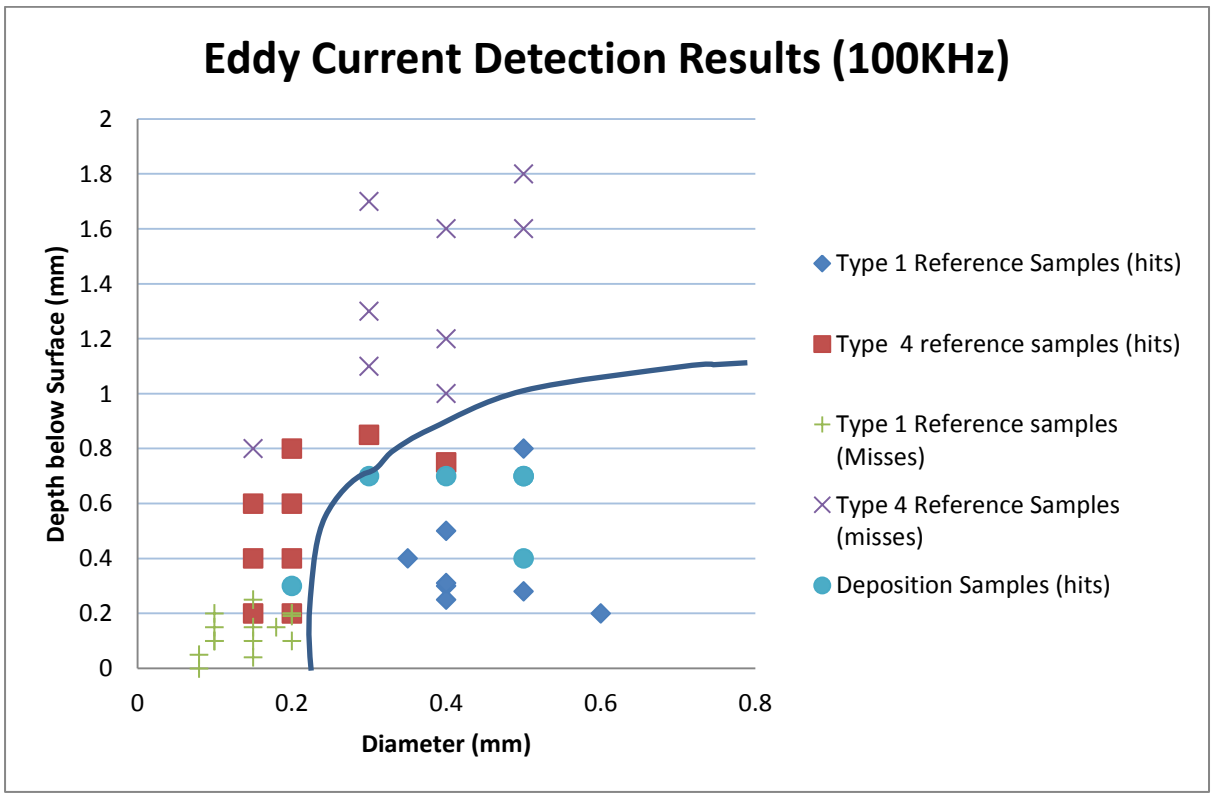

Figure 101(b) Results for Eddy Current Testing at 100KHz (results for flaws up to 0.8mm diameter)

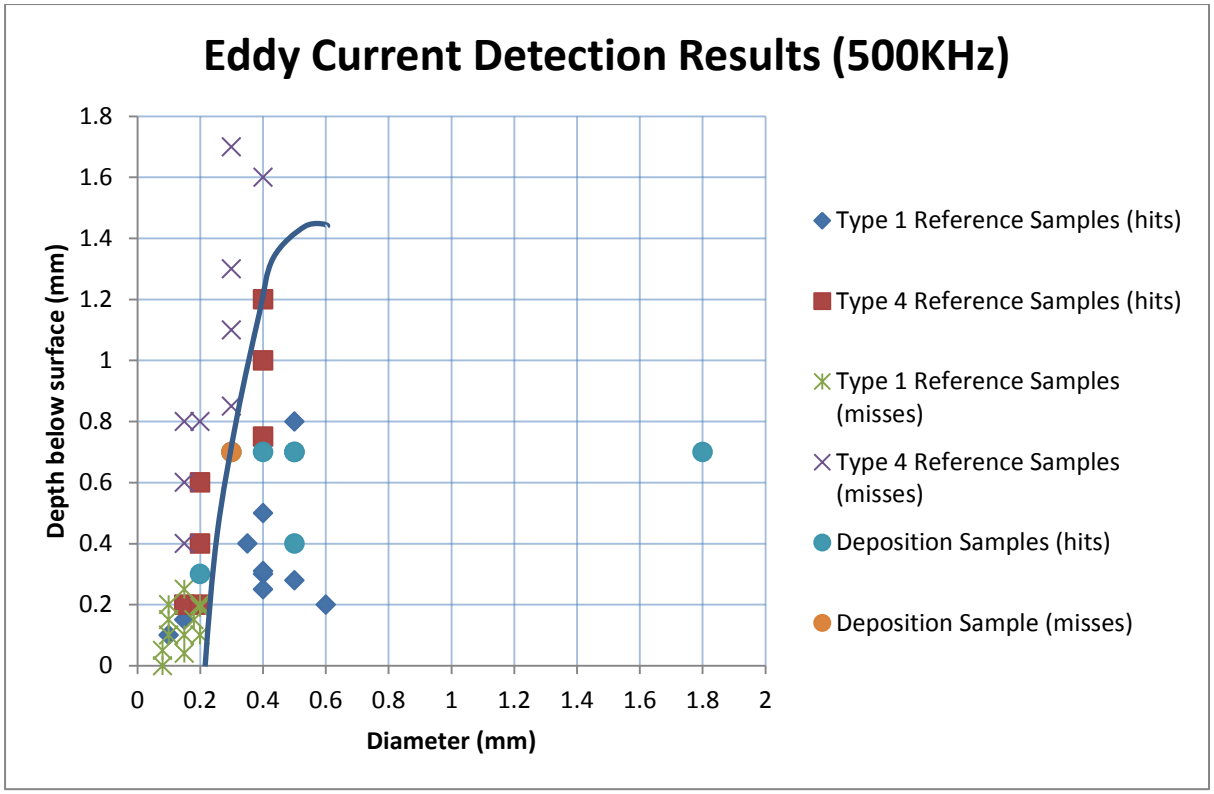

Figure 102(a) Results for Eddy Current Testing at 500KHz (all results)

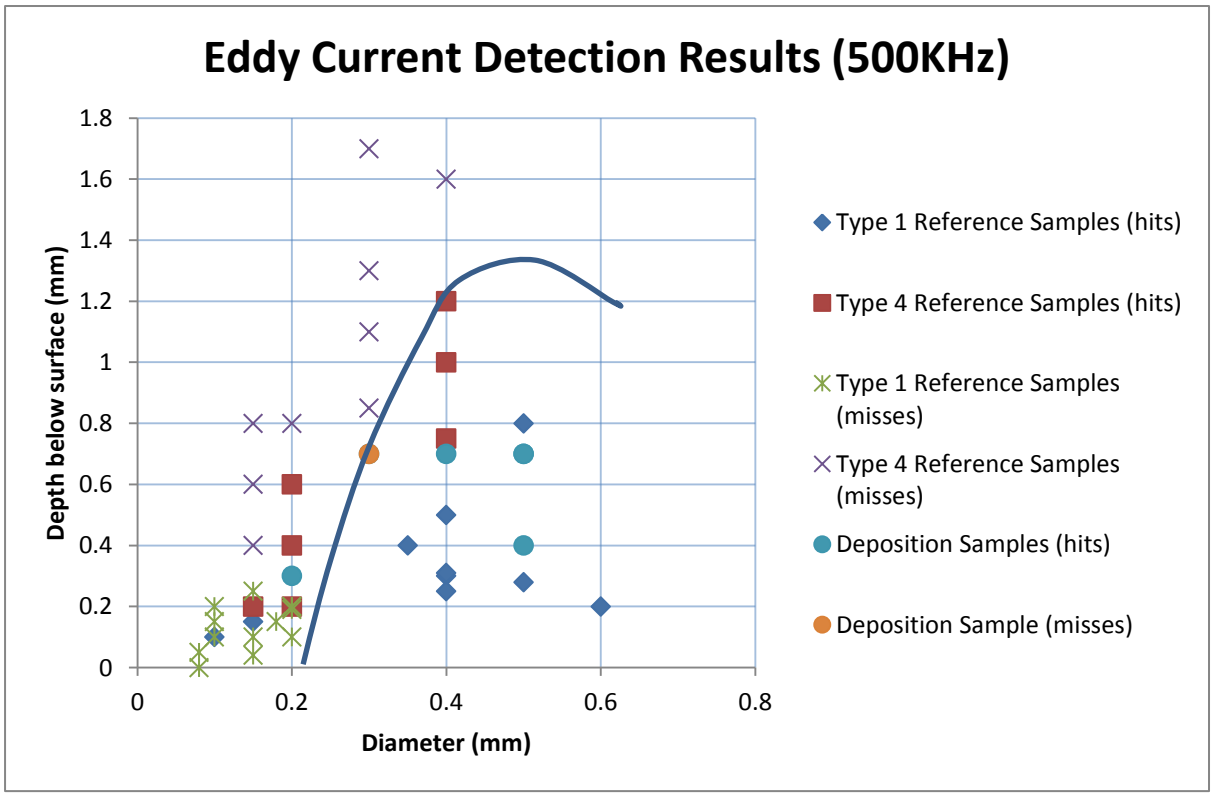

Figure 102(b) Results for Eddy Current Testing at 500KHz (results for flaws up to 0.8mm diameter))

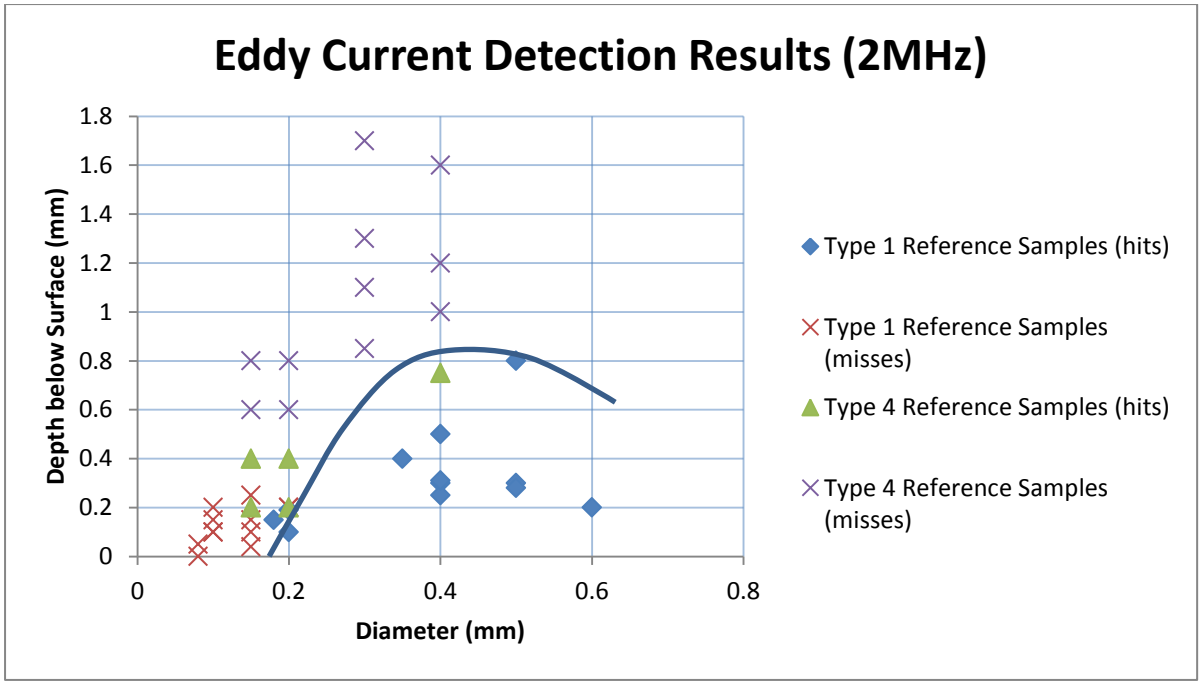

Figure 103 Results for Eddy Current Testing at 2MHz (all results)

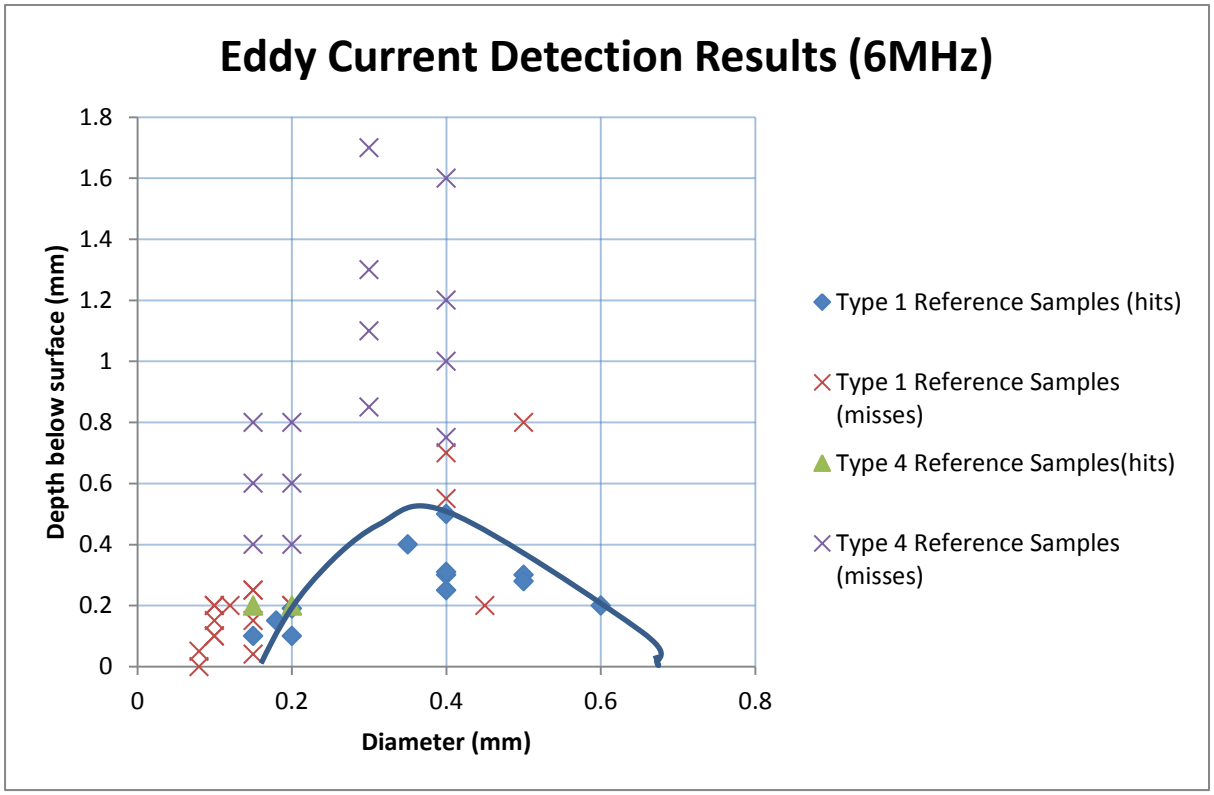

Figure 104 Results for Eddy Current Testing at 6MHz (all results)

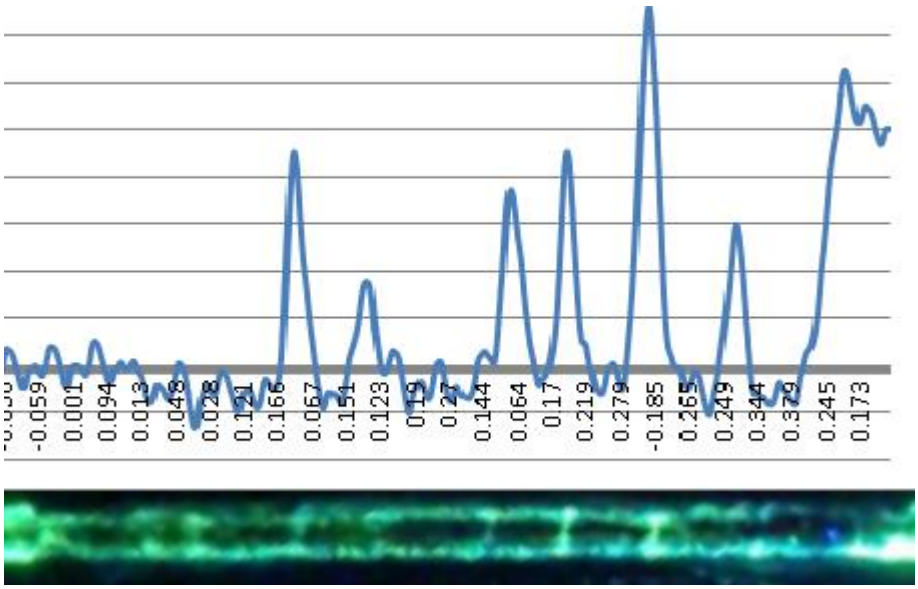

Figure 105 Comparison of dye penetrant and 6MHz eddy current results (automated scan)

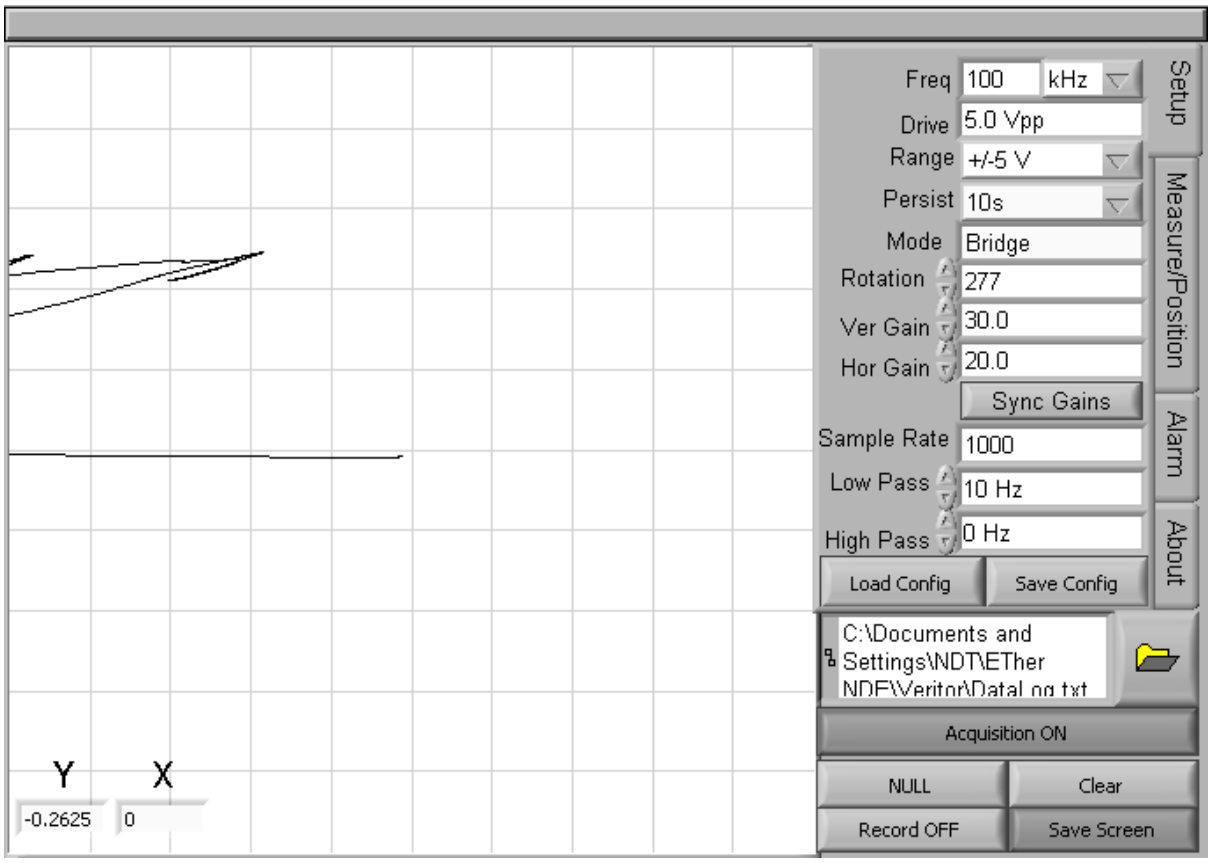

Figure 106 Sample 5 (good deposition bottom trace) and Sample 14(defective – top trace)

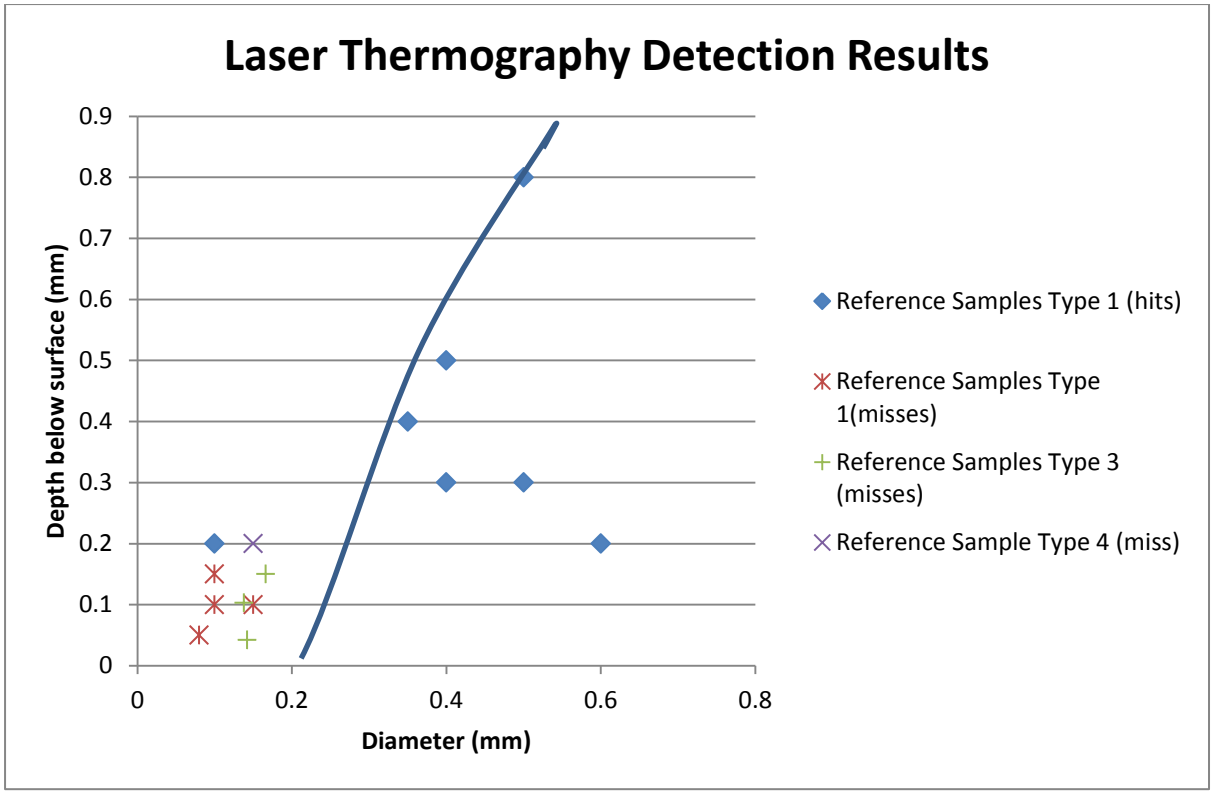

Figure 107 Laser Thermography Detection Results

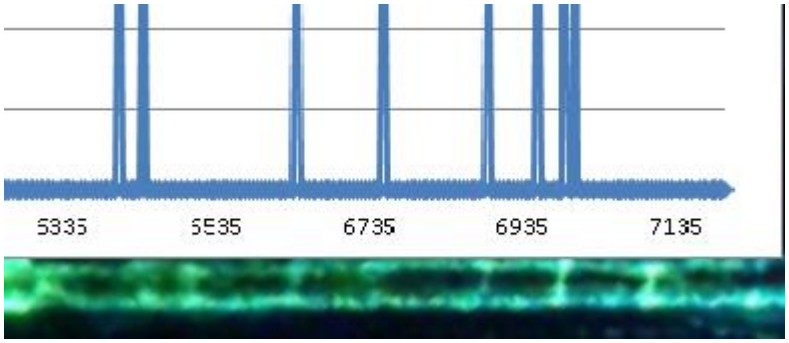

Figure 108 Comparison of dye penetrant and Laser Thermography indications (automated scan)

Materials and powders	Inconel Alloy 600 to start with Later on, nickel alloy onto aluminium substrate AC2C aluminium alloy and copper alloy powders
Bead size or width of deposit required	0.3 x 0.5mm initially 5 to 7 mm later
Flaw size of interest	<100 µm
Type of flaws to be considered	Porosity and lack of fusion
Inspection requirements	First target: Detection of 100µm holes in reference samples at different depths Detection of 100µm pores in test samples with simple geometries Detection of sub-surface flaw of 1 mm size in 5 mm width deposit (typical market requirements) If first target successful, second target: Detection of sub-surface flaw of 0.4 mm size in 5 mm width deposit (Toyota standard)
Inspection stage	Before machining process, inspection surface as clad surface

Table 1 Summary of the specifications and industrial requirements

NDT Technique	Associated Constraints and Requirements
Laser ultrasonics	Surface roughness may affect surface wave transmission Reflectivity (low for transmitter, high for receiver) requirements
Eddy current	Will be affected by proximity to edges. Temperature may affect conductivity Not remote, probe is placed close to sample
Laser thermography	Surface reflectivity (low for light) and emissivity (high for infra red) required.

Table 2 Summary of associated constraints and requirements for each NDT technique to be developed

			Diameter (mm)			Depth below surface (mm)		
Type	**Design**	**Sample**	**a**	**b**	**c**	**a**	**b**	**c**
1	1	1	0.5	0.4	0.5	0.3	0.6	0.8
		2	0.45	0.4	0.4	0.2	0.55	0.7
	2	1	0.2*	0.15*	0.1	0.2	0.15	0.1
		2	0.2*	0.1*	0.15	0.2	0.2	0.1
	3	1	0.15	0.1	0.12	0.25	0.2	0.2
		2	0.08*	0.15*	0.15*	0	0.04	0.25
		3	0.08	0.1	0.1	0.05	0.15	0.1
		4	0.18	0.2	0.1	0.15	0.1	0.19
	4	1	0.6	0.4	0.35	0.2	0.3	0.4
		2	0.5	0.4	0.4	0.28	0.25	0.31
* holes are not observable from the other side of material.								

Table 3 Summary of Targets produced in Type 1 Designs

Sample	**Side**	**Maximum Dimension (µm)**	**Depth (µm)**	**Comments**	**Image**
T5-1	B	127	287	Assume calibration is 40 µm	T5-B-1
	T	30	191		T5-T-2
T6-1	B	33	306	Max dimension / offset of one hole	T6-B-1
	T	not visible			
T7-1	B	35	304		T7-B-1
	T	66	312		T7-T-1
T8-1	B	34	272	Two images, same calibration	T8-B-1 and T8-B-2
	T	45	340	perhaps not max dimension	T8-T-1
T9-1	B	35	387		T9-B-1
	T	38	376	two holes, see image for details. Calculated max length = 71.21	T9-T-1
T10-1	B	31	312		T10-B-2
	T	47	358		T10-T-1
T11-1	B	24	331		T11-B-1
	T	44	389		T11-T-1
T12-1	B	34	234		T12-B-1
	T	40	223		T12-T-1
Note:					
T = Top, B = Bottom (of ledge)					
Offset measured from centre of hole to front surface of ledge					

Table 4 Summary of Targets in Type 2 design made by electron beam

Sample	Diameter (µm)	Depth (µm)
EDM1-1	154	135
EDM1-2	194	167
EDM1-3	160	213
EDM2-1	170	115
EDM2-2	182	139
EDM2-3	166	150
EDM3-1	160	156
EDM3-2	138	103
EDM3-3	142	137
EDM4-1	110	315
EDM4-2	100	422
EDM4-3	100	325
EDM5-1	120	97
EDM5-2	100	135
EDM5-3	100	165
EDM6-1	150	13
EDM6-2	142	42
EDM6-3	118	135

Table 5 Details of targets made in samples by EDM Microdrilling

Sample	Diameter (µm)	Depth (µm)
DB1	140	80

Table 6 Sample made by Diffusion Bonding

Temperature	Coefficient of Expansion	Electrical Resistivity	Thermal Conductivity	Specific Heat
°C	µm/m•°C	µΩ•m	W/m•°C	J/kg•°C
-150	10.9	-	12.5	310
-100	11.7	-	13.1	352
-50	12.3	-	13.6	394
20	10.4	1.03	14.9	444
100	13.3	1.04	15.9	465
200	13.8	1.05	17.3	486
300	14.2	1.07	19.0	502
400	14.5	1.09	20.5	519
500	14.9	1.12	22.1	536
600	15.3	1.13	23.9	578
700	15.8	1.13	25.7	595
800	16.1	1.13	27.5	611
900	16.4	1.15	-	628

Temperature	Young Modulus	Shear Modulus	Poisson's Ratio
°C	GPa	GPa	
22	214	80.8	0.324
100	210	79.6	0.319
200	205	78.0	0.314
300	199	76.2	0.306
400	193	74.2	0.301
500	187	71.9	0.300
600	180	69.2	0.301
700	172	65.9	0.305
800	164	62.1	0.320
900	154	57.9	0.330
1000	143	53.4	0.339

Table 7 - Thermal and elastic proprieties

ρ	Mass density	8470 kg/m^3
E	Young's modulus	214 GPa
G	Tangential modulus	80.8 GPa
υ	Poisson's ratio	0.324
Λ	Lamé constant	63.8 GPa
α	Expansion coefficient	1.04 X 10^{-5} °C^{-1}
C	Specific heat	444 Jkg^{-1}°C^{-1}
K	Thermal conductivity	14.9 Wm^{-1}°C^{-1}
$k=K/\rho C$	Thermal diffusivity	3.95 x 10^{-6} m^{2}s^{-1}
T_f	Melting temperature	1354 °C

Table 8 - Physical parameters of INCONEL alloy 600 for $T = 20^{\circ}\,\mathrm{C}$.

Notch	*Length (mm)*	*Width (mm)*	*Height (mm)*	
A	5	0.5	0.40 (80%xt)	=
B	5	0.5	0.25 (50%xt)	=
C	5	0.5	0.10 (20%xt)	=

Table 9 Dimensions of the notches added in the Inconel sheet.

Sample	Diameter (mm)	Depth (mm		100KHz		500KHz		
				Amp	Ph	Amp	Ph	
3E2	0.3	0.7		1	Vert	No ind - Noisy		
3E3	0.4	0.7	Surface Flaw by DP	1	Vert	3	TR/BL	Surface
3E5	0.2	0.3		2	TL	2	TL	
3E8			No flaw by radiography	2	BR	No ind		
5E1	0.5	0.7		1.5	TL	8	TL	Suggests surface
5E3	1.8	0.7		3	TR	1.5	TR	
5E4			No flaw by radiography	2	BR	1	BR	
5E5	0.5	0.7		8	TR	4	TR	
5E7	0.5	0.4		6	BR	2	BR	
5E9			No flaw by radiography	5	BL	4	BL	

Table 10 Eddy Current Results on Deposition Samples (automated scan)

No	Impact Identifier	Sales and savings
1	Sales of INTRAPID systems and sub-systems (ie test samples, software)	A total estimated sales of €18m*
2	Savings from reduction in materials waste	A total estimated saving of €27m**

Table 11 Impact of INTRAPID inspection system ten years after project completion

Notes:
*Business Plan compiled by SMEs at end of project
**Based on data provided by parts manufacturer. (5% global materials waste reduction).

EQUATIONS

$$c_1 = \left(\frac{\Lambda + 2G}{\rho} \right)^{1/2} = 5.16 \ \frac{mm}{\mu s} \tag{1}$$

$$c_2 = \left(\frac{G}{\rho} \right)^{1/2} = 3.09 \ \frac{mm}{\mu s} \tag{2}$$

$$c_R = \frac{0.87 + 1.12\upsilon}{1 + \upsilon} \cdot c_2 = 2.88 \ \frac{mm}{\mu s} \tag{3}$$

where Λ is the Lamé constant, G the tangential elastic modulus, and ρ the mass density.

$$\lambda \le 2\phi \quad \Rightarrow \quad \lambda \le 0.1 \text{ mm}. \tag{4}$$

$$f_1 \ge \frac{c_1}{\lambda} = \frac{5.16}{0.1} \ [MHz] \quad \Rightarrow \quad f_1 \ge 51.6 \ MHz \qquad \text{(longitudinal waves)} \tag{5}$$

$$f_2 \ge \frac{c_2}{\lambda} = \frac{3.09}{0.1} \ [MHz] \quad \Rightarrow \quad f_2 \ge 30.9 \ MHz \qquad \text{(transversal waves)} \tag{6}$$

$$f_R \ge \frac{c_R}{\lambda} = \frac{2.88}{0.1} \ [MHz] \quad \Rightarrow \quad f_R \ge 28.8 \ MHz \qquad \text{(Rayleigh waves)} \tag{7}$$

$$\Delta t = \frac{L_{\min}}{c_1} \tag{8}$$

where $L_{\min}$ is the smallest element dimension in the mesh and c_1 is the dilatational wave speed.

$$\Delta t = \frac{1}{20 \cdot f_{\max}} \tag{9}$$

where $f_{\max}$ is the highest frequency of interest.

$$l_e = \frac{\lambda_{\min}}{10} \tag{10}$$

where l_e is the element length and $\lambda_{\min}$ is the shortest wavelength of interest.

$$l_e \le \frac{\lambda}{10} = 0.01 \text{ mm}. \tag{11}$$

$$\nabla^2 T - \frac{1}{k} \frac{\partial T}{\partial t} = -\frac{A}{K} \tag{12}$$

where *T(x,y,z,t)* is the temperature distribution, *A(x,y,z,t)* is the heat produced per unit volume per unit time, and *K* e *k* are the thermal conductivity and diffusivity, respectively.

$$\frac{\partial^2}{\partial z^2} T(z,t) - \frac{1}{k} \frac{\partial T(z,t)}{\partial t} = -\frac{A(z,t)}{K} \tag{13}$$

$$T(z,t) = \frac{2I_0 \sqrt{kt}}{K} \cdot ierfc\left(\frac{z}{2\sqrt{kt}} \right) \tag{14}$$

where:

$$ierfc(\vartheta) = \frac{1}{\sqrt{\pi}} e^{-\vartheta^2} - \frac{2\vartheta}{\sqrt{\pi}} \int_{\vartheta}^{\infty} e^{-\varepsilon^2} d\varepsilon \tag{15}$$

Thus:

$$T(0,t) = \frac{2I_0\sqrt{kt}}{\sqrt{\pi}K} \tag{16}$$

$$T(z,t) = \frac{2I_0\sqrt{kt}}{K} \cdot ierfc\left(\frac{z}{2\sqrt{kt}}\right) - \frac{2I_0\sqrt{k(t-t_0)}}{K} \cdot ierfc\left(\frac{z}{2\sqrt{k(t-t_0)}}\right) \tag{17}$$

$$T(0,t) = \frac{2I_0\sqrt{kt}}{\sqrt{\pi}K} - \frac{2I_0\sqrt{k(t-t_0)}}{\sqrt{\pi}K} \tag{18}$$

$$I_0^{\max} = T_f \frac{\sqrt{\pi}K}{2\sqrt{kt_0}} \tag{19}$$

$$I_0^{\max} = 12.4 \ \frac{MW}{cm^2} \tag{20}$$

$$f_R = \frac{C_R}{d} \tag{21}$$

where f_R is the fundamental frequency of the Rayleigh surface wave field and c_R is the velocity of waves.

$$d = \frac{C_R}{f_R} = 0.1 \text{ mm} = 100 \ \mu\text{m} \tag{22}$$

$$w = \frac{d}{2} = 50 \ \mu\text{m}. \tag{23}$$

$$f_1^{2D} = \frac{c_1}{\lambda} = \frac{5.16}{0.01} \ [MHz] \quad \Rightarrow \quad f_1^{2D} = 516 \ MHz \qquad \text{(longitudinal waves)} \tag{24}$$

$$f_2^{2D} = \frac{c_2}{\lambda} = \frac{3.09}{0.01} \ [MHz] \quad \Rightarrow \quad f_2^{2D} = 309 \ MHz \qquad \text{(transversal waves)} \tag{25}$$

$$f_R^{2D} = \frac{c_R}{\lambda} = \frac{2.88}{0.01} \ [MHz] \quad \Rightarrow \quad f_R^{2D} = 288 \ MHz \qquad \text{(Rayleigh waves)} \tag{26}$$

$$V_m = 26.2 \text{ mm}^3 \tag{27}$$

$$n = \frac{V_m}{v_e} = \frac{26.2}{0.01^3 \frac{\sqrt{2}}{12}} = 222 \text{ millions} \tag{28}$$

$T(x) = I(x)/I_0 = 10^{-\alpha \cdot x}$ (29).

Where T(x) = Transmitted optical energy at depth x within the material, I(x) = light intensity at depth x within the material, I_0 = initial intensity of light entering the material, α = absorption coefficient as defined in Eq (300. X = depth of travel in the material.

$\alpha = 4 \cdot \pi \cdot k / \lambda$ (30)

where α = absorption coefficient, k = extinction coefficient or imaginary part of complex refractive index ň = n+i·k, λ = wavelength, and

$$E(x,t) = \mathrm{Re}(E_0 \cdot e^{i((2\cdot\pi(n+i\cdot k)/\lambda o)\cdot x - \omega\cdot t)}) \quad (31)$$

Where Re(ž) is an operator returning the real part of a complex number ž, E_0 = initial electric field of plane electromagnetic wave, λo = vacuum wavelength, ω = angular frequency, t = time, x = distance travelled by plane wave.